Hydrogel Cell Encapsulation for Tissue Engineering

by

Yibo Ling

B.S.E. Biomedical Engineering
B.A. English
University of Michigan, Ann Arbor, 2005

Submitted to the Department of Electrical Engineering and Computer Science
in partial fulfillment of the requirements for the degree of

Master of Science in Electrical Engineering and Computer Science at the
MASSACHUSETTS INSTITUTE OF TECHNOLOGY
[June 2008]
June 2007

Author.....
Department of Electrical Engineering and Computer Science
April 20, 2007

Certified by.....
Ali Khademhosseini
Assistant Professor
Harvard-MIT Division of Health Sciences and Technology
Brigham and Women's Hospital, Harvard Medical School
Thesis Co-Supervisor

Certified by.....
Martha Gray
Professor
Harvard-MIT Division of Health Sciences and Technology
Department of Electrical Engineering and Computer Science
Thesis Co-Supervisor

Accepted by.....
Arthur C. Smith
Chairman, Department Committee on Graduate Students

Hydrogel Cell Encapsulation for Tissue Engineering

by

Yibo Ling

Submitted to the Department of Electrical Engineering and Computer Science
on April 20, 2007, in partial fulfillment of the
requirements for the degree of
Master of Science in Electrical Engineering and Computer Science

Abstract

The engineering of artificial tissues for restoration or replacement of organ function holds the potential to alter the landscape of medical therapeutics. In many tissue engineering approaches, cells seeded within 3D porous structures are expected to remodel into tissue-like structures. Despite significant progress, difficulties in lack of control over tissue architecture as well as vascularization continue to limit the efficacy of engineered constructs. This thesis describes work aimed at tackling these two problems. First, two techniques for generating size- and shape-controlled cell-laden hydrogels are described in the context of potential modular assembly for conferring greater control over the geometry of homotypic and heterotypic cell arrangements within engineered tissues. Then, a method for producing cell-loaded microfluidic agarose hydrogels for tissue engineering is described.

Thesis Co-Supervisor: Ali Khademhosseini
Title: Assistant Professor, Harvard-MIT Division of Health Sciences and Technology, Brigham and Women's Hospital Department of Medicine, Harvard Medical School

Thesis Co-Supervisor: Martha Gray
Title: Professor, Harvard-MIT Division of Health Sciences and Technology, Department of Electrical Engineering and Computer Science, Massachusetts Institute of Technology

Acknowledgements

I would like first of all to express my gratitude to my advisor Dr. Ali Khademhosseini, whose vision, creativity, knowledge and support made this work possible. Thank you for your consistent patience in guiding me through the hills and valleys of research while simultaneously pushing me to stay focused and move full speed ahead. I would also like to thank my co-supervisor Dr. Martha Gray for shaping this thesis and supplying me with those words of encouragement that allow me believe in my work.

Next, I would like to thank all the people in the Khademhosseini Lab. To George Eng, James Blumling, Bin Ni, Giovanni Franzesi-Talei, Jay Gantz, Akash Chandawarkar, Dylan Wright, and Dave Morrison, thank you for your friendship and guidance. It was a pleasure to work with you all. But most of all, I would like to acknowledge Judy Yeh, my great friend and lab comrade. You are one of the few people in my life whom I feel genuinely proud to know; taking data points would not have been the same without you.

Finally, I wish to thank my close friends Danilo Scepanovic and Lan Xuezhao. Thank goodness we are in it together.

Dedication

To my parents,

Ling Tianjun and Xu Duohong.

Contents

List of Figures

Abbreviations

2D = two-dimensional

3D = three-dimensional

ECM = extracellular matrix

EDTA = ethylenediaminetetraacetic acid

FITC = fluorescein isothiocynate

FITC-BSA = fluorescein isothiocynate (conjugated to) bovine serum albumin

HA = hyaluronic acid

MeHA = methacrylated hyaluronic acid

PBS = phosphate-buffered saline

PCL = polycaprolactone

PDMS = poly(dimethylsiloxane)

PEG = poly(ethylene glycol)

PEGDA = poly(ethylene glycol) diacrylate

PLGA = poly(lactic-co-glycolic acid)

PLLA = poly(L-lactic acid)

TRITC = tetramethyl rhodamine iso-thiocyanate

UV = ultraviolet

μTM = microtransfer molding

VEGF = vascular endothelial growth factor

Chapter 1

Introduction

Despite the impressive ability of many tissues within the human body to regenerate in response to injury, entire classes of critical tissues such as cartilage, central nervous system, and cardiac muscle are wholly incapable of regeneration. The impairment of function accompanying common pathologies involving trauma or ischemia can be either complete, often resulting in death, or partial, resulting in varying degrees of unrecoverable functionality. One option for restoration of particularly vital functions is partial or whole organ transplantation. However, due to the limited availability of donors, only a fraction of those who could benefit from tissue transplantations actually receive them. One potential approach for remedying the shortage of transplantable organs is to artificially engineer tissues. Tissue engineering was first defined by Langer and Vacanti as, "an interdisciplinary field that applies the principles of engineering and life sciences to develop biological substitutes, typically composed of biological and synthetic components that restore, maintain, or improve tissue function."[1] Built on the premise that functional tissues will arise from cells seeded in appropriately configured scaffolds, tissue engineering techniques have been successfully applied to generate many types of tissues; yet, numerous challenges persist. The work described here offers potential workarounds to two of the most important of these challenges: nutrient/waste exchange, and the inability to control the complex three-dimensional (3D) construction and organization of cells within engineered tissues.

1.1 3D Scaffolds for Tissue Engineering

The traditional strategy for engineering 3D tissue has been to cultivate cells seeded within porous biodegradable scaffolds made from either natural[2] or synthetic[3] materials. The purpose of such scaffolds is to serve as an environment within which nutrient and oxygen transport as well as mechanical support[1] are apposite for cell growth and proliferation. In this approach, the scaffolds gradually degrade and become replaced by extracellular matrix (ECM) molecules deposited by cells, eventually leading to remodeling of the entire cell population into a macroscale tissue slab in the shape of the scaffold. Porous scaffolds are currently generated through a variety of processes such as solvent casting, particulate leaching[2], freeze-drying[3], gas foaming[4], and liquid-liquid phase separation. Processing conditions facilitate control over pore size, geometry, and interconnectivity.

Emerging techniques such as 3D printing, microsyringe deposition, and tissue spin casting confer more precise control over microscale scaffold shape and architecture. 3D printing in which a bed of powder is printed with a binder solution is typically used to generate ceramic[5] scaffolds in orthopedic tissue engineering applications. Similarly, microsyringe deposition relies on the same principle to generate poly(lactic-co-glycolic acid) (PLGA) scaffolds[6] for applications that require softer, more elastic materials. Many variations of these approaches are available and have been the subject of comprehensive reviews[7-9].

More porous scaffolds have been produced through the weaving of polymer nanofibers of a few hundred nanometers in diameter. Techniques for fabricating these nanofibers such as electrospinning, melt-blowing, phase separation, self-assembly, and template synthesis have been applied to both natural and synthetic biomaterials[10]. For example electrospinning in which a stream of discharged solvent threads via evaporation has been shown to be compatible with both naturally-derived materials such as collagen, and synthetic materials such as polycaprolactone (PCL) and poly(L-lactic acid) (PLLA), to generate scaffolds in orthopedic[11], cartilage[12], and cardiac tissue engineering[13] applications.

1.2 Strategies for Controlling Cell Remodeling

In traditional tissue engineering approaches, cells are induced to migrate within porous scaffolds upon seeding. This process is often slow (and sometimes incomplete) and, within larger scaffolds, may result in highly non-uniform cell distributions. Once cells migrate to desired regions they can remodel the surrounding environment and associate to generate functional tissues. A number of strategies have been implemented to induce remodeling of these cell populations into more desirable 3D architectures. Growth factors, chemoattractors, chemorepellents and other chemical factors have been used in soluble format or directly functionalized (in materials such as PLGA[14] and poly(ethylene glycol) (PEG)[15]) to the scaffold material. For example, it has been shown that neural and astrocyte stem cell differentiation can be modulated using hydrogel functionalized with IKVAV oligopeptides (a cell-adhesive laminin-derived sequence)[16]. Vascular endothelial growth factor (VEGF) has also been shown to improve vascularization of engineered

bone in both *in vitro*[4] and *in vivo*[17] models. Additionally, functionalized molecules have been patterned to guide cell growth and tissue remodeling. In a recent study, 3D channels of GRGDS oligopeptides (a fibronectin peptide fragment known to be cell-adhesive) were patterned into agarose matrices using a focused laser and verified to direct axon extension[18]. Alternatively, external stimuli such as the application of pulsatile electric fields have been shown to improve functionality in cardiac myocyte orientation and remodeling[5]. Similarly, cultured smooth muscle cells loaded by cyclical mechanical strain were found to upregulate elastin and collagen (standard ECM molecules) gene expression while exhibiting increased organization in comparison to cells cultured on static substrates[19].

Micro- and nano-textured substrates have been shown to significantly influence cell adhesion, gene expression [20-22] and migration[23]. These features can be incorporated within tissue engineering scaffolds to provide physical environmental cues to cells. For example, textured surfaces have been shown to improve osteoblast adhesions in a number of orthopedic replacement/augmentation applications[24]. Although the exact mechanism is not clear, it is believed that improved adhesion is caused by increased surface area. Nanotextures with features less than 100 nm may be produced by a number of techniques such as chemical etching in metals[25], the embedding of carbon nanofibers in composite materials[26], and the embedding of constituent nanoparticles in materials ranging from metals to ceramics to composites[27-30]. These approaches to improving cell remodeling for tissue engineering have been extensively reviewed in the literature[24].

1.3 Current Challenges and Obstacles

Although tissue engineering approaches described above have been successfully applied to the engineering of a variety of simple tissues such as skin and bone, more complex structures with higher cell densities, greater metabolic requirements, and intricate 3D architectures have been more difficult to engineer. Therefore it is believed that alternatives to the traditional 'seed-in-a-scaffold' approach are worth exploring. Two of the important immediate tissue engineering challenges are: 1) to enable nutrient and waste exchange in macroscale tissue constructs[31,32] and, 2) to overcome the lack of control of microscale 3D cell architectures in tissues in which proper function requires the formation of complex homotypic and heterotypic structures.

A common strategy for enhancing nutrient/waste exchange is perfusion of cell-laden macroporous scaffolds; however, this approach is suitable only for *in vitro* experimentation. Alternatively, vascularization of tissue engineered constructs through growth-factor induced angiogenesis[33-35] has produced promising results; yet, it is unclear that such an approach is amenable for the production of stable blood vessels or larger vasculature. Recently, tissue engineered constructs have been fabricated with soft lithography to produce synthetic vasculature for enabling nutrient/waste exchange[36,37]; however, the cells were coated within the channels as opposed to being embedded within the device material itself. Furthermore, while strategies for recapitulating function and complex 3D architecture in tissue engineered constructs by following the 'soluble factor' and 'external stimuli' strategies described in Section 1.2 have afforded important successes, most techniques have failed to produce fully or partial-but-substantially

functional tissue. Therefore, the goal of the work presented in this thesis is to address the challenges of nutrient/waste exchange and complex 3D architecture.

Chapter 2

Background and Motivation

Traditional tissue engineering in which cells are seeded within scaffolds is limited by difficulties in producing large, vascularized, complex tissues. Strategies such as tissue/organ printing of cells and materials have been explored as a means of generating complexity[38,39]. While tissue printing is promising for reproducing native three-dimensional (3D) architecture involving multiple cell types, the scalability of such approaches is unclear given that sequential layer-by-layer deposition also implies sequential exposure to potentially toxic gelling conditions. Alternatively, highly porous cell-seeded tissue engineering structures have been perfused as a means to maintain cell viability. This is a clever approach but it is unclear how such constructs would be connected to the blood supply *in vivo* as there is very little control over the specific porous architectures. Therefore, other strategies for conferring more precise control over the 3D architecture of engineered tissues as well as for enabling nutrient/waste exchange may be worth exploring. This thesis presents three standalone works developing three techniques, each described within separate chapters (Chapters 3-5). Chapters 3 and 4 document two techniques for fabricating the same types of shape- and size-controlled microstructures; these structures are considered in the context of a single strategy for generating complexity. Chapter 5 describes a technique for fabricating a different type of structure, for use in an unrelated strategy for enabling nutrient/waste exchange.

This chapter will orient the reader by 1) describing previous work in which hydrogel materials (the materials used here in all three works) were used for cell encapsulation, 2) reviewing the existing techniques for generating microscale features in cell encapsulated hydrogels, 3) providing an overview of the soft lithography technology employed by all three techniques described in the thesis, and 4) defining the basic design criteria for the structures produced to be compatible with tissue engineering. To reiterate, the three techniques presented in this thesis are considered in the context of two disparate strategies for addressing two separate problems in tissue engineering. For clarity, we will now discuss background issues of common relevance to all three techniques (Section 2.1, 2.2). We will then discuss the two strategies separately and in turn (Section 2.3, 2.4).

2.1 Hydrogels for Cell Encapsulation

Hydrogels are synthetic or naturally-derived hydrophilic polymer networks that swell greatly in water. They are commonly found in household items such as contact lenses and disposable diapers[40,41]. Among numerous other applications, hydrogels have been used for cell encapsulation since their mechanical properties resemble that of native tissues while intrinsically exhibiting high permeability to oxygen, nutrients, and other water-soluble metabolites[42,43]. In addition, hydrogels display mechanical and chemical properties that may be engineered (addition of functional groups, modulation of degradation rates) to exhibit other desirable characteristics. Due to this customizability, hydrogels have been widely used in tissue engineering and drug delivery applications[44,45].

In traditional tissue engineering, cells are seeded upon the surface of porous scaffolds (with pores sufficiently large to enable cell migration) and induced to migrate and populate the inner regions. In many cases cells do not evenly seed within the scaffold because of the large distances they must migrate in order to populate the scaffolds. Attempts have been made to homogenize cell seeding distribution through, for example, the application of centrifigual force to surface-seeded scaffolds[46] or the continuous perfusion of scaffolds with cell suspended solutions[47-49]. These techniques require cumbersome equipment and have not, to our knowledge, been demonstrated for microscale scaffold constructs. In contrast, the techniques described here use the encapsulation of cells within hydrogel materials[a]. The advantage of cell encapsulation to cell seeding in porous scaffolds for tissue engineering is the homogeneity of cell distribution that may be achieved. In cell encapsulation applications, cells are embedded within hydrogels by suspending the cell in a liquid hydrogel precursor, followed by crosslinking of the polymer network. In this way, uniformly-distributed hydrogel-encapsulated cells are required to migrate much shorter distances during the subsequent remodeling of cells into tissue.

To encapsulate cells, they are mixed with the hydrogel precursors and subsequently crosslinked. The crosslinking reaction may be controlled by a variety of non-cytotoxic stimulating factors such as temperature, pH or the addition of ions. Furthermore, hydrogels can be photopolymerized in the presence of photoinitiators via exposure to ultraviolet (UV) light[50]. Both biologically-derived hydrogels (e.g. fibrin[51], hyaluronic

[a] Note that hydrogels are also porous, though at nanoscales, so that while liquid diffusion is unhindered cell (~8 μm diameter for mammalian cells) migration is initially (prior to matrix degradation) unlikely.

acid (HA)[52], agarose[53]) and synthetic hydrogels (e.g. poly(ethylene glycol) (PEG)[54,55]) have been used to encapsulate cells. For example, photopolymerized PEG diacrylate hydrogels were explored for the transplantation of islets of Langerhans for the development of a bioartificial pancreas[56-58]. Similarly, photopolymerized HA hydrogels have been investigated as potential implantable/injectable cell delivery vehicles for cartilage regeneration[59]. Alternatively, alginate polymers that crosslink with the addition of calcium ions have been studied for the encapsulation of islet cells[60,61].

2.2 Soft Lithography

Soft lithography is a suite of techniques inspired by the semiconductor industry in which 'soft' materials are used to replicate micro- and nano-scale patterns[62]; it provides one avenue for creating microfeatured hydrogel materials. These patterns are often generated through photolithography (Figure 2.1A, 2.1B, 2.1C), in which a planar mask enables selective exposure of a thin film of photoresist upon a silicon wafer to UV. Exposed regions of photoresist then crosslink, transferring the features of the mask onto the thin film. Reusable patterned silicon masters[63,64] produced through photolithography have been utilized to generate relief structures in materials such as polyimides, polyurethanes, and most commonly, poly(dimethylsiloxane) (PDMS). The reusability of the silicon masters streamlines the fabrication process and greatly minimizes the need for costly photolithographic equipment and cumbersome clean room facilities. However, a disadvantage of soft lithography is that the features created are inherently planar. In soft

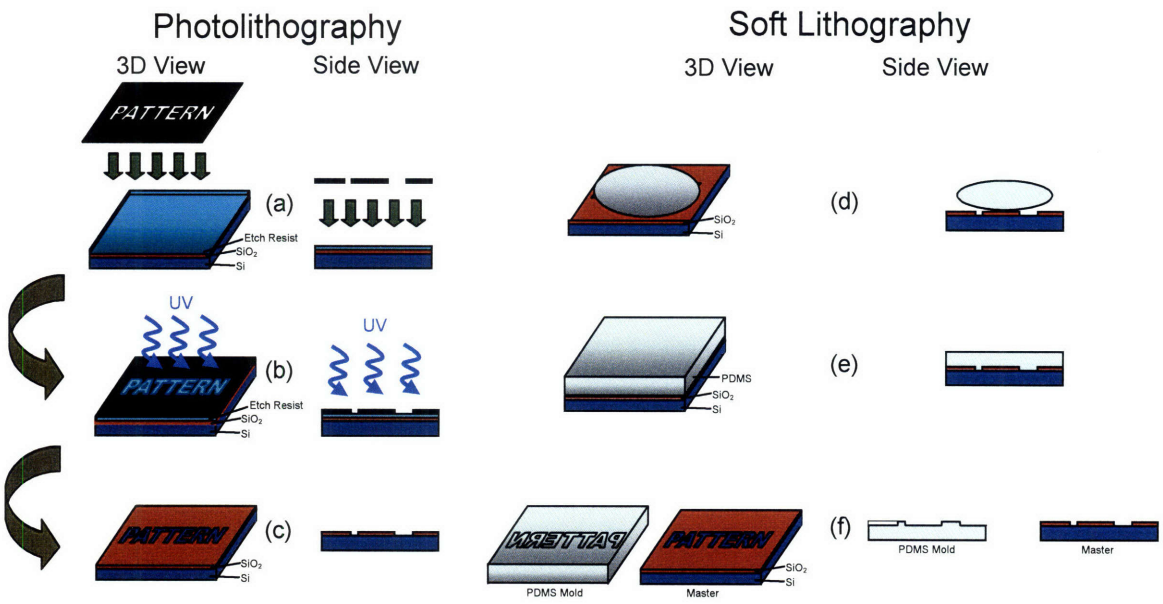

Figure 2.1: **Schematic comparison of photolithography (left) and soft lithography (right)**. Photolithography uses, (a) a patterned mask to (b) selectively expose and crosslink regions of polymer, (c) resulting in patterned silicon wafers. Soft lithography utilizes these patterned wafers to (d) mold liquid prepolymer which can be (e) cured or polymerized to produce negative copies of the patterned silicon wafer *in relief*.

lithography, cast molding (Figure 2.1D, 2.1E, 2.1F), is typically employed to generate relief structures in the elastomeric material.

Although many variations exist, the fundamental process is as follows: 1) a prepolymer solution is poured on top of a patterned silicon master, 2) a curing or polymerization-inducing agent is mixed into the prepolymer solution either before or after the pouring, 3) the material is cured or polymerized, 4) the solidified material with an imprint of the features of the silicon master in relief is peeled away from the master; the master can now be reused. A wide range of variations on the fundamental dogma of soft lithography such as replica molding, microtransfer molding, and microcontact printing have been developed[62]. Among many applications, elastomeric materials have been used to microcontact print surfaces for cell patterning[64], form microfluidic channels for the study of chemotaxis[65], and micromold arrays of microwells for high-throughput cell studies[66]. The production of both cell-loaded hydrogel microstructures and channel-featured constructs described here are based on soft lithography technology.

2.3 Bottom-Up Tissue Engineering: Overview and Background

Chapters 3 and 4 describe methods developed in this work for producing microstructures that may be used to generate complexity in a 'bottom-up' approach in which, like Lego blocks, assembly would begin from smaller microscale components in which cells are embedded. These shape-fitting microscale components containing different cell types may then be built up into larger meso- or macroscale constructs in a controlled manner. This two-step process can therefore be broken up into the fabrication of these

microstructures and the achievement of self-assembly. The work described in Chapters 3 and 4 is aimed at developing the fabrication techniques; self-assembly is left for future work although further rationale and background data regarding potential approaches are provided in the concluding chapter.

Previous techniques for encapsulating cells within microscale hydrogels were motivated by a desire to improve cell viability in the center of encapsulation constructs due to lack of appropriate levels of oxygen and nutrient diffusion through macroscale constructs[56,67]. As such, spherical microcapsules with high surface area to volume ratios and coated annuli of cells immobilized within polymers were generated to overcome these transport difficulties[59]. To date most synthetic cell-laden microstructures have been limited to spheres because of the incompatibility of current technologies, based on emulsification[68,69] or shear-induced droplet formation from syringes[53], to generate microscale structures of other shapes. While these techniques have been shown to be capable of forming spherical cell-laden microgels of controlled sizes, the lack of ability to generate non-spherical shape-fitting modular components circumscribes their efficacy for bottom-up tissue engineering.

Recently, photolithography[70-72] and soft lithography[73] (discussed previously in Section 2.2) were used to encapsulate live cells within small units of polymeric hydrogels anchored upon two-dimensional (2D) surfaces. These systems offer great potential for diagnostic and cell screening applications[74]. However, the specific techniques are incompatible with the formation of free components[63,64]. Nonetheless the fabrication

techniques involved in the generation of free cell-laden microstructures were inspired by the general approaches of these previous works.

Micromolding was used in the work documented in Chapters 3 and 4 to produce shape- and size-controlled cell-laden microstructures. Micromolding is a straightforward derivative of soft lithography in which microstructures are molded from elastomeric materials generated by the previously described cast molding process. In short, the liquid prepolymer solution is sandwiched between a patterned elastomeric surface and a flat surface and induced to cure or polymerize so as solidify in the shape of the mold. In principle, micromolding is capable of producing free hydrogel microstructures of controlled size and shape for tissue engineering.

Various micromold-able materials may be polymerized in different ways. Therefore, to enable the use of a wide range of hydrogel materials for bottom-up tissue engineering it is desirable to formulate alternative methods to fabricate microstructures from various cell encapsulation compatible hydrogels. Chapters 3 and 4 of this thesis describe the production of two classes of cell-loaded hydrogel microstructures for bottom-up tissue engineering: UV photopolymerizable, and chemical crosslinkable. Photopolymerizable polymers were previously discussed in Section 2.1; the third chapter is devoted to work demonstrating the photopolymerization approach with PEG diacrylate and methylacrylated hyaluronic acid (MeHA) as model photopolymerizable cell encapsulation materials. This work is straightforward in that the sandwiched material will polymerize upon UV exposure.

This simple micromolding approach could not be applied to a wide variety of chemical or pH-dependant crosslinking hydrogels such as alginate, chitosan and fibrinogen. Previously[75], alginate microfluidic devices were fabricated by pouring the hydrogel precursor over a mold followed by the immersion of the setup in a bath containing the gelling agent. However, this procedure cannot be easily adapted to produce individual microparticles. The essential challenge to the micromolding of chemical or pH-dependant crosslinking hydrogels is their rapid gelling, which occurs immediately upon contact with the gelling agent. Controlling the shape and size of microparticles and microstructures made from these hydrogels has not been possible by using previously reported techniques. In the fourth chapter of this work, the controlled release of a gelling agent from a soft lithographically generated hydrogel mold is used overcome this limitation.

For self-assembly of cell-laden microstructures to be feasible for tissue engineering, the following set of criteria were considered. First, the processing conditions had to be sufficiently mild so as to maintain an acceptable percent viability of encapsulated cells (~80% initial viability is conventionally accepted[76]). Different cell types were expected to be more or less resilient to processing conditions; since the technique was not intended to be organ-specific the identity of the cell type was not important and a convenient and commonly used cell line could be used (the NIH-3T3 fibroblasts are extremely well-characterized and commonly used as a conventional 'model' cell in tissue engineering[76]). Next, the technique had to allow for the production of various controlled shapes using (possibly charged or charge-functionalizable) materials that could potentially fit together

(for examples, cubes or other hexahedrons) in a charge and shape complementary fashion. At this early proof-of-concept stage a rigorous analysis of shape reproduction was not so important but future characterization will be essential for application to bottom-up tissue engineering[b]. To be consistent with the size range of previous mesoscale self-assembly methods[77], the microstructures needed to roughly be in the range of 50 – 1000 μm in each dimension.

2.4 Cell-Laden Microfluidic Constructs: Overview and Background

Chapter 5 describes a method for fabricating synthetic microfluidic flow channels within macroscale cell-loaded constructs as a means of enabling nutrient/waste exchange. These channels could then be perfused to facilitate controlled diffusion-based maintenance of cell viability.

In microfluidics, the controlled flow of fluids within microscale channels has be used to perform biological analyses and assays[78,79]. Microfluidic devices require minimal reagent consumption, allow for the laminar flow of fluids, and may be used for high-throughput analysis[80]. Currently, microfluidic devices are most commonly fabricated using soft lithography from poly(dimethyl siloxane) (PDMS) [81-84], a flexible silicone rubber that is optically transparent and therefore amenable for analyte visualization. Since PDMS is non-toxic, cells may be cultured on its surfaces or along the walls of its microchannels. However, cells cannot be cultured within the PDMS bulk material. In addition, materials such as poly(DL-lactic-*co*-glycolide) (PLGA) and poly(glycerol

[b] Please note that specific discussions on the types of shapes most conducive to self-assembly (i.e. number of potential slip planes, symmetry) were considered outside of the scope of our work but are discussed to some degree in the final chapter (which considers future self-assembly work).

sebacate) (PGS) as well as PDMS have been used to engineer microvasculature within synthetic scaffolds [85]. In these works [86-88], endothelial and hepatic cells were seeded within complex microfluidic channel patterns as a potential method to generate blood vessels and liver constructs for 3D tissue engineering. This approach is potentially powerful for engineering vasculature, which is an important challenge in making 3D constructs. While PGS and PLGA are biocompatible and biodegradable, potential limitations of this approach include the difficulty of achieving uniform cell seeding, the high volume of the scaffold material which must be degraded, and the 2D surface microenvironment of the scaffolds. The alternative approach presented here aims to overcome these limitations by utilizing hydrogel cell encapsulation technology. Recently, the first hydrogels, calcium alginate[75] and gelatin[89], were used to fabricate microfluidic devices. Also, it was demonstrated that cells could be seeded on the surface the microchannels within these devices.

However, no previous work has shown the capacity to perfuse, using highly controlled channels, cells encapsulated within the surrounding material. As such, primary consideration in our work was given to cell maintenance within the perfused construct. The mechanical properties of the material were considered only insofar as their compatibility with the fabrication of sufficiently stiff and perfusable channels (with the simplest channel patterns available and cross-sectional areas in the range of typical arterioles or capillaries). As with the cell-loaded microstructures described above, the processing conditions had to be sufficiently mild so as to maintain an acceptable percent viability of encapsulated cells (~80% initial viability is conventionally accepted[76]).

Again, cell type was not considered an important parameter and so a commonly used cell line (AML-12 here) could be used. Since the criterion considered most important for this first demonstration was that the material allow for nutrient/waste exchange, it was necessary to verify the capacity of such a construct to maintain cell viability over time.

In summary, Chapters 3 and 4 will describe micromolding approaches for producing shape- and size-controlled cell laden microstructures. To increase the number of micromoldable cell encapsulation materials that may be used in bottom-up tissue engineering, techniques for utilizing both photocrosslinkable (Chapter 3) and chemically crosslinked (Chapter 4) hydrogels are developed. Chapter 5 will then describe the fabrication of microfluidic cell-laden hydrogel constructs with a brief discussion of future directions. Finally, the thesis will conclude with a chapter detailing future bottom-up tissue engineering work and the specific ways by which shape- and size-controlled cell laden microstructures could be self-assembled.

Chapter 3

UV Crosslinked Hydrogel Microstructures

This chapter discusses the fabrication and characterization of ultraviolet light (UV) crosslinked cell-laden microstructures which could potentially be used in bottom-up tissue engineering. Two model UV-crosslinkable materials, poly(ethylene glycol) diacrylate (PEGDA) and hyaluronic acid methacrylate (MeHA) were used (reactions illustrated in Figure 3.1). Briefly, NIH-3T3 fibroblast cells were suspended in a hydrogel precursor solution containing photoinitiator, deposited onto hydrophilic poly(dimethylsiloxane) (PDMS) patterns, crosslinked under UV radiation, and retrieved upon hydration. Application of this technique yielded size- and shape-controlled microstructures with generally homogeneous cell distributions at various cell densities.

Hyaluronic acid (HA) is a negatively charged natural component of the extracellular matrix (ECM) known for its biodegradable and bioresistant properties[90,91] as well as its role in facilitating cellular functions such as adhesion, proliferation, and migration[92]. PEG is a synthetic, inert, non-biofouling material often used in templates for immobilizing cells on two-dimensional (2D) surfaces[63,64] or within microfluidic channels[63]. A large body of literature exists describing the addition of functional groups to PEG to modulate characteristics such as charge and degradation rate[72].

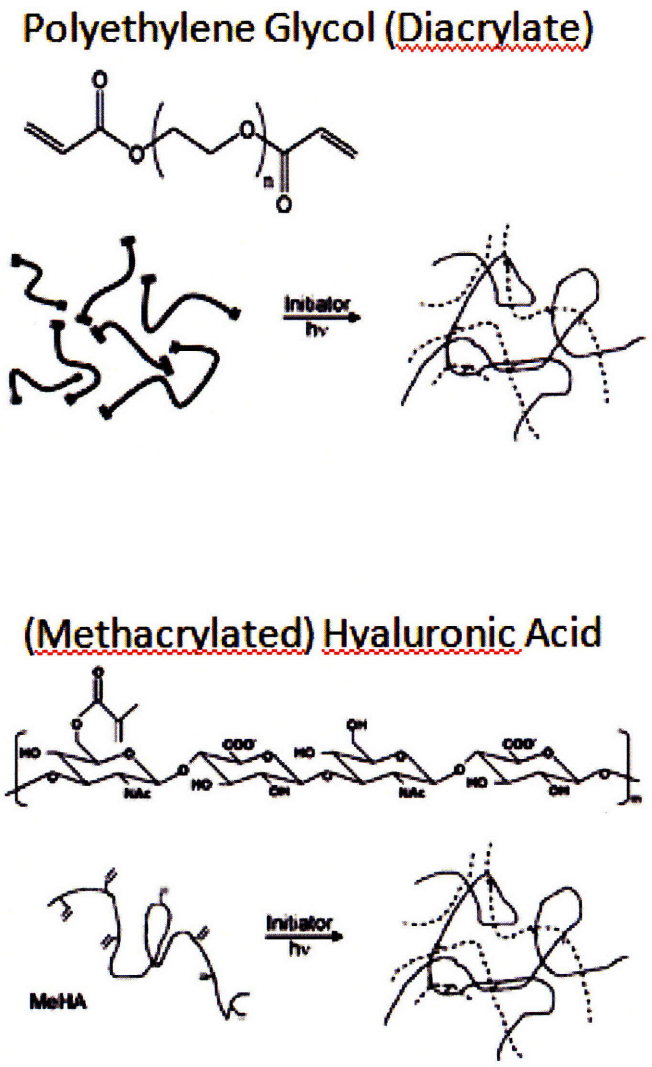

Figure 3.1: Photopolymerization of PEGDA and MeHA. PEGDA hydrogel networks undergo polymerization at the carbon-carbon double bonds of the acrylate group functionalized to the ends. Two primary radicals, generated by the photoinitiator when exposed to UV light, propagate through the electron-rich acrylate groups. The subsequently generated kinetic chains result in crosslinked PEG. Similarly, the functionalized methacrylate groups of MeHA enable free radical polymerization in the presence of photoinitiator.

The goal of this work was to provide a proof-of-principle that a photopolymerization micromolding approach could be used to produce free shape- and size-controlled microstructures. Previous work has thoroughly explored the properties and design considerations of hydrogels[93]. Rather than a rigorous and thorough analyses of biological and mechanical properties, this work was focused on demonstrating the possibility of producing free microstructures with acceptable viability (~80% viable), reproduction fidelity (produced in the general shape of their molds), and structural integrity (could be harvested in solution without dispersing into debris). The mechanical and biological properties of PEGDA are more thoroughly characterized than MeHA in existing literature. While cells were encapsulated in both PEGDA and MeHA systems, processing parameters (using our model materials) like UV exposure length, prepolymer concentration and photoinitiator concentration were only explored to increase cell viabilities for MeHA[c]. Despite differences in biocompatibility the processing properties were not expected, and were not found in this work, to differ substantially between the two materials.

[c] An additional reason we focused more on MeHA is that the mechanical and cell viability characteristics in PEG encapsulation systems have been thoroughly well-characterized in the past.

3.1 Materials and Methods

3.1.1 Cell Culture

All cells were manipulated under sterile tissue culture hoods and maintained in a 95% air/5% CO_2 humidified incubator at 37°C. NIH-3T3 mouse embryonic fibroblast cells were maintained in Dulbecco's modified Eagle media (DMEM) supplemented with 10% FBS. Confluent dishes of NIH-3T3 cells were passaged and fed every 3-4 days.

3.1.2 Prepolymer Solution

Two macromers were used: PEGDA and MeHA. The synthesis of MeHA was previously reported[95]. In brief, the synthesis was performed by the addition of 1 wt% methacrylic anhydride (Sigma) to a solution of 1 wt% HA (Lifecore, MW = 67 kDa) in deionized water. The reaction was performed for 24 h on ice and maintained at a pH of 8-9 through the addition of 5N NaOH. The macromer solution was then purified by dialysis (Pierce Biotechnology, MW cutoff 7 kDa) for 48 h in deionized water and lyophilized for 3 days, resulting in a final dry form which was frozen for storage. The prepolymer form of MeHA was created by dissolving dry MeHA in PBS (Gibco) at 37°C for 24 h to facilitate full dissolution. Immediately prior to UV photopolymerization, varying concentrations of photoinitiator solution were added to the prepared prepolymer solution. The photoinitiator solution used was 33 wt% 2-hydroxy-1-(4-(hydroxyethoxy)phenyl)-2-methyl-1-propanone (Irgacure 2959, CIBA Chemicals) in methanol.

To generate PEG hydrogels, a solution containing 10% (w/w) PEGDA (MW 575, Sigma) in PBS (Gibco) was prepared prior to experiments in order to allow the PEGDA to

adequately dissolve into solution. Immediately preceding UV photopolymerization, photoinitiator solution was added to the prepolymer solution at 1 wt%. The photoinitiator solution used was also 33% (w/w) 2-hydroxy-1-(4-(hydroxyethoxy)phenyl)-2-methyl-1-propanone (Irgacure 2959, CIBA Chemicals) in methanol.

3.1.3 PDMS mold fabrication

PDMS molds of various shapes were fabricated by curing prepolymer (Sylgard 184, Essex Chemical) on silicon masters patterned with SU-8 photoresist. The patterns on the masters had protruding patterns (squares, circles, long rectangles) of various sizes (ranging from 50 to 400 μm), which allowed for the formation of shaped wells in PDMS replicas. PDMS molds were generated by pouring 1:10 curing agent to silicon elastomer onto the master and curing for 2 h at 37°C. Finally, the PDMS molds were peeled from the silicon masters, cut into small rectangular shapes, and placed over glass slides to facilitate ease of manipulation. The use of glass slides allowed direct manipulation of the slides, thereby minimizing the possibility of damaging the molds. Before use the molds were rendered hydrophilic by plasma cleaning for 45 s on medium power (PDC-001, Harrick Scientific). Untreated (hydrophobic) flat sections of PDMS were similarly placed over glass slides and used as coverslides to reversibly seal the prepolymer solution within individual volumes during the micromolding procedure.

3.1.4 Microstructure Polymerization

The micromolding procedure schematized in Figure 3.2 was used to fabricate microstructures of controlled shapes and sizes. To suspend NIH-3T3 cells within the

prepolymer solution, the cells were first trypsinized with 0.23% trypsin and 0.13% ethylenediaminetetraacetic acid (EDTA) in PBS (Gibco). The suspension was then centrifuged at 1000 rpm for 2 min to produce a cell pellet. The pellet was resuspended in controlled volumes of the prepolymer solution. This yielded differing concentrations of cells in prepolymer solution (cell density values are reported as cells/ml of the prepolymer). 20 - 25 $\mu L\ cm^{-2}$ of this cell/polymer mixture was then pipetted onto freshly plasma oxidized PDMS molds. The tip of the pipette was gently brushed on the mold surface to remove any bubbles. A PDMS coverslide was then carefully applied on top of the mold and gently rotated under slight finger pressure to ensure PDMS/PDMS contact. The mold/polymer-solution/coverslide assembly was then exposed to ~1 $W\ cm^{-2}$ 360-480 nm UV light for various durations. Finally, the coverslide was carefully removed and PBS was immediately pipetted onto the coverslide surface upon which the microstructures were adhered to hydrate the newly formed hydrogels.

3.1.5 Microstructure Harvesting

After photopolymerization, the coverslide was separated from the PDMS mold to retrieve the microstructures. In this process, a fraction of the microstructures adhered within the wells of the mold while the other fraction adhered to the PDMS coverslide. For convenience, those microstructures which adhered to the PDMS coverslide upon removal of the coverslide from the PDMS mold were then harvested while those which remained adhered within the microwells were discarded. After hydrating the microstructures upon the coverslide, a number of individual microstructures spontaneously detached from the coverslide while a number remained adhered. A pipette tip was gently brushed over the

coverslide to mechanically detach the remaining microstructures. Reproduction fidelity for (10% MeHA, 1% photoinitiator, 180 s UV exposure) 400 x 400 μm square hexahedrons (these became slightly rectangular) was determined by dividing the length of the short axis by that of the long axis (n = 6). Planar swelling was determined for (10% MeHA, 1% photoinitiator, 180 s UV exposure) square hexahedrons molded within 400 μm x 400 μm x 50 μm by dividing the top-down planar surface area by 400 x 400 μm (n = 6).

3.1.6 Imaging and Analysis of Encapsulated Cells

Initial encapsulated cell viability was assessed by applying a live/dead (calcein AM and ethidium homodimer) fluorescence assay to a model polymer system, consisting of cells encapsulated in thin layers of HA hydrogel made by deposition of 20 μl cell/prepolymer mixture between a glass slide and a flat PDMS coverslide. After photopolymerization, the PDMS coverslide was removed, leaving a thin layer of cell-loaded polymer adhered to the glass slide. The thin layer was subsequently hydrated with 200 μl PBS solution containing 2 μg/ml calcein AM and 4 μg/ml ethidium homodimer-1 (Molecular Probes) and visualized under a fluorescent microscope (Zeiss, Axiovert 200). Initial cell viability assessments were made using NIH-3T3 cells encapsulated within MeHA thin layer hydrogels in which the macromer concentration, UV exposure duration, and photoinitiator concentrations were varied.

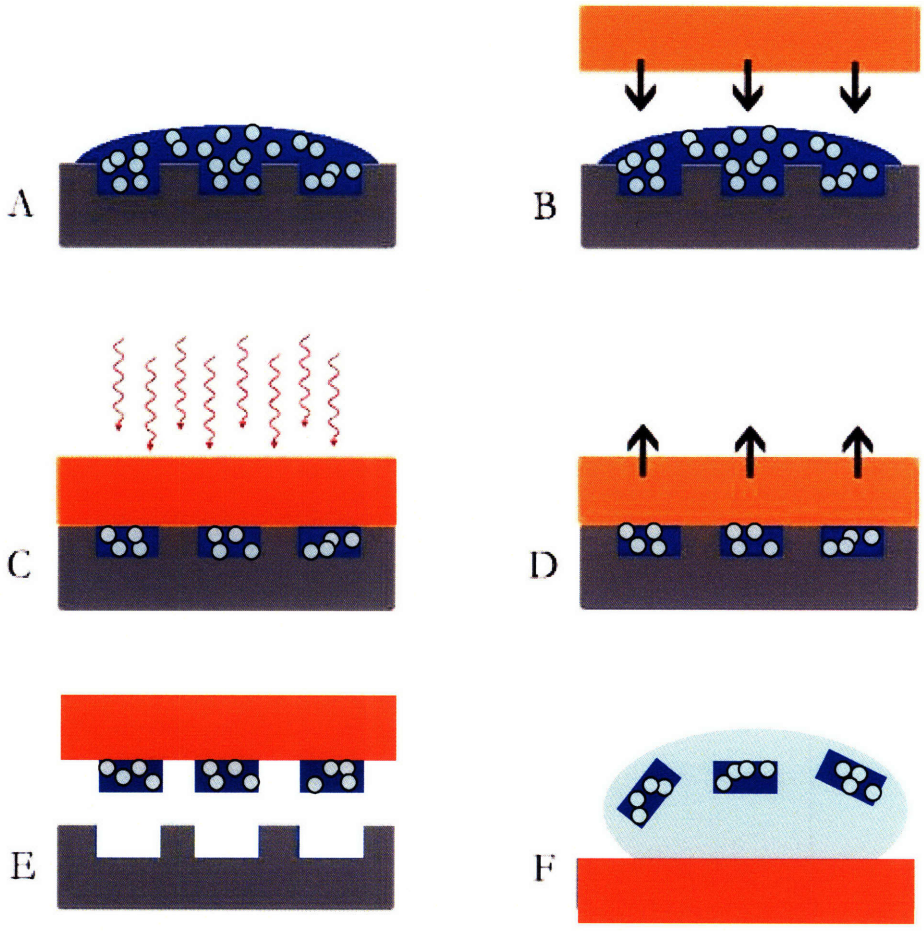

Figure 3.2: Process of cell encapsulation and microstructure formation. (A) Cells are suspended in prepolymer solution and deposited onto a plasma-cleaned PDMS mold. (B) A PDMS coverslide is placed on top, forming a reversible watertight seal. (C) Liquid prepolymer is photopolymerized via exposure to UV light. (D) The PDMS coverslide is lifted, (E) permitting removal of the microstructures which are then (F) hydrated and harvested.

Two recognized parameters of cell viability – intracellular esterase activity and plasma membrane integrity – were tracked. Live cells fluoresced green, exhibiting intracellular esterase activity that hydrolyzed the fluorogenic esterase substrate (calcein AM) to a green fluorescent product; dead cells fluoresced red, their plasma membrane being compromised and therefore permeable to the high-affinity, red fluorescent nucleic acid stain (ethidium homodimer-1). Percent viability values were calculated by counting the number of live (green) cells and the number of dead (red) cells in a representative 400μm × 400μm square area magnified at 50X (or embedded within individual microstructures) and dividing the number of live cells by the number of total cells (live plus dead). Measurements were taken in triplicates, and error bars were based on standard deviation values for n=3 unless otherwise indicated.

For confocal microscopy, cells were stained with Vybrant DiD (Molecular Probes) at 20μl/ml in PBS, fixed with Fluoromount-G, and covered with a No. 1 thickness coverslip. Confocal images were taken at 40× magnifications through a Rhodamine filter with a maximum focal depth of 248 μm. CFSE and PKH26 staining were performed[96] at room temperature prior to microscopy.

3.2 Results

3.2.1 Microstructure Fabrication

Using the micromolding approach schematized in Figure 3.2, cell-free MeHA and PEGDA microstructures of various shapes at 10% macromer and 2% photoinitiator concentrations exposed for 180 s to UV light were generated. Representative images of a

few of these cell-free square hexahedrons, cylinders, and strings are shown in Figure 3.3. The planar swelling of 10% MeHA, 1% photoinitiator, 180 s UV exposed microstructures produced from 400 x 400 μm square molds was 73% with a standard deviation of 22%. The ratio of short to long axes of 10% MeHA, 1% photoinitiator, 180 s UV exposed microstructures produced from 400 x 400 μm square molds was 0.94 with a standard deviation of 0.05. This places it slightly over one standard deviation away from the value of a perfect square (1).

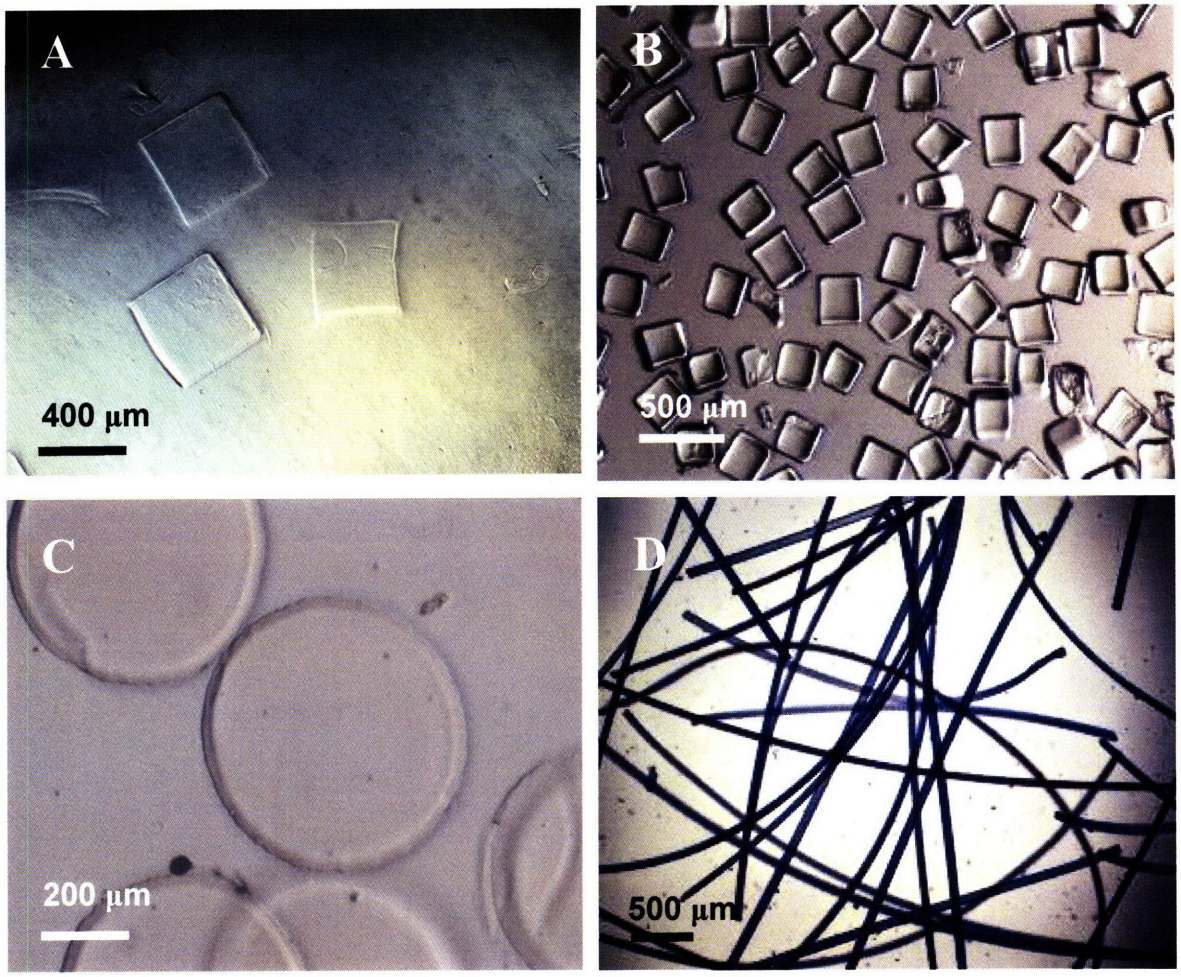

Figure 3.3: Versatility of microstructure shapes. Microstructures of various shapes can be micromolded: square hexahedrons (A, B), cylinders (C), and string-like rectangular hexahedrons (D, stained with trypan blue to facilitate visualization) using different prepolymer solutions: (A) MeHA and (B, C, D) PEGDA.

3.2.2 Characterization of Initial Cell Viability

Cell viability was tracked as a function of photoinitiator concentration, UV exposure length, and macromer concentration in a thin-layer MeHA model (Figure 3.4). Viability exhibited significant decreases with increasing UV exposure length for any given photoinitiator and macromer concentrations (Figure 3.4). When other parameters were held constant increasing either macromer concentration or photoinitiator concentration individually also decreased cell viability.

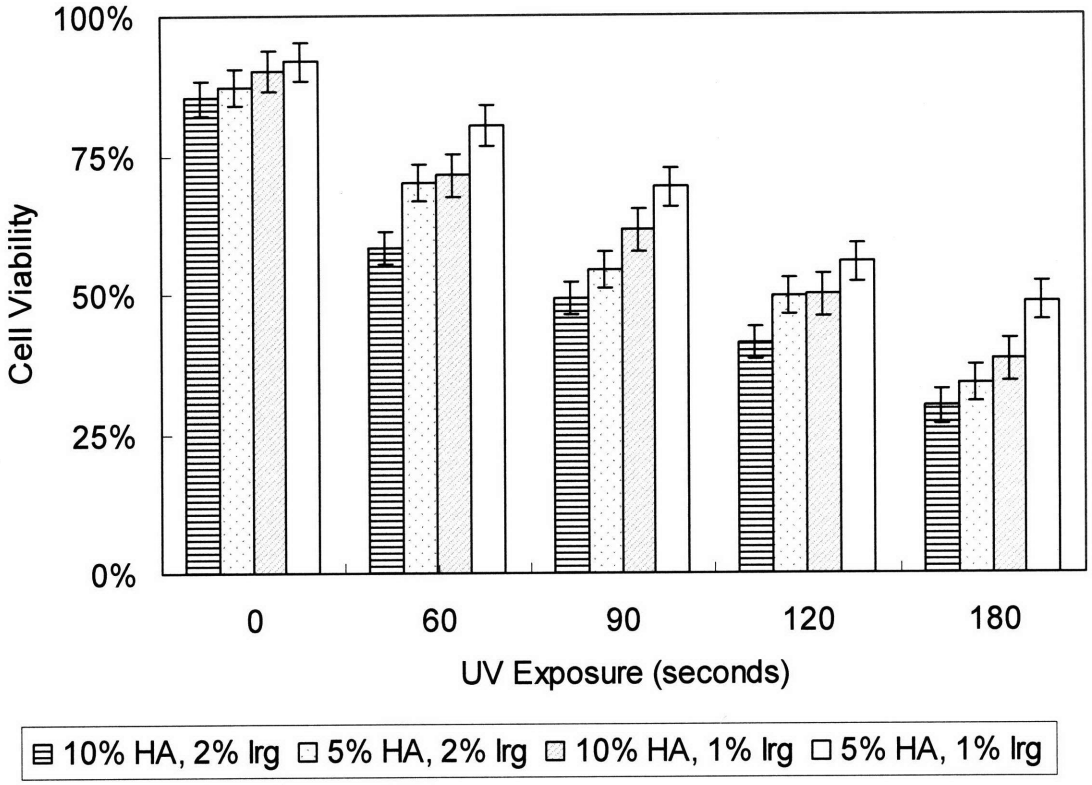

Figure 3.4: Characterization of initial cell viability. Varied parameters include macromer (HA) concentrations, photoinitiator (Irg for Irgacure) concentrations, and UV exposure durations. Control values (0 s) are provided for reference. Error bars indicate standard deviation values for n = 3.

3.2.3 Cell Encapsulation within Microstructures

Facile retrieval is shown between Figure 3.5A/3.5C, in which the microstructures were initially fabricated (and left residing as an array attached to the coverslide), and Figure 3.5B/3.5D, in which the microstructures were subsequently hydrated and suspended (now at oblique angles). Upon being pushed with a micromanipulator, the dead (stained red) cells at the periphery of the microstructures were found to be mobile while those presumably embedded within the hydrogel material moved in registration with the outline of the microstructures. The ability to vary cell density while maintaining viability >85% is shown in Figure 3.6.

MeHA and PEGDA microstructures fabricated at 10 wt% macromer, 1% photoinitiator, and UV exposed for 45 s yielded initial viability values >85% for both materials (Figure 3.7). The microstructures were qualitatively observed to exhibit more uniformity in a top-down view (Figure 3.7A-D) and somewhat less uniformity throughout the depth (Figure 3.7E). Time-course viability remained >85% for up to 4 days in MeHA microstructures (Figure 3.8). In the day 4 fluorescent image (Figure 3.8), one microstructure in the lower left corner appears to have substantially lower viability than surrounding structures.

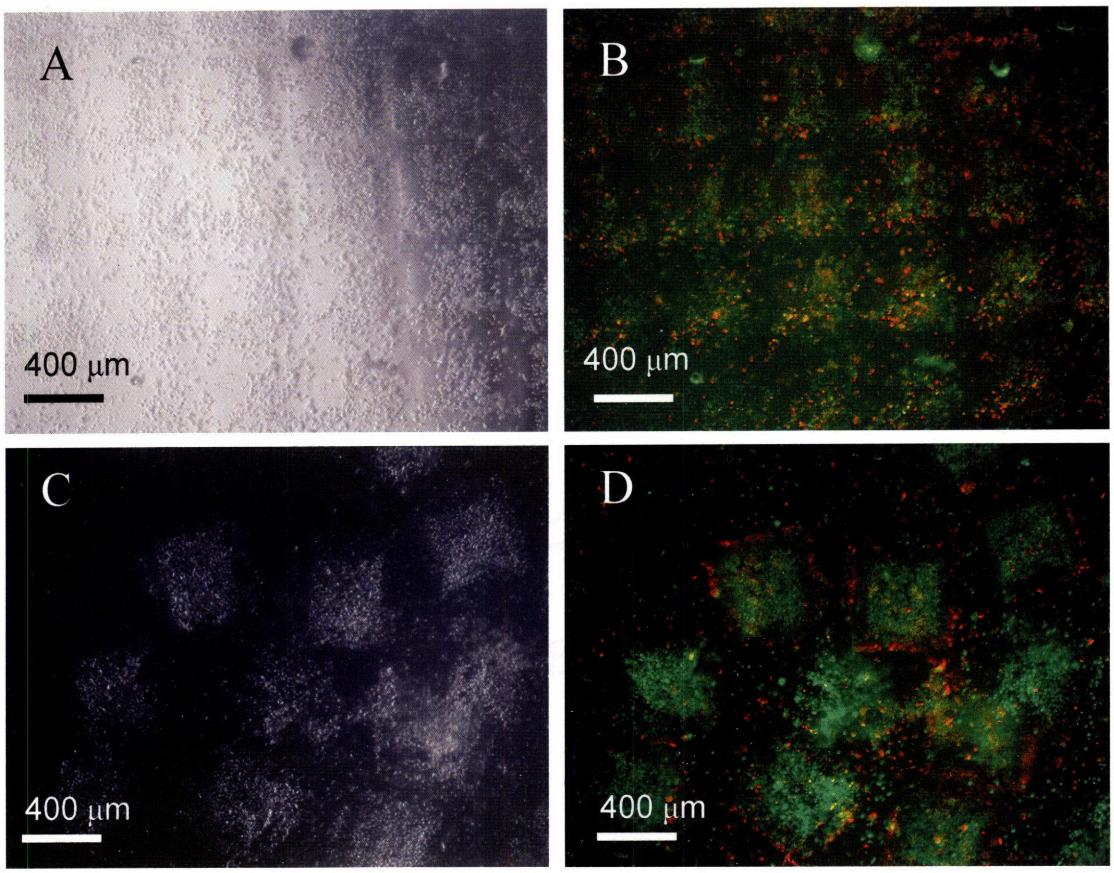

Figure 3.5: Harvesting microstructures. Removal of the PDMS coverslide following UV exposure yields (A) a uniform array of HA microstructures with cells encapsulated within. Subsequent hydration (C) allows these microstructures to be dislodged and suspended in solution. Viability stains (B, D) indicate >85% (n = 3) cell viability.

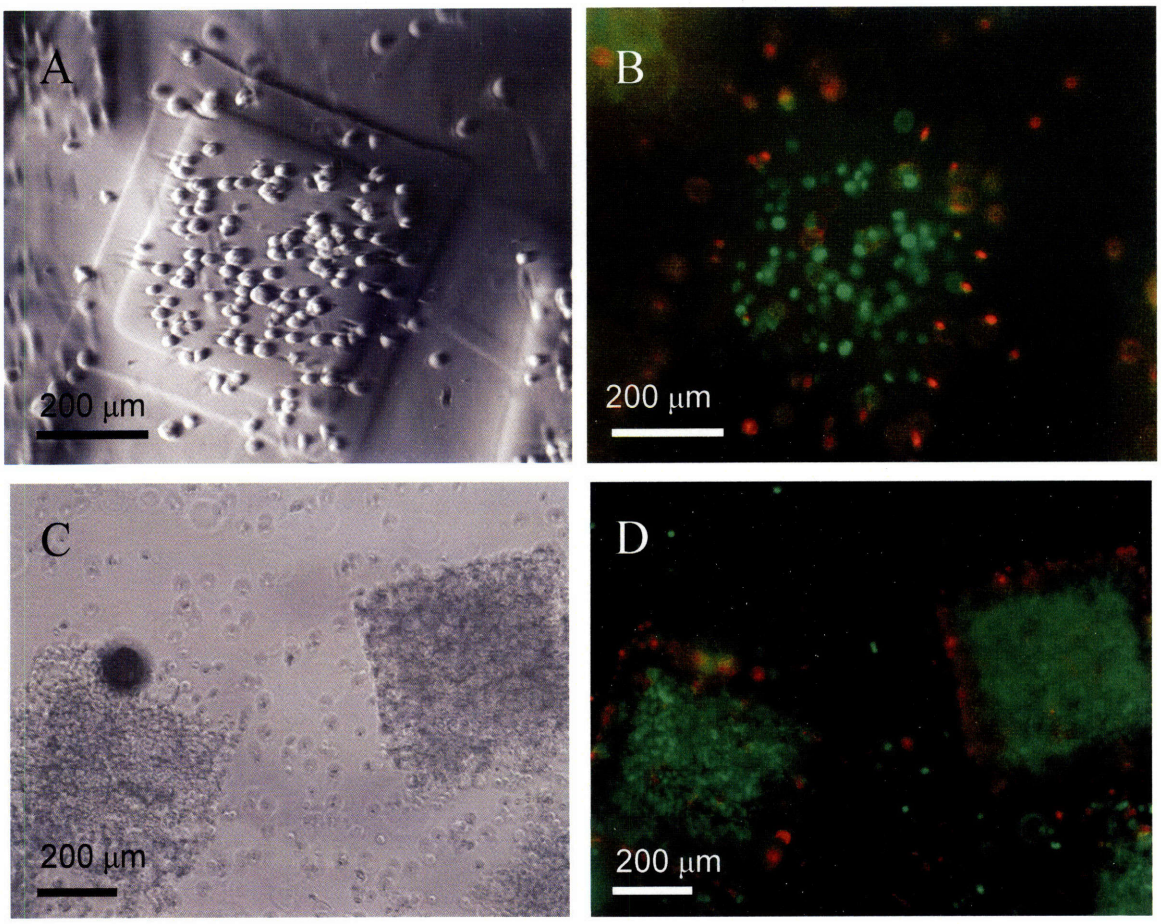

Figure 3.6: Variation in cell density. Cell density in microstructures can be controlled. Variations shown range from (A,B) 5×10^7 cells/ml to (C,D) 20×10^7 cells/ml MeHA prepolymer solution. Viability stains (B, D) show >85% (n = 3) viability. Light micrographs (A,C) were taken at different phases and so the images look different. The appearance of cells in A as outside of the microstructures is a function of the optical phase used; the cells were determined to be embedded within the microstructures by verifying the motion of cells in registration with the microstructures when jostled with a micromanipulator. The focus was slightly adjusted between C and D to produce sharper images so not all cells visible in C are visible in D.

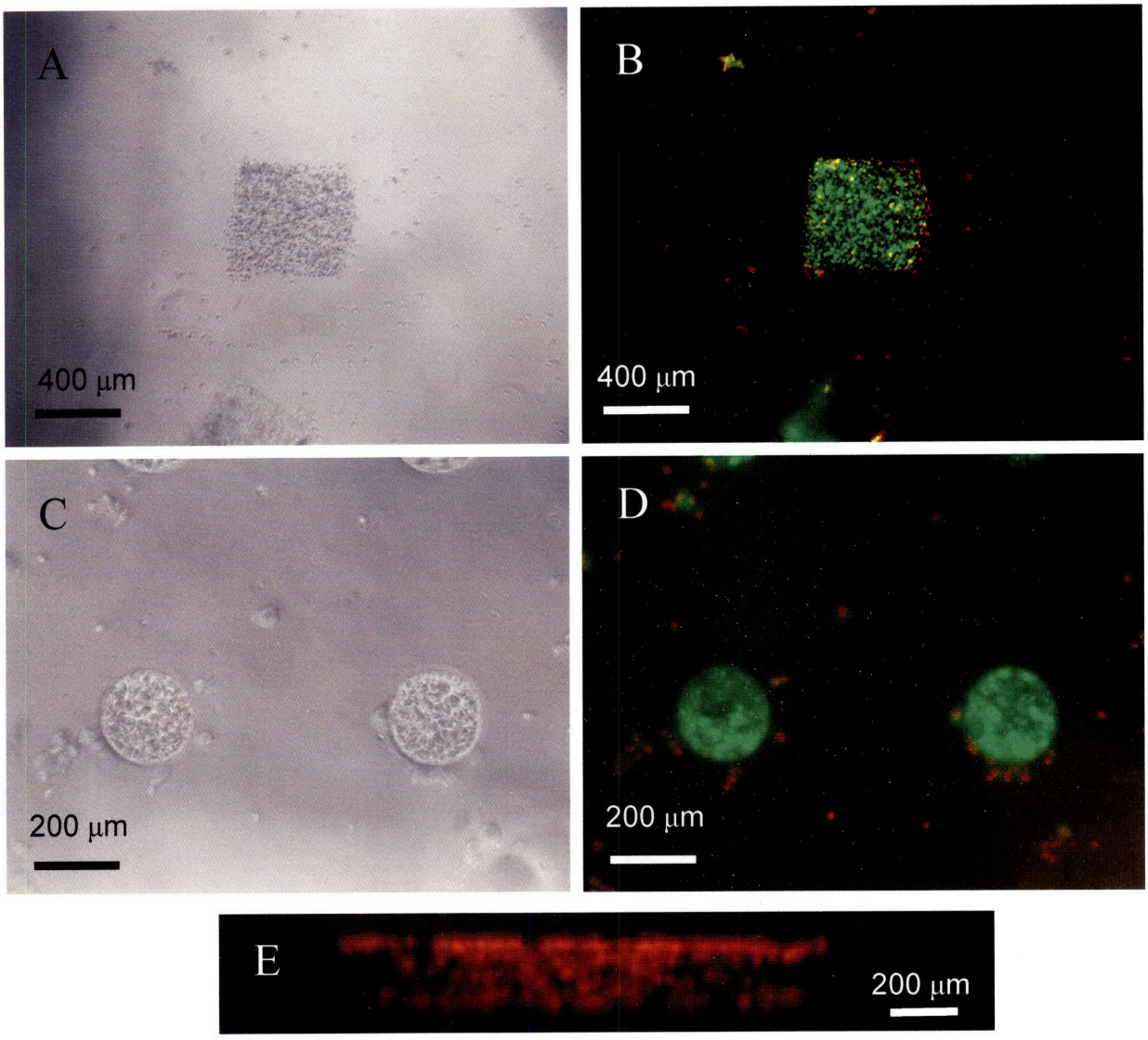

Figure 3.7: Cell encapsulation, viability, and distribution. Cells were encapsulated in (A) MeHA and (C) PEGDA microstructures and stained with viability markers (B, D). (E) Confocal imaging shows some inhomogeneity in the lateral portions (rhodamine-stained) throughout the depth of one MeHA microstructure.

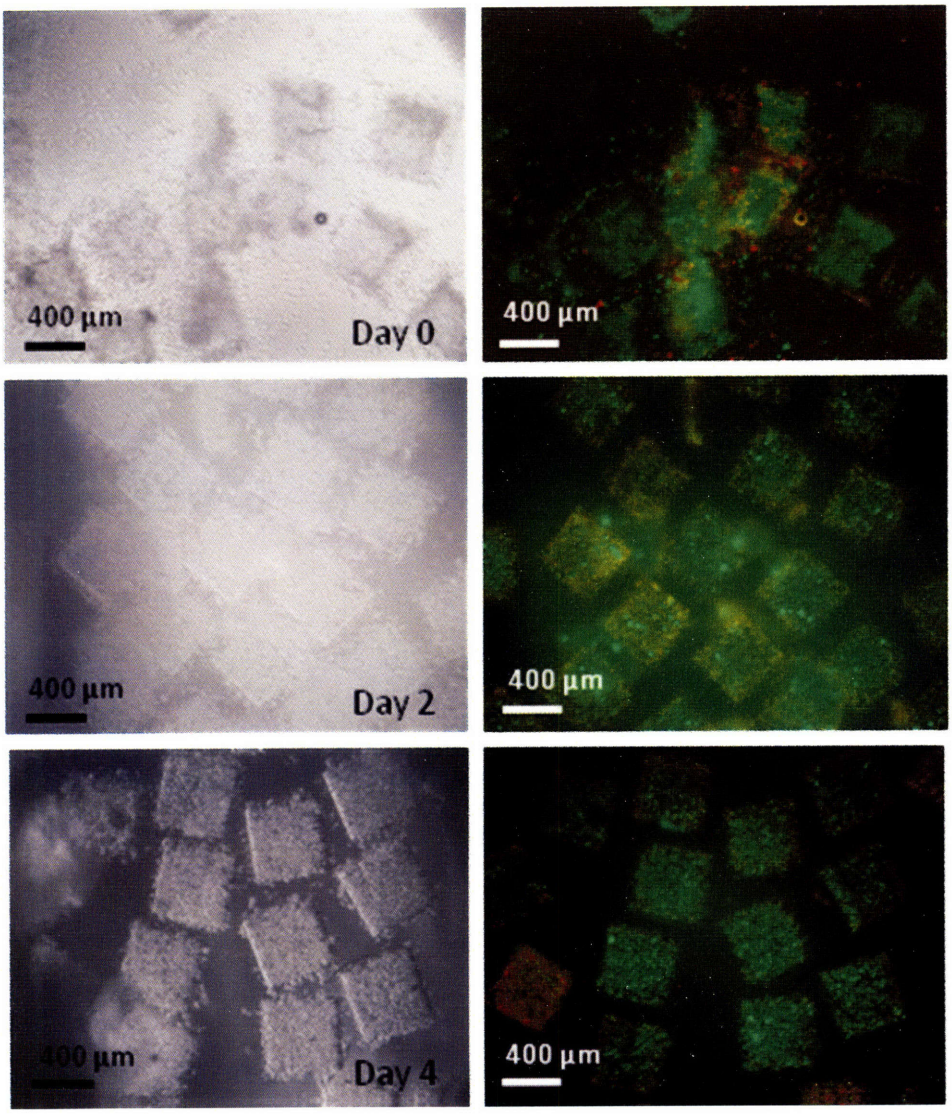

Figure 3.8: Cell viability over 4 days. These representative live/dead stained and corresponding light microscope images of cell-loaded microstructures show the maintenance of cell viability >85% (n = 9) for up to 4 days.

3.3 Discussion

3.3.1 Microstructure Fabrication

In comparison to previous methods for producing microscale hydrogels (limited to spheres), the advantage of a soft lithographic fabrication technique is that it can be used to produce free microstructures of virtually any planar shape and fixed height as long as the desired pattern can be fabricated in the PDMS molds. Figure 3.3 demonstrates this ability to generate different shapes (square hexahedrons, cylinders, rectangular hexahedrons) using different materials (MeHA, PEGDA).

It has previously been shown in quantitative characterizations that macromer concentration can significantly alter hydrogel properties such as swelling and elasticity[52]. We did not replicate these analyses but did qualitatively observe this swelling property (as well as assess it quantitatively for 10% MeHA) in our own experiments. We further expected and observed that the mechanical robustness of the microstructures increased with increasing macromer concentrations: mechanical stimulation of MeHA microstructures of low macromer concentrations tended to fragment them into debris while stimulation of microstructures of higher macromer concentrations had no apparent effect. Since the material properties of hydrogels are well-characterized in the literature we chose to focus more on a biocompatibility parameter—cell viability.

3.3.2 Characterization of Initial Cell Viability

It has previously been shown that increasing photoinitiator concentration, UV exposure length, and macromer concentration negatively impacts the viability of cells encapsulated within PEGDA and other photopolymerized hydrogels[52,97,98]. This was found to be the case in thin layers of photopolymerized MeHA (Figure 3.4). Based on these results, parameters of 5% MeHA, 1% photoinitiator, and 60 s UV-exposure was determined, of the parameters tested, to be most satisfactory for maintaining cell viability within thin hydrogel films. This was in line with our expectation, based on past work[52], that lower macromer concentrations, lower photoinitiator concentration, and shorter UV exposure lengths would increase cell viability. Although even lower parameter values would likely have further increased cell viability, it was observed that further lowering any of these three parameters resulted in noticeable debris formation upon photopolymerization. Though a thin-layer may not be a perfect model for the viability of cells loaded within microstructures, it was useful for screening parameters.

3.3.3 Cell Encapsulation within Microstructures

A number of difficulties in realizing the ability to harvest free cell-laden MeHA microstructures in solution (Figure 3.5) were encountered that were not experienced in harvesting cell-free microstructures. Using PDMS molds in which the microwells accounted for ~25% of the planar area, the fabrication of microstructures was plagued by formation of a thin film between the PDMS coverslide and the PDMS pattern upon photopolymerization of the prepolymer/cell mixture. This film interfered with the harvesting of individual microstructures as the particles were attached to the thin film.

This phenomenon transpired presumably as a result of cells (which did not fall into the molds) being sandwiched between the coverslide and non-well areas of the pattern pieces, thereby preventing complete sealing between the coverslide and pattern. It was minimized by using PDMS patterns with smaller spacing (~70% of the planar area) between the negative features such that the cells could more easily be displaced to the microwells and decreased the likelihood that a cell would be sandwiched between the coverslide and the non-well areas of the pattern pieces. In addition, the PDMS coverslip was maintained in a hydrophobic state to maximize dewetting of the solution from the surface and thus minimize the formation of thin films between microstructures. In the future the problem may also potentially be overcome by utilizing microwell patterns with hydrophobic surfaces and hydrophilic wells. An additional complication of generating photopolymerized cell-loaded microstructures versus cell-free microstructures was the added viscosity of prepolymer solution in which cells are suspended. This additional viscosity is believed to be responsible for the difficulties encountered in making cell-loaded microstructures smaller than 400 μm. Using PDMS molds with microwells that were smaller than 400 μm (as low as 50 μm), it was found that gels of the proper shape and size rarely formed; it appeared post-photopolymerization that the cell/prepolymer solution did not properly fill the wells and that the wells were instead filled with air bubbles. In contrast, cell-free microstructures formed adequately under the same macromer concentration, photoinitiator concentration, and UV duration parameters within PDMS micropatterns of features as low as 50 μm in diameter.

The parameter values (5% MeHA, 1% photoinitiator, 60 s UV exposure) found to be most satisfactory for producing cell viable hydrogels with the thin-layer model produced a noticeable quantity of debris when used to generate cell-laden microstructures. This was visibly observed during experimentation to be a result of the physical stimulation (the microstructures were pushed around with a micromanipulator to verify that they were untethered) required to harvest free microstructures which was not required to produce thin-layers of hydrogel. In the end, parameter values of 10% MeHA macromer concentration, 1% photoinitiator, and 45 s UV exposure duration were found to be acceptable for maintaining both cell viability and microstructure stability.

Our finding that initial viability with differing encapsulated cell densities (Figure 3.6) remained relatively stable (>85%) was in line with expectations. However, longer term viability may differ with respect to cell density if diffusion mediated nutrient/waste exchange becomes limited. In these scenarios, the size of the microstructures would also be expected to affect the capacity of diffusion-reliant processes to maintain cell viability. In the future it may be useful to model as well as experimentally assess diffusion-limited cell death. Diffusion-limited death does not appear to be relevant for the cell-laden 400 μm (50 μm thick) square hexahedrons (Figure 3.8) used here, as there appears on the fourth day to be no more cell death in the middle than near the periphery. Note that the red cells in Figures 3.5-3.8 located around periphery of the microstructures are believed to be adhered to the surface rather than embedded within the surface layers of the microstructure since they were found to be mobile and detachable from the surface upon physical contact with a micromanipulator.

Two phenomena remain unexplained which future work may aim to address. One is the issue of cell distribution homogeneity within cell-laden microstructures. The fluorescently stained cells in Figure 3.7 were qualitatively assessed to have fairly uniform distributions with the exception of the confocal-produced side view (Figure 3.7E). It is unclear from the data collected whether this is real and reproducible. The second phenomenon is the existence of occassional microstructures exhibiting much lower viability values than the majority of the other microstructures (lower right, Figure 3.8). It may be of value in the future to determine whether this is reproducible, and if so, to identify the cause so as to minimize these occurrences.

Taking a step beyond easy retrieval, microstructures generated using the photocrosslinking technique were arranged into specific configurations. A representative example is an alternating checkerboard pattern (Figure 3.9) assembled from fluorescently red- and green-stained cells in separate sets of microstructures. This was performed by physically directing individual microstructures into the pattern using a micromanipulator. Although this operation was time-consuming due to difficulties encountered in manipulating individual microstructures and unfeasible for bottom-up tissue engineering, the successful ordered arrangement of shape-specific components containing different cell types may be beneficial for generating cellular structures with controlled 3D structures *in vitro*.

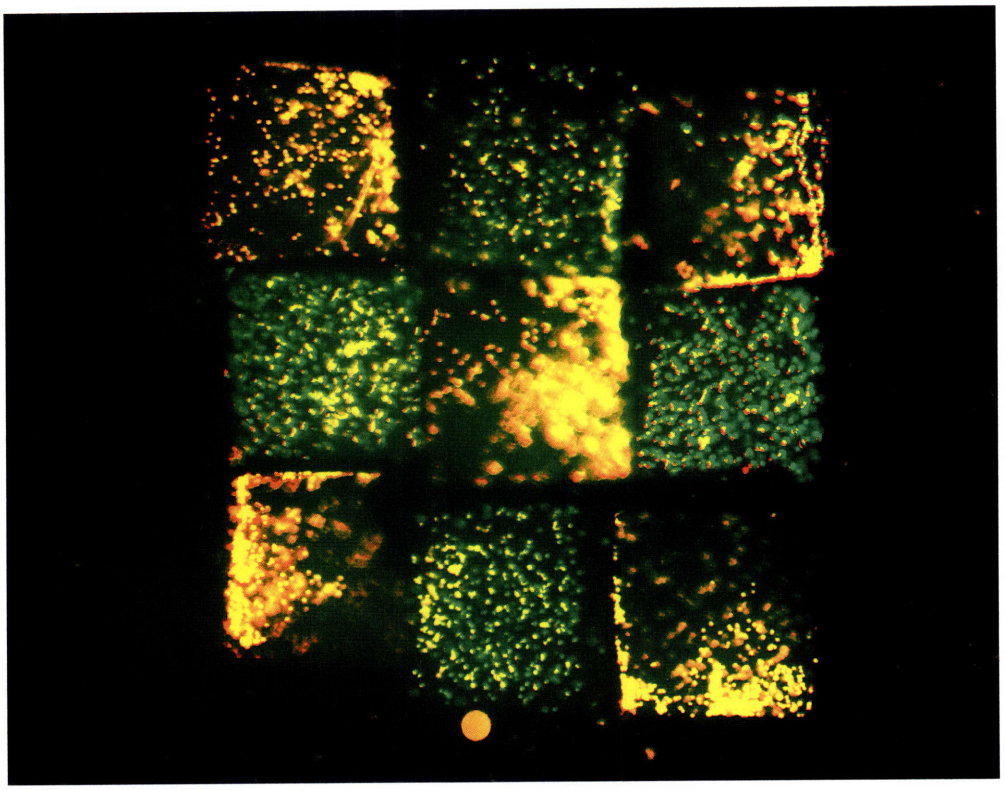

Figure 3.9: Microstructure arrangement and assembly. PKH26 (red) and CFSE (green) stained cells were encapsulated in separate MeHA microstructures and subsequently arranged in an alternating checkerboard pattern.

3.4 Conclusion

This work was originally undertaken as a general proof-of-principle of a technique for which bottom-up tissue engineering was but one of multiple potential applications. As such, we showed that it is possible to produce MeHA and PEGDA microstructures of controlled size and shape with initial cell viabilities >85%. In the future, materials which polymerize through alternative chemistries that do not require UV exposure such as 450 nm visible light[97] may be beneficial for enhancing cell viability. We recognize that the utilization this technique for bottom-up tissue engineering would necessitate more rigorous and thorough characterizations than we have performed here of important properties like reproduction fidelity, elasticity/plasticity as a function of cell density, and cell viability as functions of cell type or microstructure size. Nonetheless, this work lays out a facile technique for producing photocrosslinkable shape- and size-controlled microstructures as well as identifying the important processing difficulties and considerations that should be taken into account in future work. As such, micromolding through UV photocrosslinking may potentially be a useful and important component in a bottom-up tissue engineering strategy.

Chapter 4

Chemically Crosslinked Microstructures

The rapid crosslinking of hydrogel materials such as alginate which polymerize through the addition of a secondary soluble factor (which we refer to as 'chemically crosslinkable') requires a modification to the micromolding approach utilized for ultraviolet (UV) light photopolymerizable hydrogels. The technique discussed in Chapter 3 involves initiating the crosslinking reaction (UV exposure) after the liquid prepolymer has already been molded. Similarly for chemically crosslinked hydrogels, it is necessary to introduce the crosslinking agent after molding so as to avoid producing masses of partially crosslinked hydrogel that obstruct the molding process. This may be facilitated by the use of a (crosslinking) agent-delivering agarose mold. By pre-loading the crosslinking agent within the mold itself, the liquid prepolymer hydrogel can be crosslinked post-molding by the diffusion of the agent out of the mold. To demonstrate the efficacy of this controlled-release technique we focused on generating alginate microstructures which polymerize with the addition of divalent calcium ions (schematically illustrated in Figure 4.1). We furthermore verify its applicability by producing alternate structures (such as patterned membrane) and using alternate materials (pH-modulated chitosan).

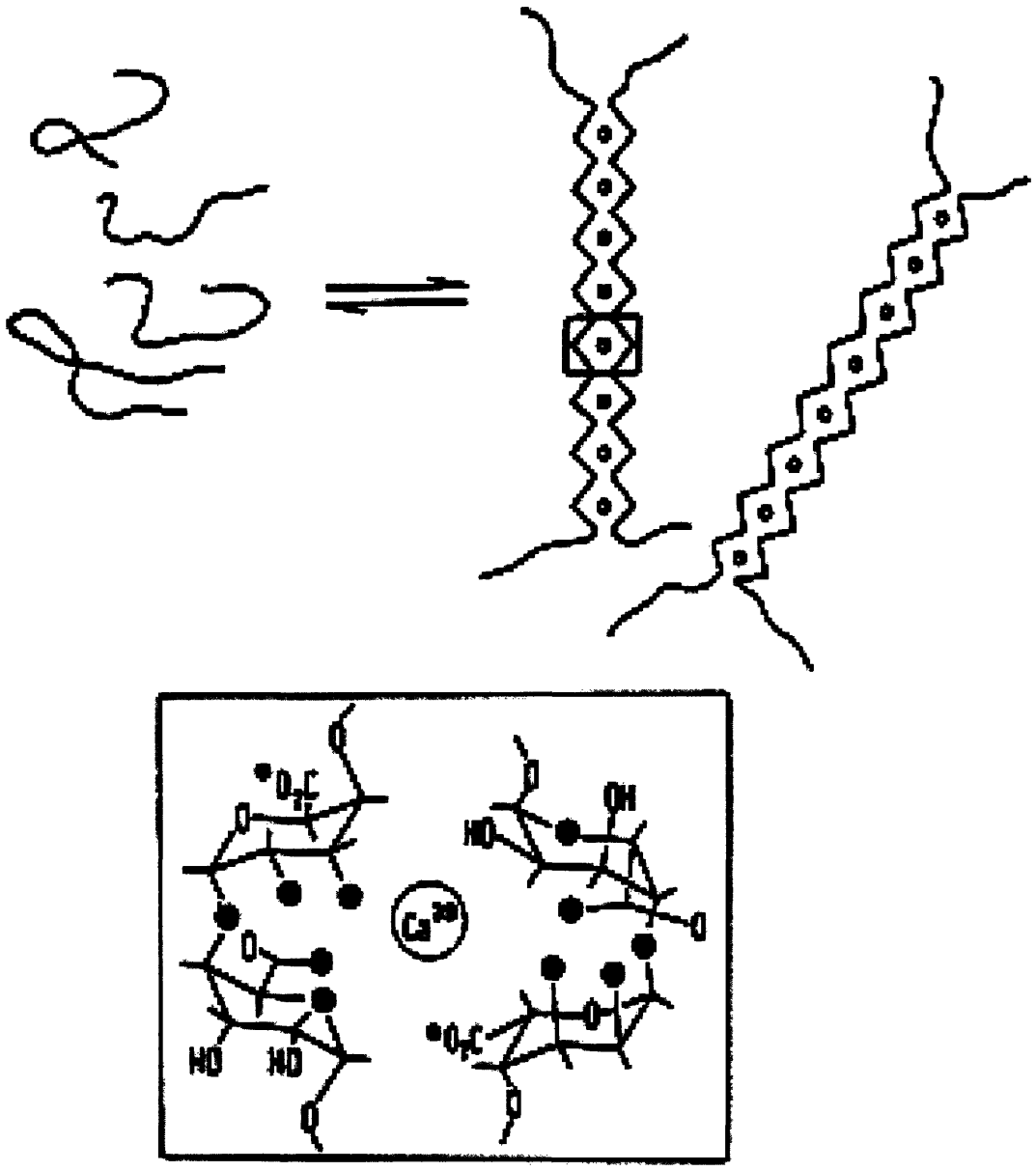

Figure 4.1: Photopolymerization of calcium alginate. Alginate consists of linear chains of alternating (1-4)-linked ß-D-mannuronate (M) and C-5 epimer α-L-guluronate (G) blocks which can be stably crosslinked by divalent cations such as calcium. Since crosslinking occurs at the G-blocks the relative number of G- and M-blocks dictate the structural characteristics of crosslinked alginate networks.

The goal of this work is similar to Chapter 3 in that we intended to demonstrate a controlled-release approach could feasibly generate free shape- and size-controlled microstructures. While the processing requirements of the materials used in this work (calcium alginate, chitosan) were essential in driving the motivation behind developing this technique, the specific biological and mechanical properties were only dealt with peripherally. This work was intended as a proof-of-principle[d] of a controlled-release technique for producing microstructures and microfeatures that could be used in any number of applications (and so patterned membranes are also demonstrated). We fully recognize that specific future applications such as bottom-up tissue engineering would require more rigorous and comprehensive assessments of the biological and mechanical properties of shape- and size-controlled microstructures. However, such characterizations were considered beyond the scope of this particular work. Nonetheless, most of the work was performed used calcium alginate (with only a brief demonstration of producing chitosan microstructures) because it is commonly used in tissue engineering[43,99-101], drug delivery[102-104], immunoisolation[105-107], and cell encapsulation[108,109] applications. Indeed, it has been shown to be stable over long periods of time *in vivo* in both animals and humans[110]. We have here assessed processing parameters (crosslinker and macromer concentration) for their effects on gelation time and initial cell viability in a particular (calcium alginate) model system. However, this controlled-release technique may potentially be used with other similar chemically crosslinked materials.

[d] Please note this work was carried out for publication as a 2-page Communication. The relative lack of characterization data reflects this.

4.1 Materials and Methods

4.1.1 Cell Culture

All cells were manipulated under sterile tissue culture hoods and maintained in a 95% air/5% CO_2 humidified incubator at 37°C. NIH-3T3 mouse embryonic fibroblast cells were maintained in Dulbecco's modified Eagle media (DMEM) supplemented with 10% FBS. Confluent dishes of NIH-3T3 cells were passaged and fed every 3-4 days. Murine embryonic stem (mES) cells (R1 strain) were maintained on gelatin treated dishes with media comprised of 15% ES qualified FBS in DMEM knockout medium. ES cells were fed daily and passaged every 3 days at a subculture ratio of 1:4. AML12 murine hepatocytes were maintained in a medium comprised 90% of 1:1 (v/v) mixture of DMEM and Ham's F12 medium with 10% FBS. Confluent dishes of AML12 cells were passaged and fed every 3-4 days.

4.1.2 Prepolymer Solutions

Alginate hydrogel precursor was prepared by dissolving alginic acid (Sigma) in cell-culture media prepared as described above, or in ddH_2O to obtain the desired final concentration (1% w/v, 1.5% w/v, 2% w/v, 3% w/v, 4%w/v) at 37°C. For the preparation of fluorescently-labeled alginate hydrogels, rhodamine (Sigma) or fluorescein isothiocynate conjugated to bovine serum albumin (FITC-BSA, from Sigma) were dissolved in ddH_2O to obtain a concentration of 200μg/ml prior to addition of the alginic acid. Chitosan hydrogel precursor was prepared by dissolving 2% w/v chitosan (practical grade from crab shells, Sigma) in a pH 5.7 solution of hydrochloric acid (Fisher Scientific) diluted in ddH_2O

4.1.3 Poly(dimethylsiloxane) (PDMS) Mold Fabrication

PDMS micropatterns of various shapes were fabricated by curing prepolymer (Sylgard 184, Essex Chemical) on silicon masters patterned with SU-8 photoresist. The patterns on the masters had shapes in relief (squares, circles, long rectangles) of various sizes (ranging from 20 to 400 μm) as well as in depth, so that molds with both wells and protruding features could be produced. PDMS patterns were generated by pouring 1:10 curing agent to silicon elastomer onto the master and curing for 2 h at 70°C. Finally, the PDMS patterns were peeled from the silicon masters, and cut into small rectangular shapes. Before molding, the PDMS patterns were rendered hydrophilic by plasma cleaning for 10 minutes on medium power (PDC-001, Harrick Scientific).

4.1.4 Agarose Mold Fabrication.

Agarose replicas were molded by pouring molten agarose on positive and negative SU-8 patterned silicon masters, as well as on flat surfaces to create patterned and flat molds, respectively. Agarose solutions were generated by heating 4% w/w agarose (Aldrich) in ddH_2O until dissolved. For use with the alginate hydrogel precursor, $CaCl_2$ (Sigma) was added to the molten agarose to obtain a final concentration of 10mM, 50mM, 100mM, 200mM or 500mM. For use with chitosan hydrogel precursor, the agarose mold was removed from the SU-8 master, allowed to dry at room temperature overnight, and hydrated in a bath of 5% NaOH (Sigma) in ddH_2O for 5-6 hrs before use.

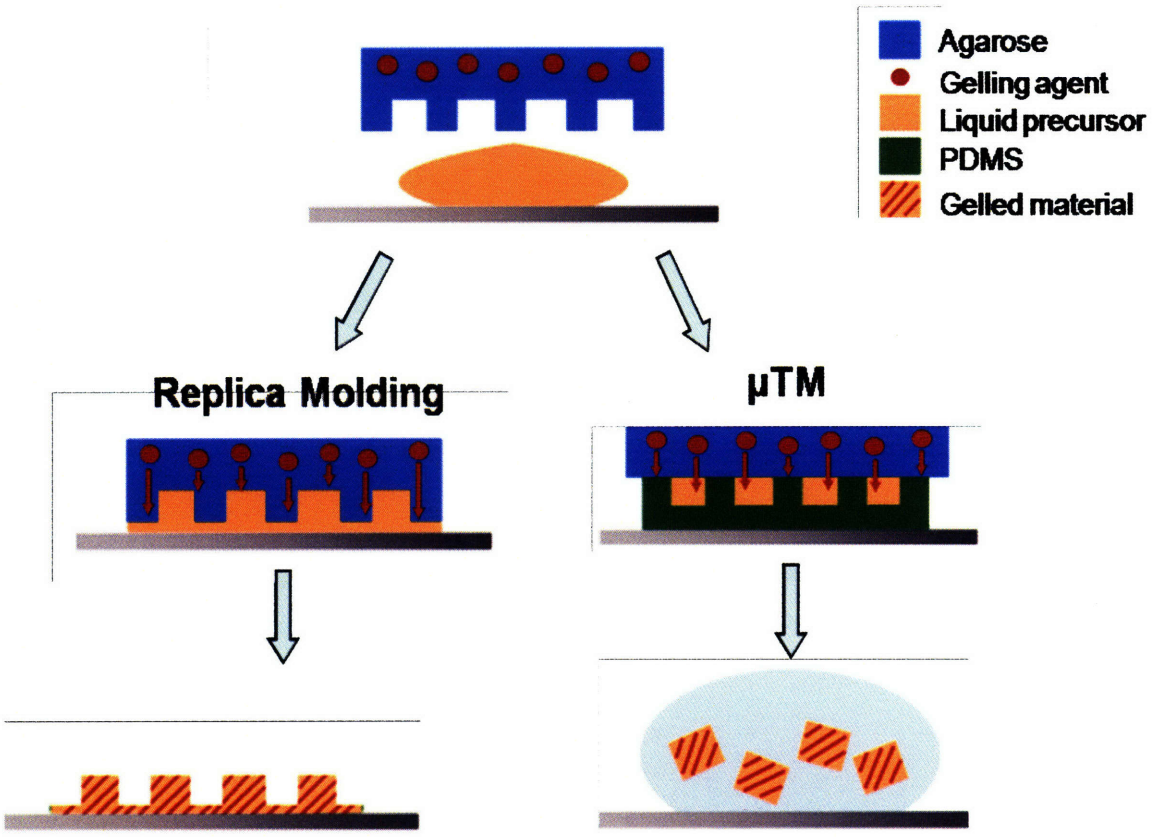

Figure 4.2: Schematic of controlled release crosslinking technique. Replica molding can be used to produce patterned membranes while microtransfer molding may be used to generate free shape- and size-controlled microstructures. Note that the primary difference between the two techniques is whether the crosslinker-loaded agarose is the molded or flat piece.

4.1.5 Cell Encapsulation

For encapsulation experiments, cells were trypsinized with 0.23% trypsin and 0.13% ethylenediaminetetraacetic acid (EDTA) in PBS (Gibco) and then centrifuged at 1000 rpm for 2 min to produce a cell pellet. The pellet was then resuspended in the prepolymer solution at 8 x 10^6 cells/ml (this choice was arbitrary—we intended only to show cells encapsulated within the hydrogels).

4.1.6 Replica Molding and Micro-Transfer Molding (μTM)

Replica molding was used to produce micropatterned hydrogel membranes. The hydrogel precursor was poured on top of a flat substrate, and an agarose mold containing the gelling agent was applied directly to the liquid hydrogel precursor. To produce the structures seen in Figure 4.6B, replica molding was used to produce PKH-26 (Sigma) stained AML-12 cells loaded within patterned membranes. Cell-tracker blue (Invitrogen) stained mES cells were then deposited atop the patterned membranes with excess cells (outside of the wells) gently scraped away using a coverslide To produce the structures seen in Figure 4.6C, a FITC-loaded (10% w/w in alginate precursor) membrane was first produced using replica molding. A secondary rhodamine-loaded (10% w/w) precursor was then molded (gelled for 4 min) atop of the membrane using a flat agarose slab containing the gelling agent. Micro-transfer molding (μTM) was employed to obtain free microstructures. A thin layer of hydrogel precursor was coated over the PDMS mold; after briefly (~30s) degassing in a vacuum chamber (PDC-001, Harrick Scientific) and scraping away excess material, the agarose slab containing the gelling agent was pressed

against the mold. This procedure was required to overcome the weak seal formed between PDMS and agarose, which otherwise led to the formation of a continuous film.

4.1.7 Harvesting of Free Microparticles

After gelling, the agarose slab was removed to retrieve the free microstructures. In this process, most pieces remained attached to the microwells. After hydrating the microstructures upon the mold, a number of individual pieces spontaneously detached from the microwells. To remove any remaining pieces, a pipette tip was gently brushed over the surface the mold.

4.1.8 Imaging and Analysis

Phase contrast and fluorescent images were taken on a Nikon TE2000 fluroescent microscope. Cell viability within the microstructures was assessed using live/dead stain. The microstructures were stained with 200 μl PBS solution containing 2 μg/ml calcein AM and 4 μg/ml ethidium homodimer-1 (Molecular Probes) and visualized under fluorescein isothiocynate (FITC) and tetramethyl rhodamine iso-thiocyanate (TRITC) filters. Two recognized parameters of cell viability – intracellular esterase activity and plasma membrane integrity – were tracked. Live cells fluoresced green, showing intracellular esterase activity that hydrolyzed the fluorogenic esterase substrate (calcein AM) to a green fluorescent product, and dead cells fluoresced red, their plasma membrane being compromised and therefore permeable to the high-affinity, red fluorescent nucleic acid stain (ethidium homodimer-1). Co-cultured cells were labeled

using PKH26 (Sigma) and CellTracker Blue (Invitrogen) dyes, and processed according to the manufacturer specifications.

4.1.9 Cell Viability Measurements

To assess the effects of the fabrication process on encapsulated NIH-3T3 cell viability, cells were suspended in 4% w/v alginate precursor solutions and molded into micropatterned membranes. Percent viability values were calculated by counting the number of live (green) cells and the number of dead (red) cells in a representative 1500μm × 1000μm rectangular area magnified at 4X and dividing the number of live cells by the number of total cells (live plus dead). Measurements were taken in quadruplicate, and error bars were based on standard deviation values for n=4.

4.2 Results

4.2.1 Cell-Free Microstructures

As shown in Figure 4.3, 4% w/v calcium alginate (Figure 4.3A, 4.3B) and 2% w/v chitosan (Figure 4.3C, 4.3D) could be polymerized for 4 min to generate patterned membranes as well as shape- and size-controlled microstructures as small as tens of microns. These representative structures exhibit roughly (qualitatively) sharp corners with what appear to be minor imperfections along the edges of the microstructures (Figure 4.3B, 4.3D).

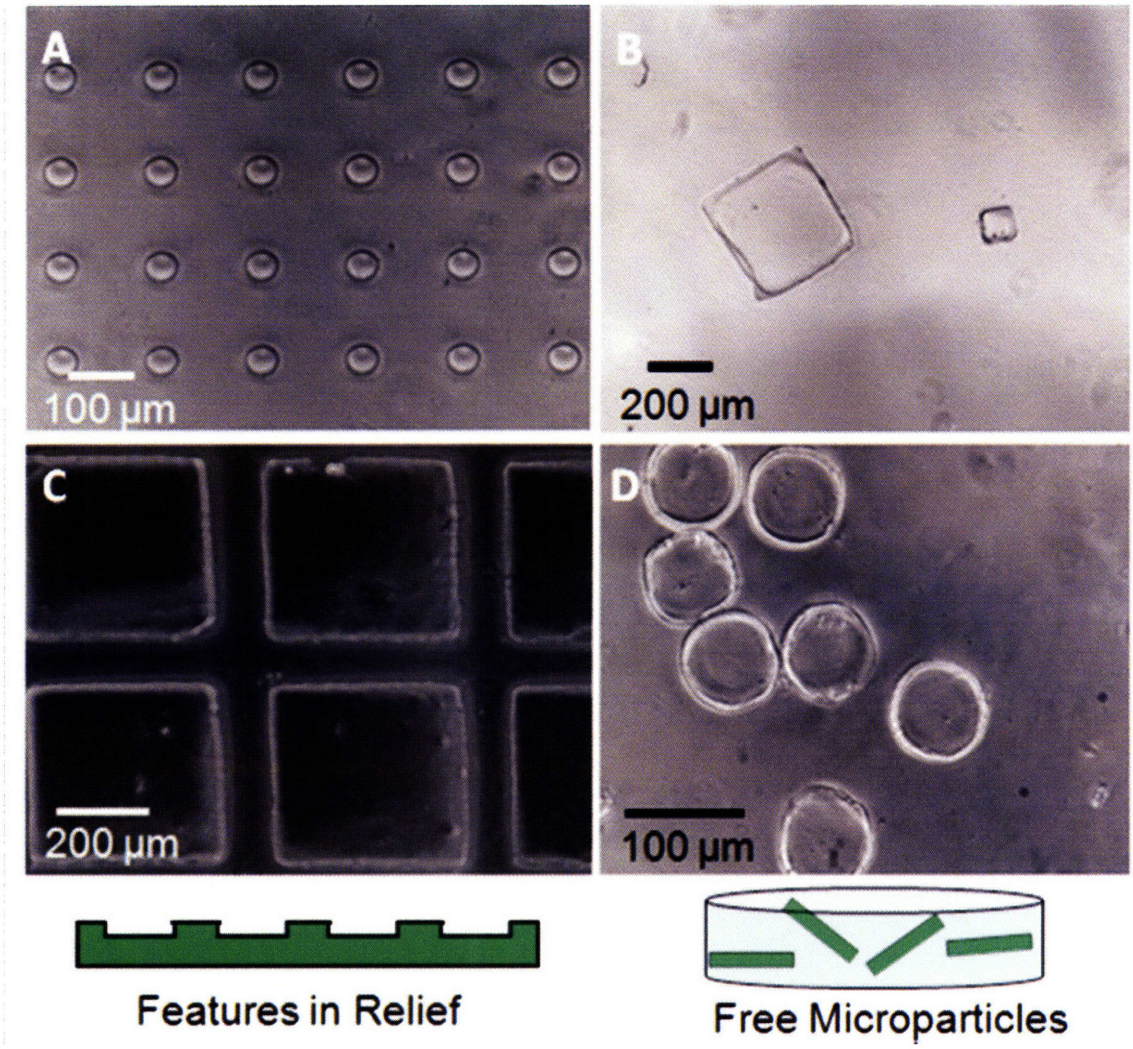

Figure 4.3: Photomicrographs of free microstructures and patterned membranes. Replica molding generated patterned (A) calcium alginate and (C) chitosan membranes with features in relief while µTM generated (B) calcium alginate and (D) chitosan microstructures.

4.2.2 Polymerization Properties

We investigated the effect of alginate concentration in the hydrogel precursor as well as agarose and calcium chloride concentration in the mold on the polymerization properties of the microstructures (Figure 4.4). Increases in both alginate precursor concentration and agarose Ca^{2+} concentration are shown to vary inversely with the time required to form mechanically stable structures.

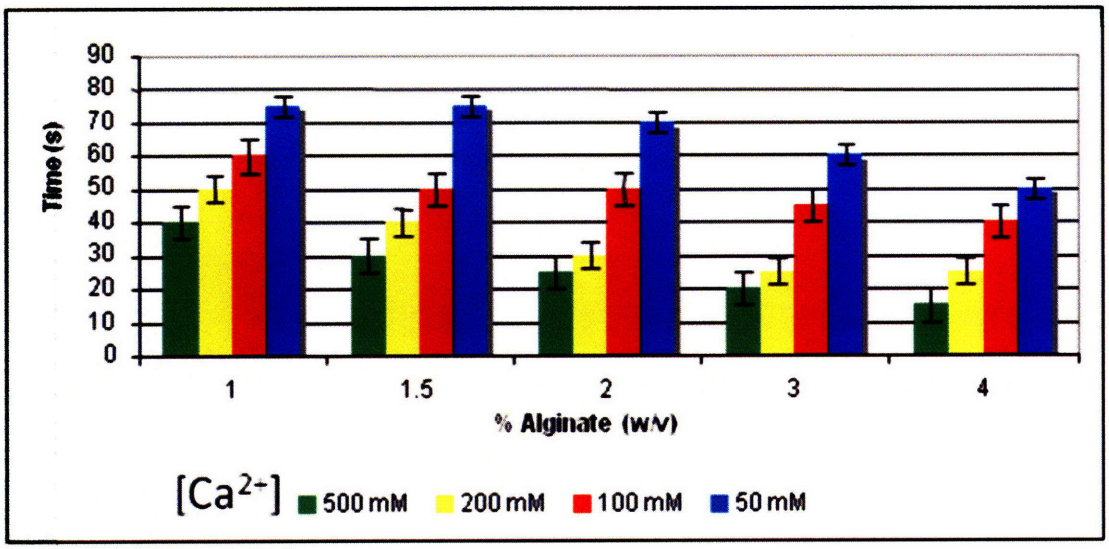

Figure 4.4: Polymerization time as a function of alginate concentration. The data shows the time required to achieve complete gelation using replica molding under varying alginate and $CaCl_2$ concentrations. In general, higher calcium and alginate concentrations facilitate shorter gelation times.

4.2.3 Initial Cell Viability

Initial cell viability (Figure 4.5) measurements were made with a fixed alginate concentration of 4%. This data indicates uniformly high cell viabilities for the parameter ranges tested with the exception of 500 mM calcium for 2.5 minutes.

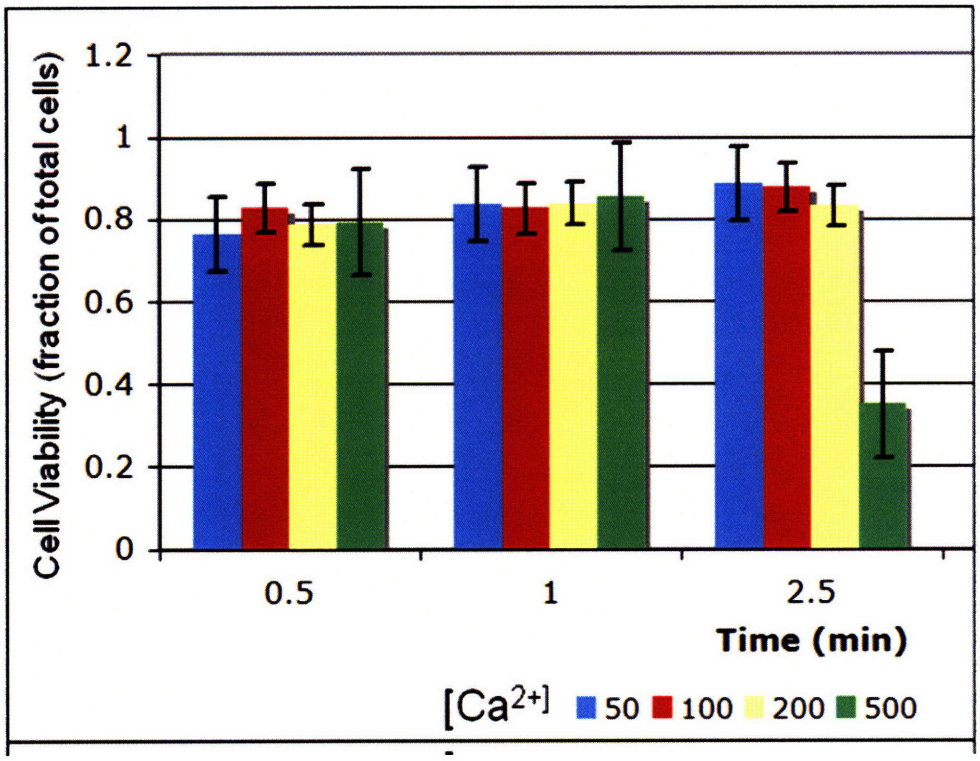

Figure 4.5: Cell viability as a function of calcium concentration and gelation time. Initial encapsulation viability of NIH-3T3 in 4% alginate w/v under varying $CaCl_2$ concentrations and molding times. With the exception of the 500 mM / 2.5 min data point, cell viability remains relatively uniform at ~80%.

4.2.4 Cell- and Soluble Factor-Laden Microstructures

To illustrate the potential utilization of this controlled release technique for producing cell-laden shape- and size-controlled microstructures, cells were encapsulated in rectangular hexahedron microparticles (Figure 4.6A). Though considered outside of the scope of this work, it was qualitatively observed that the mechanical properties of the microstructures appeared to vary with the precursor concentration. The ability to produce various other structures (not relevant to bottom-up tissue engineering) is demonstrated using the controlled-release technique as well. In Figure 4.6B, the potential use of cell-laden micromolded hydrogels to control cell-cell interactions *in vitro* is shown. Here, Cell-Tracker Blue stained mouse embryonic stem cells (blue) were seeded within microwells formed from alginate hydrogels embedded with PKH26 stained AML12 hepatocytes (red). To produce the structures seen in Figure 4.6C, the controlled-release technique was used to produce multilayered soluble factor-loaded hydrogel constructs by sequential molding of hydrogels. Finally, free alginate microstructures containing a fluorescence FITC-BSA marker are shown in Figure 4.6D.

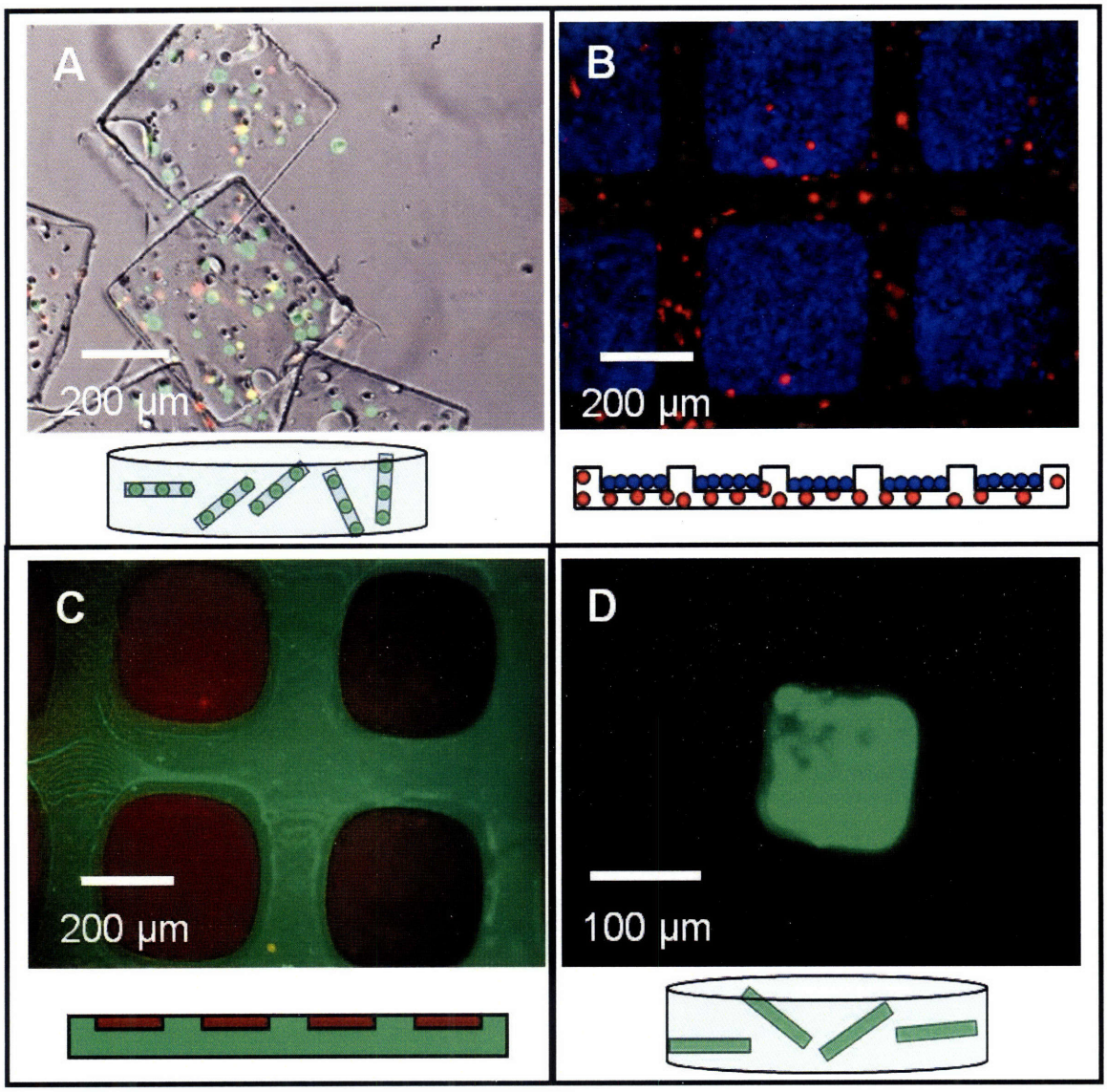

Figure 4.6. Fluorescent images of various microstructures. (A) Micrograph of NIH-3T3 cell-laden microparticles overlayed with live/dead staining (green/red, respectively). The yellow represents a cell which stained both green and red; yellow presumably indicates that a cell that was initially alive died before imaging. (B) Co-culture of AML12 cells, stained with PKH26 (red) and mES cells, stained with CellTracker Blue. AML12 cells were encapsulated within the alginate membrane, while mES cells were seeded within wells. (C) Composite structures of FITC (green) and rhodamine (red) loaded alginates and (D) alginate microparticle loaded with FITC-BSA are also shown.

4.3 Discussion

4.3.1 Polymerization Properties

Gelation time was hypothesized to be an important parameter since extremely long durations may not be compatible for maintaining high cell viability in encapsulation applications. Therefore, we measured the minimum time required for the formation of mechanically stable structures (that could be easily handled and spontaneously released from the agarose mold) under each set of conditions. The key conclusion we drew from these results was that gelation time within the range of parameters tested appears well-suited for cell encapsulation. Even the lowest alginate and calcium concentrations tested yielded a gelation time of only 90s (as opposed to many hours).

4.3.2 Initial Cell Viability

From our experiments (Figure 4.4) 90 s was determined to be a reasonable ceiling for gelation time and so our cell viability (Figure 4.5) data range did not extend beyond 2.5 minutes. Integration of data from both figures 4.4 and 4.5 imply that there is a wide parameter range in terms of calcium and alginate concentrations in which it is possible to maintain high cell viabilities. Therefore, these processing conditions should not limit the cell viability of alginate microstructures produced using this controlled-release technique.

4.3.3 Cell- and Soluble Factor-Laden Microstructures

Though Figure 4.6A demonstrates the ability to encapsulate cells within free shape- and size-controlled microstructures, important questions regarding biological performance remain unresolved. Chief among them is viability over time which, due to diffusion limitations, we would expect to vary as a function of the size and shape of the

microstructure. Reproduction fidelity (rough edges in Figure 4.3) and mechanical characteristics as a function of polymer and calcium concentration (not to mention cell density) also remain unexplored.

With the exception of Figure 4.6A, the structures shown in Figure 4.6 are not compatible with bottom up tissue engineering. The original intent of the work was to present the concept of the controlled-release technique and to demonstrate the range of interesting and potentially useful structures that could be produced. As such, the setup in Figure 4.6B was intended to suggest the potential co-culture of one type of cells with another immobilized supporting type, Figure 4.6C novel cell and material patterning applications, and Figure 4.6D drug delivery applications.

4.4 Conclusion

The controlled-release technique represents the second of two methods discussed in this thesis for fabricating shape- and size-controlled microstructures. While in this work we focused on assessing processing conditions for cell-loaded calcium alginate microstructures, the technique we present, based on replica molding or μTM by controlled release of the gelling agent, was also demonstrated with pH dependent chitosan hydrogels. For bottom-up tissue engineering, comprehensive and rigorous biological and mechanical characterization work must be performed on free microstructures. Nonetheless, we believe this controlled-release soft lithographic technique is practical to implement and useful for producing shape- and size-controlled microstructures.

Chapter 5

Cell-Laden Agarose Microfluidics

This chapter discusses the fabrication and characterization of cell-laden agarose microfluidic devices that maintain cell viability through diffusion-based nutrient/waste exchange. In this soft lithographic fabrication technique, cells were suspended in low-temperature molten agarose and molded on an SU-8 patterned silicon wafer to generate channel features. To seal the two pieces of agarose to form microchannels, they were placed on a glass coverslip and heated on a hot plate so as to slightly melt the bonding interfaces. The two slightly melted surfaces were then annealed to one another to form water tight microchannels.

Although microfluidics devices have traditionally been fabricated from dry non-hydrogel polymers[111], agarose is not the first hydrogel to be used for microfluidics. Recently, calcium alginate[75] and gelatin[89] hydrogels were reported. But in these papers, the extent of the biological work was limited to cells seeded on the surface of microchannels. The work documented in this chapter is to our knowledge the first involving the formation of cell-containing microfluidic hydrogels for diffusion-based nutrient/waste exchange.

Agarose is a thermally reversible polysaccharide consisting of alternating copolymers of (1-3)-linked β-D-galactose and (1-4)-linked (3-6)-anhydro-α-L-galactose[61]. It can be induced to melt or gel in a variety of temperatures ranging from 17 °C to 80 °C depending on the molecular weight and chemical modification of side groups. Agarose hydrogels

are commonly used in a variety of biological and biomedical applications and are used ubiquitously in electrophoresis applications[112] for their ability to control the diffusion of biological moieties. Importantly for this work, agarose is amenable for soft lithography [113,114] and can be used to produce micropattern surfaces. In addition, cell encapsulation in agarose has been used for a variety of applications ranging from biosensing to therapeutics [53,115] and agarose has been shown to be biocompatible when implanted *in vivo* [116]. While agarose does not directly provide an active attachment substrate, it can be supplemented with collagen or gelfoam to provide attachment sites for anchorage-dependent cells [61].

The goal of this work was to present a microfluidic technique for facilitating nutrient/waste exchange in macroscale tissue engineering constructs. Agarose has not previously been shown to be useful as a microfluidic material but its physical and biocompatibility properties are extremely well-characterized in the literature[61]. Therefore, we focused in this work on the specifics of its application as a microfluidic biomaterial by showing the diffusion of molecules from the microfluidic channels into the surrounding bulk material as a result of flow through channels. Furthermore, we show that encapsulated cells exhibit a zone of high cell viability (in comparison to controls) around the microchannels after 3 days of continuous flow of media through the microchannel. Because this is the first use of microfluidics for facilitating nutrient/waste exchange for cells in the surrounding bulk material, the work did not aim to provide a full characterization of the system.

5.1 Materials and Methods

5.1.1 Cell Culture

AML-12 murine hepatocytes were kept at 37 °C in a 95% air/5% CO_2 incubator and maintained in 45% Dulbecco's Modified Eagle Media (DMEM), 45% Ham's F12 Media, and 10% Fetal Bovine Serum (FBS). Confluent flasks of AML-12 cells were passaged and fed every 3-4 days.

5.1.2 Agarose Mold Fabrication

Agarose replicas (1 cm thick, so as to provide sufficient mechanical stability to allow handling) were molded by gelling molten agarose solution on the positive microchannel features of SU-8 patterned silicon masters (Figure 5.1). Agarose solutions were generated by heating Low Gelling Temperature Agarose (Type VII-A, Sigma) in Phosphate-Buffered Saline (PBS) until dissolved. For experiments in which cells were embedded within agarose, 6% agarose (autoclaved/sterilized to dissolve in PBS) was allowed to cool to 70 °C and supplemented with equal volume of cell suspension in media (cells at controlled densities) to yield a 3% agarose mixture loaded with cells. The molten agarose-cell mixture was then poured onto the silicon master and allowed to gel for 2 h at 25°C in a sterile tissue culture hood. To form the base of the microchannel, a thin flat slab of agarose was fabricated in a plastic culture dish. The agarose molds were gently peeled from the silicon masters and trimmed to a suitable shape. To make holes for inlets and outlets, a metal feeder wire of ~2 cm in length was used as a guide for insertion of the flexible polyethylene tubing (inner diameter 0.58 mm, outer diameter 0.965 mm,

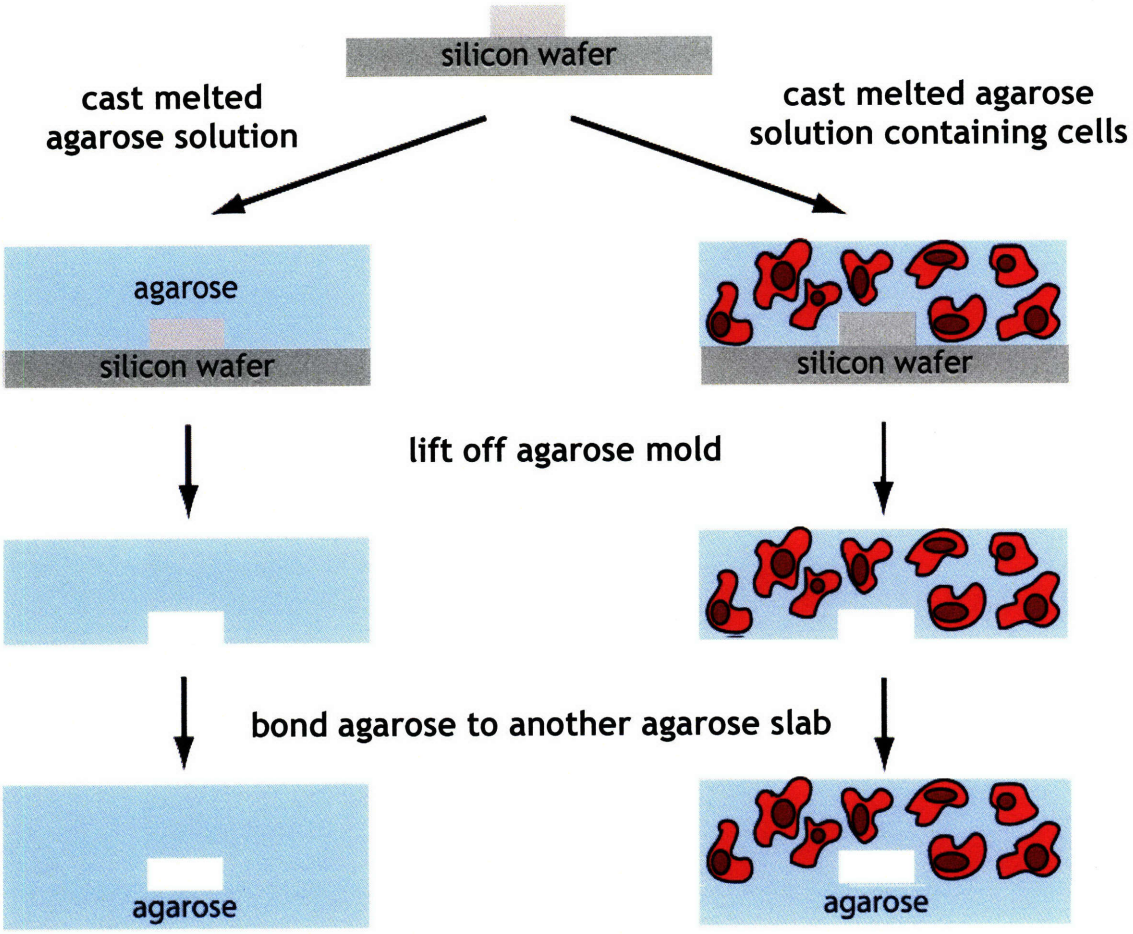

Figure 5.1: Schematic of the fabrication of agarose microfluidic devices with (right) and without (left) embedded cells.

Becton Dickinson). Finally, the agarose molds were heated on glass slides on a hot plate for 3 s at 71 °C and pressed against one another to form sealed microfluidic channels. The device was allowed to cool for 10 min before fluid was introduced into the channel. The processes involving cells were maintained under sterile conditions.

5.1.3 Channel Flow Experiments

To control the flow rate of fluids through the microchannel, the agarose microfluidic device was connected to a syringe pump (AL-1000, World Precision Instruments) via flexible polyethylene tubing. The channel effluent was removed by collection from an outlet tube connected using a procedure similar to that of the inlet tube.

For experiments in which AML-12 hepatocytes were embedded at 2 x 10^6 cells/ml (density given as cells within pre-gelled agarose) in microchannels, medium was pumped through 150 μm deep x 800 μm wide channels at a rate of 10 μl/min. Sterile conditions were maintained throughout the fabrication and operation of the microfluidic device by fabricating and operating the device entirely within a biosafety cabinet. For time dependant studies, the entire apparatus was kept inside a sterilized vessel placed within an incubator at 37 °C and 95% air/5% CO_2.

5.1.4 Sectioning and Analytical Techniques

Channel flow and diffusion were verified by flowing fluorescein isothiocyanate conjugated to bovine serum albumin (FITC-BSA, green fluorescence, excitation/emission = 506/529 nm) through (cross-sectional area) 220 μm x 100 μm microchannels at a rate

of 100 μl/min. To qualitatively assess diffusion into the surrounding agarose, intensity measurements were calculated from fluorescent images taken every minute for 45 min. These fluorescent intensities, which were taken at a fixed distance from the channel boundary using fixed optical and image capture parameters, were then processed. Specifically, the images were registered, cropped, and averaged over the length of the channel using MATLAB. The fluorescence intensities, assumed to be proportional to the concentration of FITC-BSA, were normalized to the mid-channel intensities of each captured image to account for increasing intensities in progressive images caused by diffusion into the ceiling and floor of the channel.

Initial cell distribution throughout cell-loaded devices was visualized by incubating cells with CFSE (carboxyfluorescein succinimide ester) stain for 15 min prior to encapsulation followed by fluorescence microscopy after device fabrication. Cell viability within the microchannels was assessed by applying a live/dead fluorescence assay to slices of agarose microchannels with encapsulated cells. To analyze agarose cross-sections, slices were gently removed with a flat razor blade into ~ 1 mm thick sections. Live/dead stain was applied directly to the slices, which were incubated for 10 min and visualized under a fluorescent microscope (Nikon, TE2000). Two recognized parameters of cell viability—intracellular esterase activity and plasma membrane integrity—were tracked with the live/dead stain, consisting of PBS solution containing 0.5 μg/ml calcein AM and 2 μg/ml ethidium homodimer-1. Live cells fluoresced green due to intracellular esterase activity that hydrolyzed the fluorogenic esterase substrate (calcein AM) to a green fluorescent

product. Dead cells fluoresced red since their compromised membranes were permeable to the high-affinity red fluorescent nucleic acid stain (ethidium homodimer-1).

Percent viability values of slices were calculated by counting the number of live (green) cells and the number of dead (red) cells in zones above each channel magnified at 4X. Viability data were taken in triplicate for any given condition from the beginning (0 cm), middle (1.5 cm), and end (3.0 cm) of channels. In Figure 5.6B, values were obtained for each control or experimental condition (n = 9 for each value, an average of 230 cells/zone) by dividing the number of live cells by the total number in a 1.25mm x 1.25mm zone above the channels. To average the potential effect of nutrient depletion on cell viability along the axial length of the channel, sections were taken in triplicates from three axial (0 cm, 1.5 cm, 3.0 cm) sections of the channel (resulting in n = 9 for each data point). Percent viability values for Figure 5.6C were determined in a similar manner except that that the data was binned into 5 vertical zones (demarcated in Figure 5.6A) of 1.25 mm x 0.25 mm each (n = 9 for each value, an average of 46 cells/zone). The exception is that the initial viability value shown in Figure 5.6C was obtained from the 1.25 mm x 1.25 mm square zone located above the channel (n = 9). To determine the viability of cells in channels as a function of both axial distance along and vertical distance away from the channel, the viability of cells within 1.25 mm x 0.25 mm zones are reported (n = 3 for each value, an average of 46 cells/zone) in Figures 5.7-5.14. Zones were defined at various vertical distances (50 μm, 300 μm, 550 μm, 800 μm, 1050 μm; the labeled values indicate the distance from the channel floor to the floor of the zone) and axial distances (0.0 cm, 1.5 cm, 3.0 cm). Paired t-tests were used to assess statistically significant differences in viability. Due to potential human error in cell counting we considered $p <$

0.005 to be statistically significant (conservative when compared to $p < 0.05$ used in many typical biological experiments).

5.2 Results

5.2.1 Channel Fabrication

The important parameters for channel sealing, agarose concentration and heating, are explored in Figure 5.2. It appears that the degree of heating required to produce sealed microchannels increases with increasing agarose concentrations. Using agarose of any given concentration, low heating resulted in imperfectly sealed and leaky microchannels; however, excessive heating resulted in melted channel features. In addition, lower concentrations produced moderately transparent but weak bulk materials which tended to fracture upon even careful handling, while higher concentrations produced more opaque (hinders microscopy) but also more robust bulk materials. From these experiments, an agarose concentration of 3% was accepted as both sufficiently transparent for imaging and sufficiently robust for careful mechanical handling. At this concentration, 3 s of heating at a temperature of 71°C was found to adequately seal channels while avoiding melting of features.

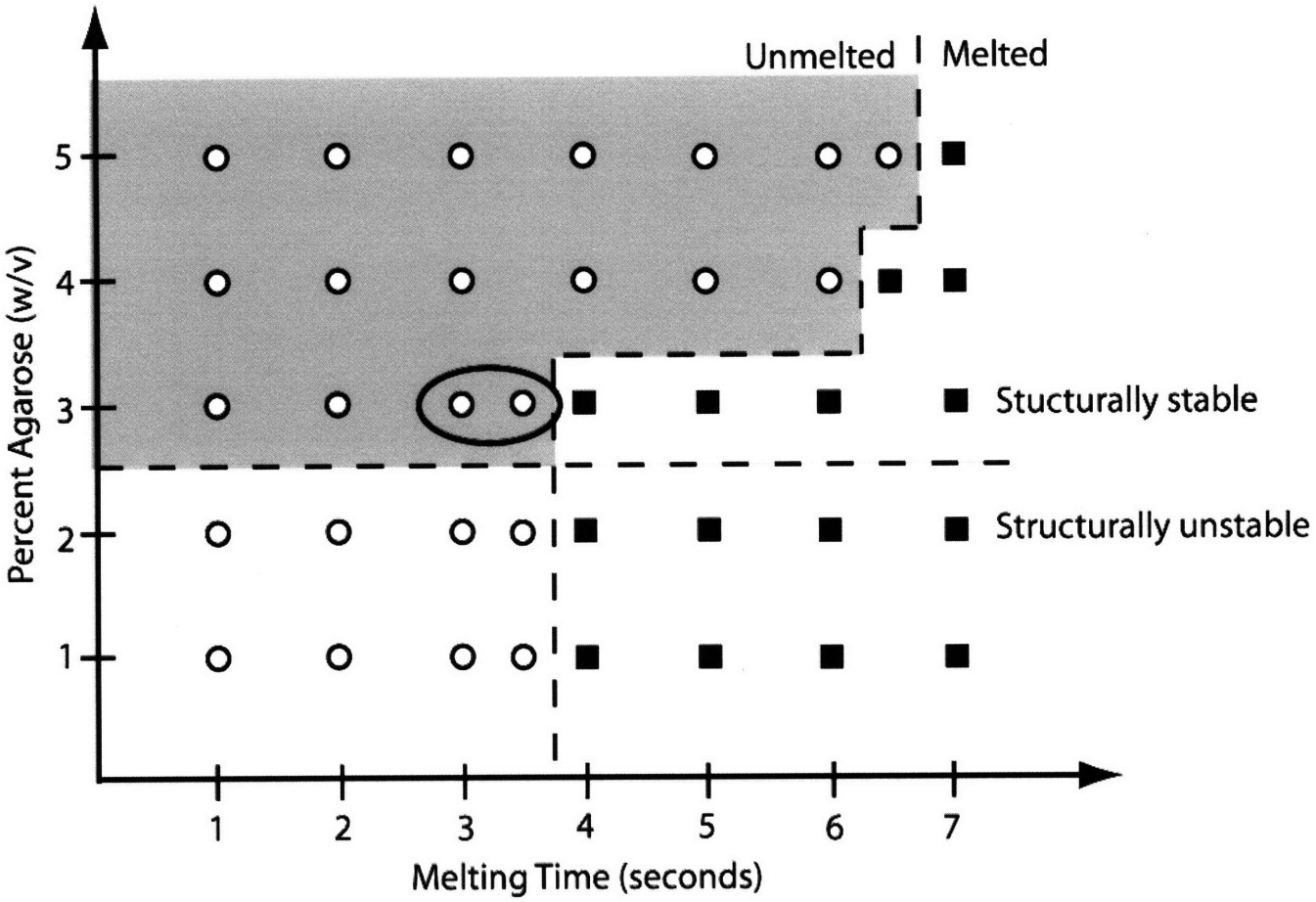

Figure 5.2: Characterization of agarose concentration and melting time for sealing of surfaces. Circles indicate that channel features were unmelted, and squares indicate melting. Dashed lines mark the boundary between melted and unmelted features and between structurally stable and unstable agarose, where stability was defined as the ability to maintain channel features in the agarose without tearing or deformation. The circled region indicates the chosen experimental conditions.

Figure 5.3 shows that agarose microchannels of different sizes and aspect ratios from 50 μm wide by 70 μm tall (Figure 3A) to 1000 μm wide by 150 μm tall (Figure 3B) can be fabricated. The channel in Figure 5.3B demonstrates that 3% agarose, at an elastic modulus reported between 19 and 32 kPA [117,118], is sufficiently rigid to support a large aspect ratio channel without noticeable deformation. While there appear to be black spaces at the interface of the two agarose slabs; we believe these to be optical artifacts. They are likely a product of our sectioning technique (impossible to manually produce perfect 1mm thick slices) as well as the lack of complete melting of the two surfaces upon attachment. Despite the presence of this black edge in light microscopy the devices are known to be sealed as the channels have been verified as sealed in dozens of flow experiments with tracer dyes.

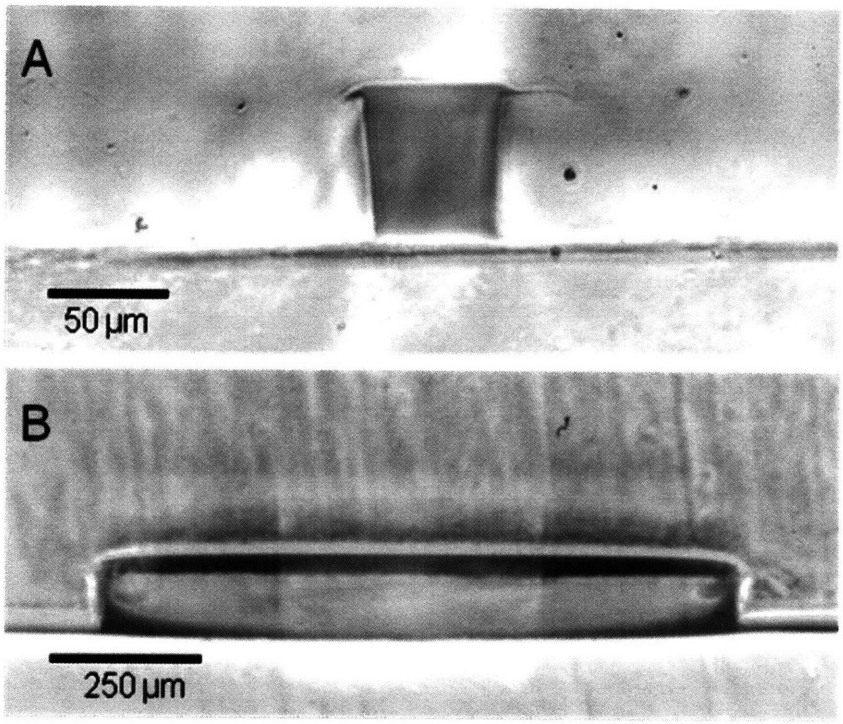

Figure 5.3: Light micrograph cross sectional images of agarose channels. Channels (A) 50 µm in width x 70 µm in height and (B) 1 mm in width x 150 µm in depth are depicted.

To visualize the diffusivity of molecules as a result of flow through 3% agarose microchannels, a series of fluorescent images were taken at 1, 5, and 30 min (Figure 5.4A). The immediately visible and sharply defined boundaries of fluorescence in Figure 5.4A at 1 minute indicate proper sealing. By 30 min into flow conditions, diffusion of FITC-BSA (MW 69 kDa) into the surrounding channel material is apparent. As graphed in Figure 5.4C, the fluorescence intensity rises with time at any given distance from the channel. .

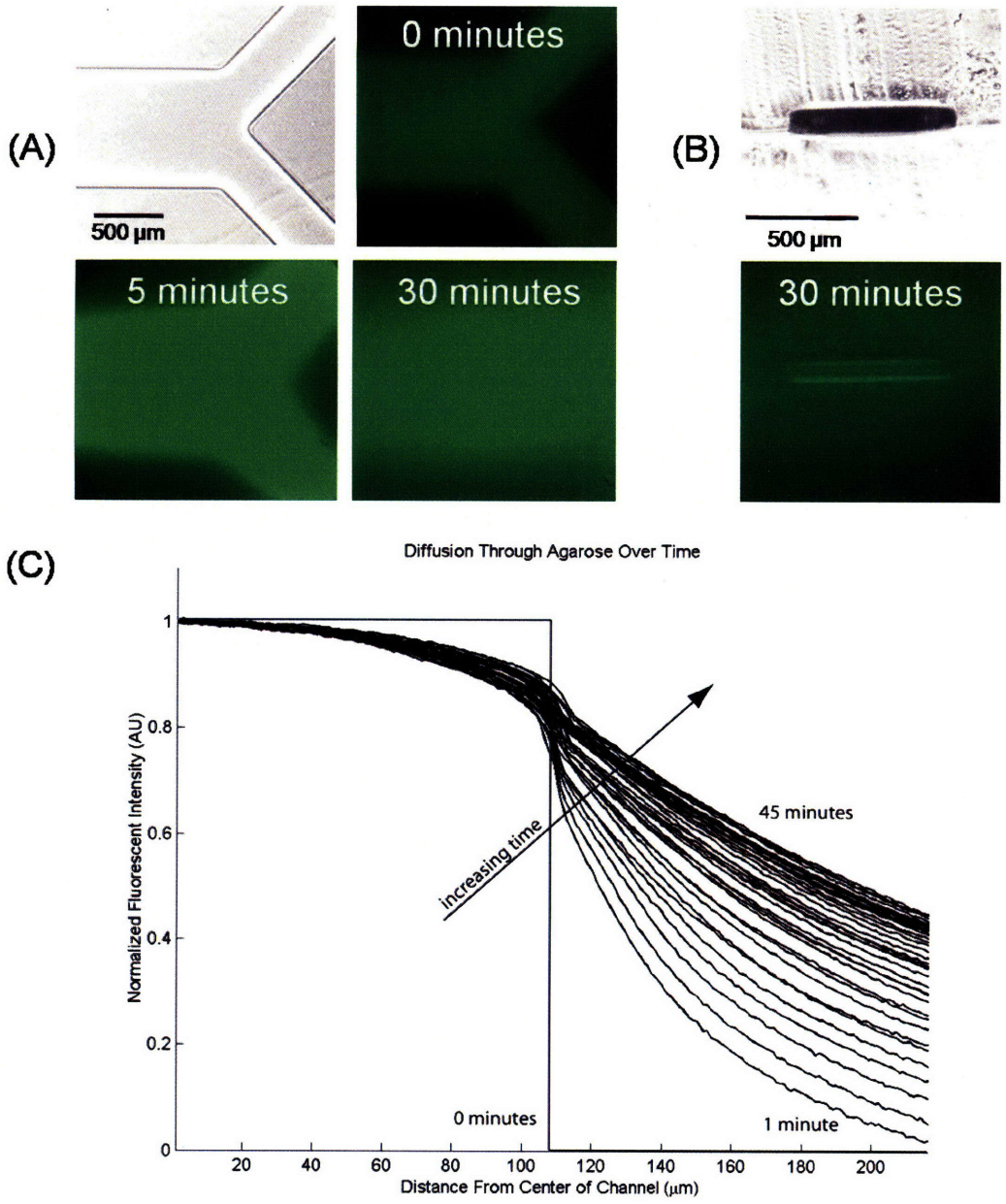

Figure 5.4: Diffusion of FITC-BSA into surrounding agarose. The series of top-down fluorescent images with corresponding phase image in (A) qualitatively depict diffusion with time. In (B) the phase and corresponding fluorescent image of the cross-section of a channel 30 min after FITC-BSA flow are shown. Overlaid intensity profiles (C) are plotted for times ranging from 1 min to 45 min.

5.2.2 Cell Encapsulation within Agarose

Figure 5.5 shows a microfluidic channel in which cells were embedded within the bulk material of the molded upper layer but not within the bulk material of the flat bottom layer. Light microscopy (Figures 5.5C, 5.5D) and CSFE-labeled fluorescence (Figures 5.5A, 5.5B) images of encapsulation reveal a fairly homogeneous distribution of cells throughout the molded bulk agarose material. Further observation of sections of different channel regions (not shown) indicated that the cells were homogeneously distributed throughout the rest of the device as well.

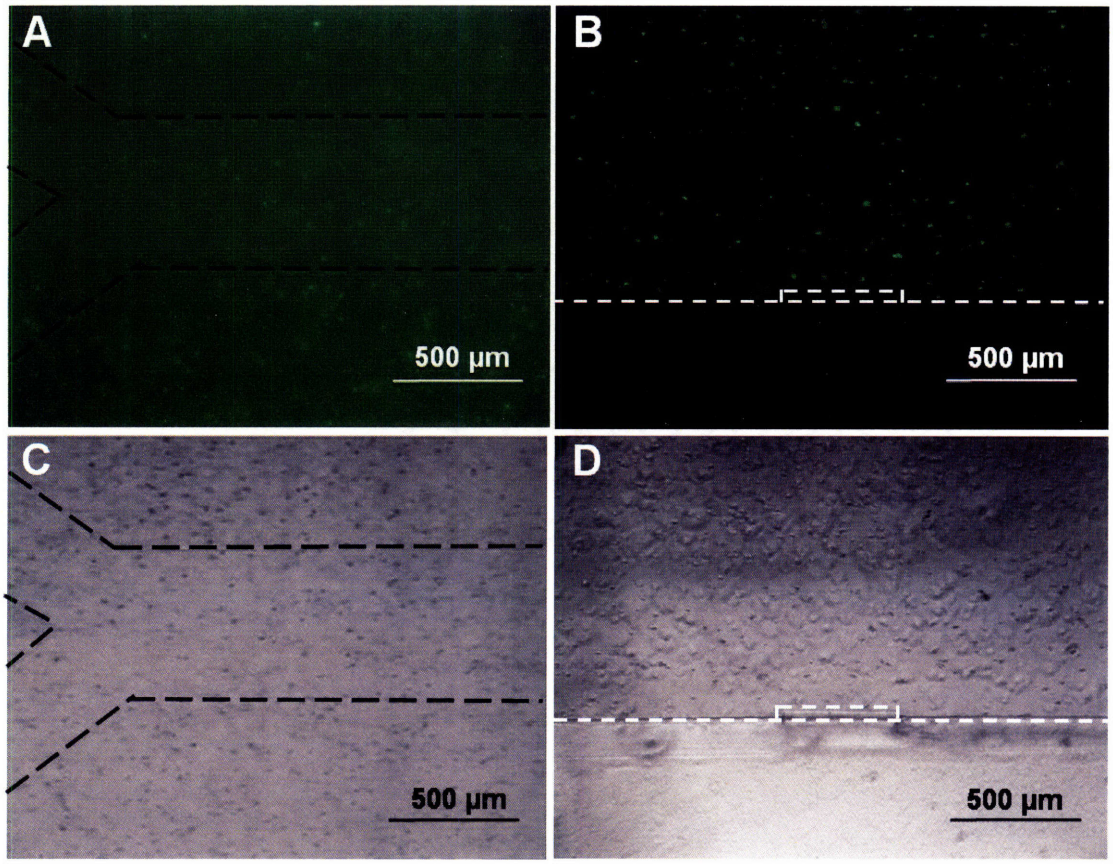

Figure 5.5: Fluorescent and brightfield micrographs of CFSE-stained cells embedded in an agarose microchannel. Panels A and C show a channel from above while panels B and D show the cross-sectional image of another channel. Dotted lines were added to the images to facilitate visualization at print resolutions.

5.2.3 Viability of Encapsulated Cells

Please note that while Figure 5.6 sums up the interesting viability findings and presents them for comparative purposes, more detailed data is reported in Figures 5.7-5.14. Upon formation of microchannels, cell culture media was pumped through the channels for up to three days. The flow rate of 10 μl/min yielding a shear stress value of 1.18 Pa (using previously described method [119]) was chosen because it falls within the physiological shear stress range of mammalian arteries (0.51 – 5.0 Pa [120]).

As shown in the left panel of Figure 5.6A, the majority of cells were viable upon initial device fabrication. Control experiments that exposed trypsinized but unencapsulated cells to identical processing temperatures (as high as 70 °C, including cooling time) exhibited similar viability values (~85%). The live/dead staining indicates no disproportionate degree of cell death at the adherent boundary between the two agarose pieces, indicating that the brief surface heating (71 °C for 3 s, to facilitate bonding of the two pieces) did not cause additional cell death.

From the no-flow and PBS flow controls (Figure 6B), it appears a fraction of cells are able to survive up to 3 days with no nutrient delivery. However, viability results under experimental conditions in which media was continuously pumped through the device show statistically significant increases between experimental and the two control conditions for day 1, day 2, and day 3. By day 3, the difference between experimental and the two control conditions was dramatic. While there were significant drops in viability between each day up to day 2, there was no significant difference in the viability

of the either control condition between days 2 and 3. Additionally, PBS flow control viability values exhibit statistically significant differences in time-course viability when compared to the values obtained under no-flow control condition on days 1 and 2; this difference disappears by day 3.

No significant variations in viability with respect to distance above the channel were observed immediately after the encapsulation process (Figure 5.6C, 50 μm). Over time, cells further from the microchannel gradually lost viability, as shown in a representative image from day 3 in the right half of Figure 5.6A in which zones further from the channel may be qualitatively compared to the zones that are closer. To quantitatively assess the effect of distance above the microchannel as a function of time under experimental conditions, the percent viability of zones roughly 1.25 mm x 0.25 mm (visualized in Figure 5.6A by dashed white lines) centered atop and binned at progressively greater distances above the channel are plotted individually in Figure 5.6C. This data shows significantly larger drops in viability over time for regions at greater (1050 μm) distances from the channel. In the region closest to the channel (50 μm), there is a small (in comparison to regions at greater distances) but significant drop in viability on day 1 in comparison to initial viability, but no significant differences are found between day 1 and 2 or between 2 and 3.

Detailed PBS control (Figures 5.7 – 5.9) and experimental media flow (5.10 – 5.14) viability data are reported to assess the possibility of nutrient depletion along the axial direction (direction of flow) of the channel. For each time point (day) and condition

(PBS/experimental), no statistically significant differences were found between zones of different axial distances along the channel (left panel in Figures 5.7-5.9). These three axial values were therefore binned and plotted together (n = 9, right panel in Figures 5.7-5.9).

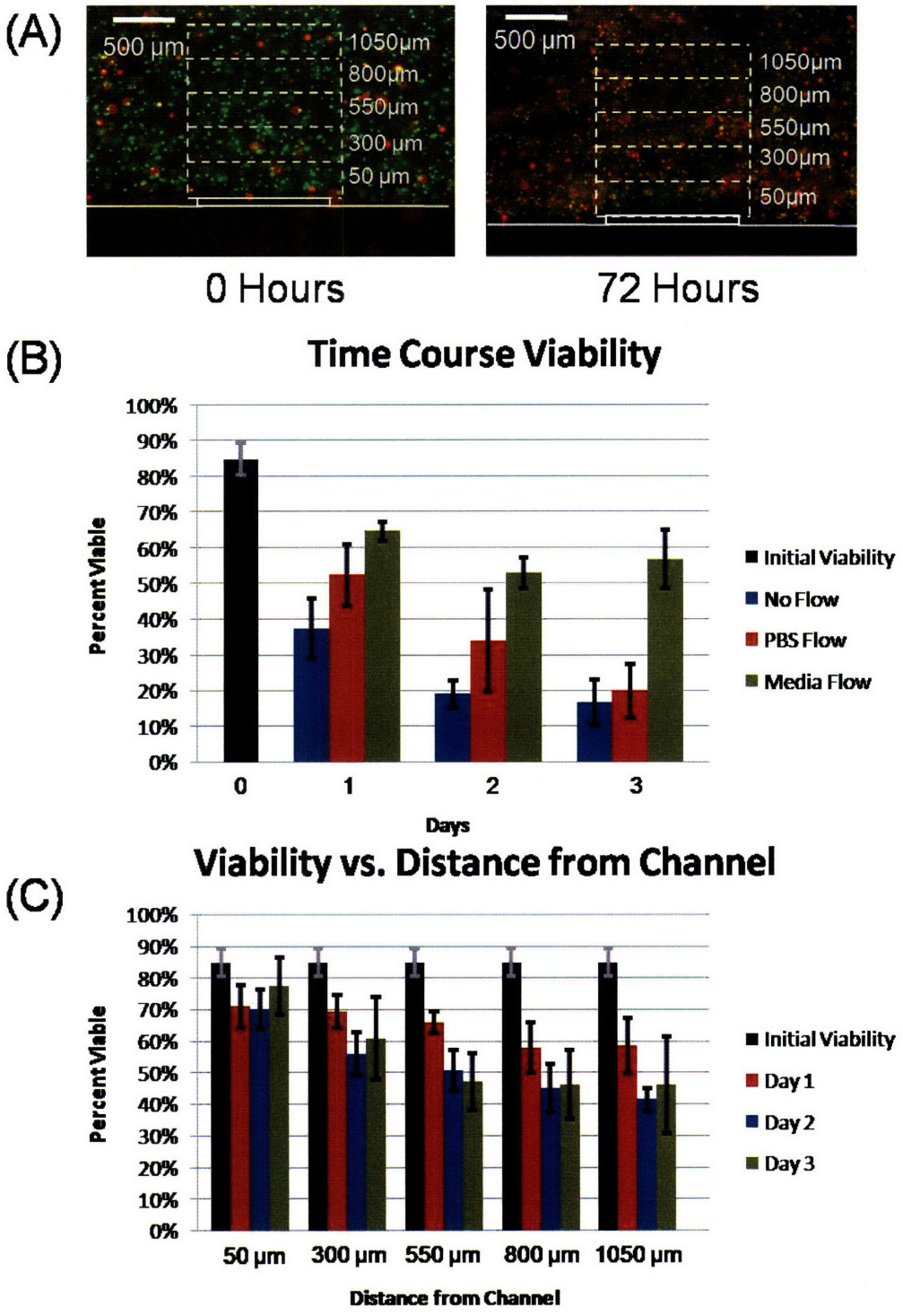

Figure 5.6: Quantification of cell viability in the agarose microchannels over time. The images in (A) are representative live-dead staining of AML-12 murine hepatocytes encapsulated in agarose channels after 0 (left) and 3 days (right). Rectangular regions demarcated by dashed white lines correspond to ~250 µm thick zones where the labeled

height values correspond to the mean distance of each zone above the channel floor. The graph in (B) plots percent viability values for initial (n=27) as well as for up to three days under 2 control conditions (No Flow, PBS Flow) and experimental media flow conditions (n=9 for all three conditions). In part (C) the time course viability under experimental media flow conditions for 1.25 mm x 0.25 mm zones of progressively increasing distances (50 μm, 300 μm, 550 μm, 800 μm, 1050 μm) from the channel are shown (n=9). Error bars span one standard deviation from the mean.

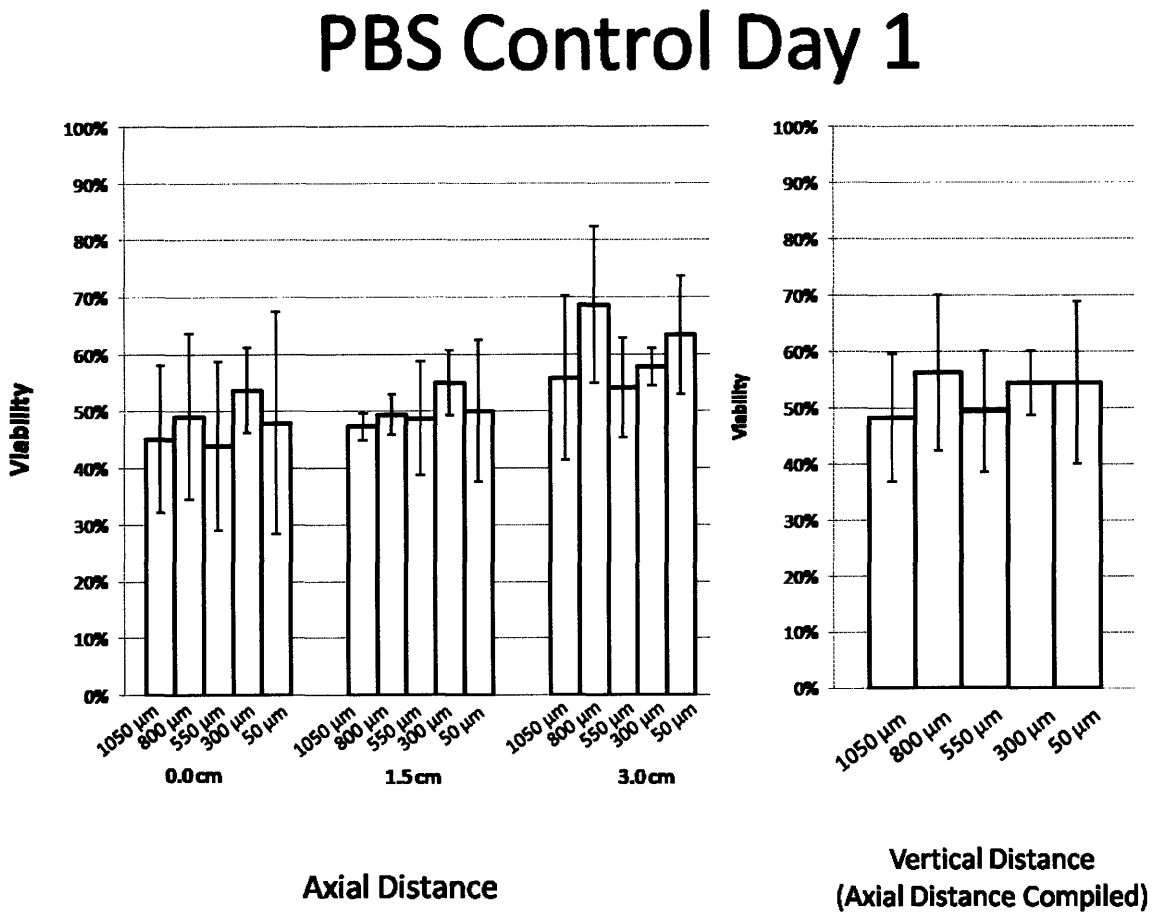

Figure 5.7: Viability data for PBS flow control experiments at day 1 in zones binned by vertical distance above and axial distance along the channel (left panel, n=3) as well as only by vertical distance above the channel (right panel, n = 9). Error bars span 1 standard deviation from the mean.

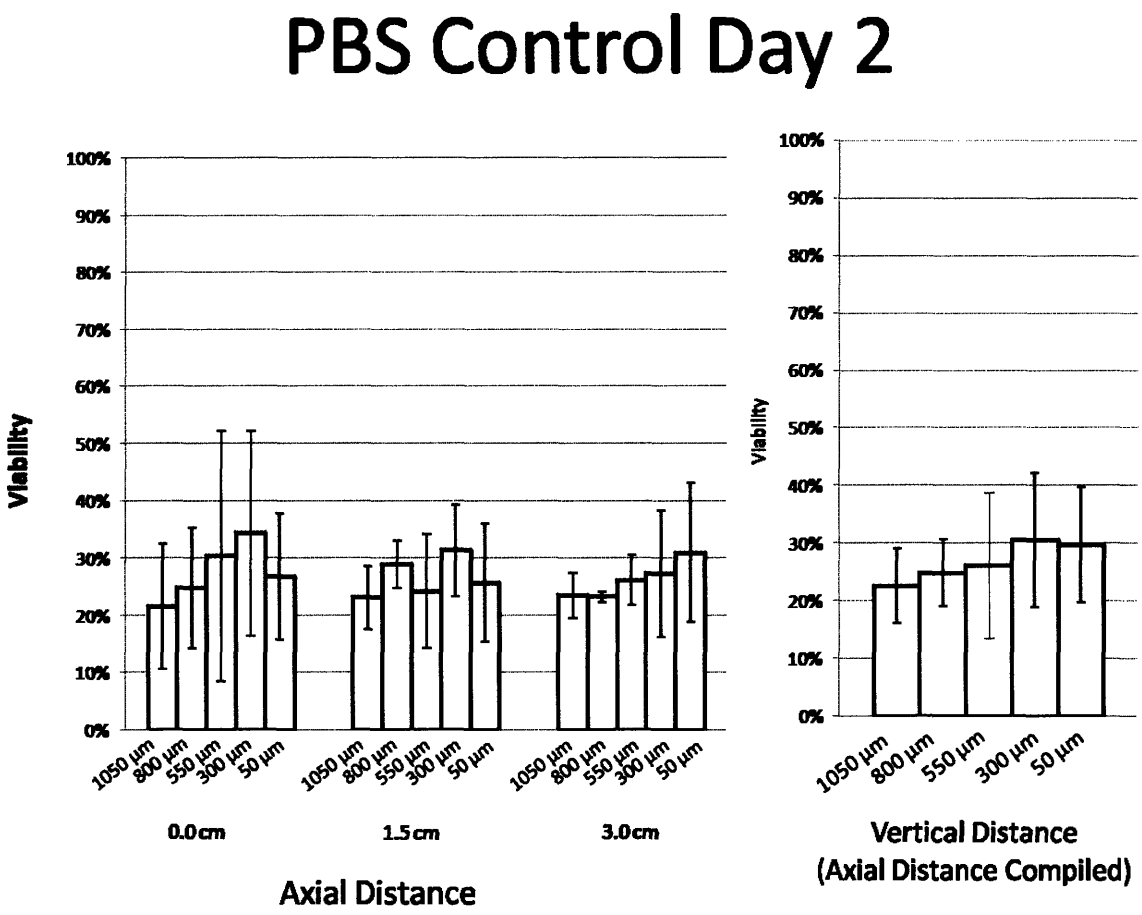

Figure 5.8: Viability data for PBS flow control experiments at day 2 in zones binned by vertical distance above and axial distance along the channel (left panel, n=3) as well as only by vertical distance above the channel (right panel, n = 9). Error bars span 1 standard deviation from the mean.

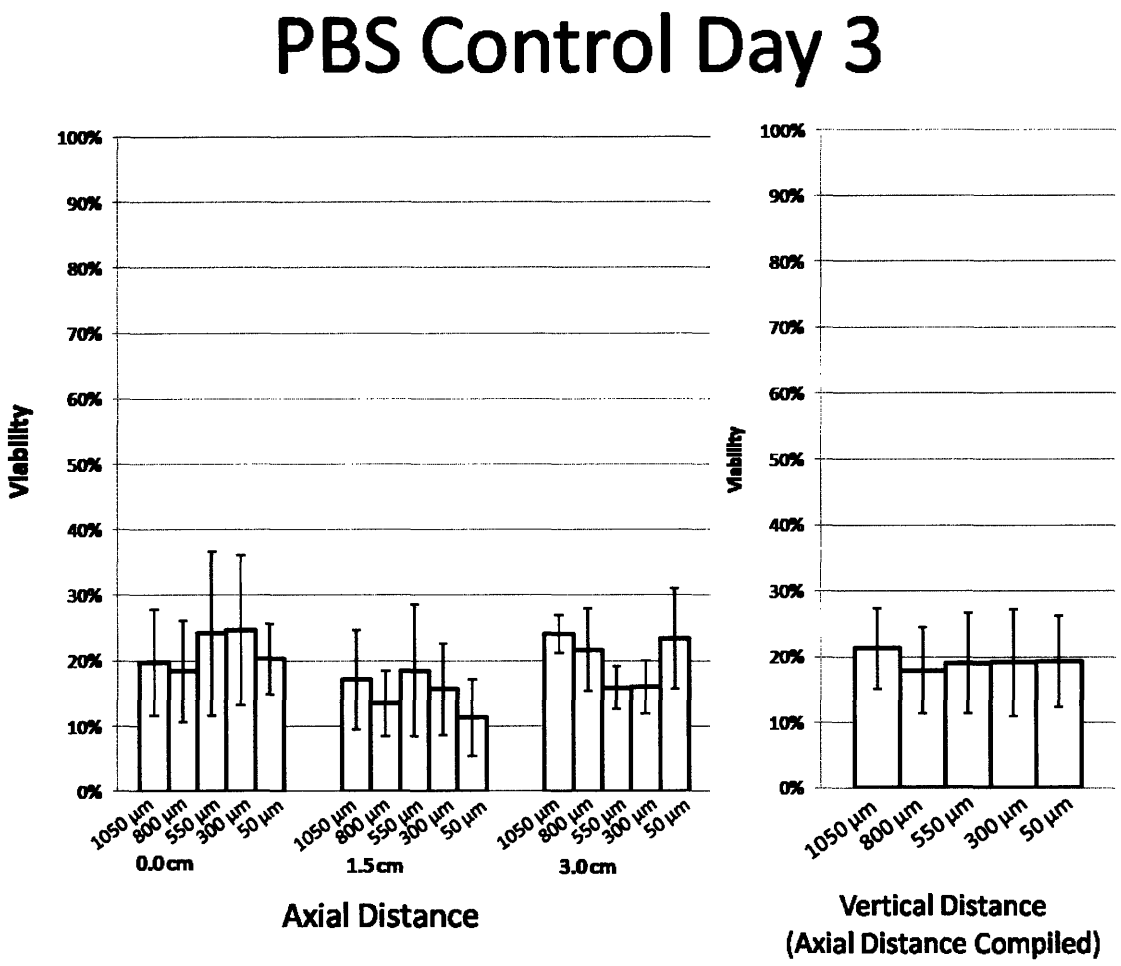

Figure 5.9: Viability data for PBS flow control experiments at day 3 in zones binned by vertical distance above and axial distance along the channel (left panel, n=3) as well as only by vertical distance above the channel (right panel, n = 9). Error bars span 1 standard deviation from the mean.

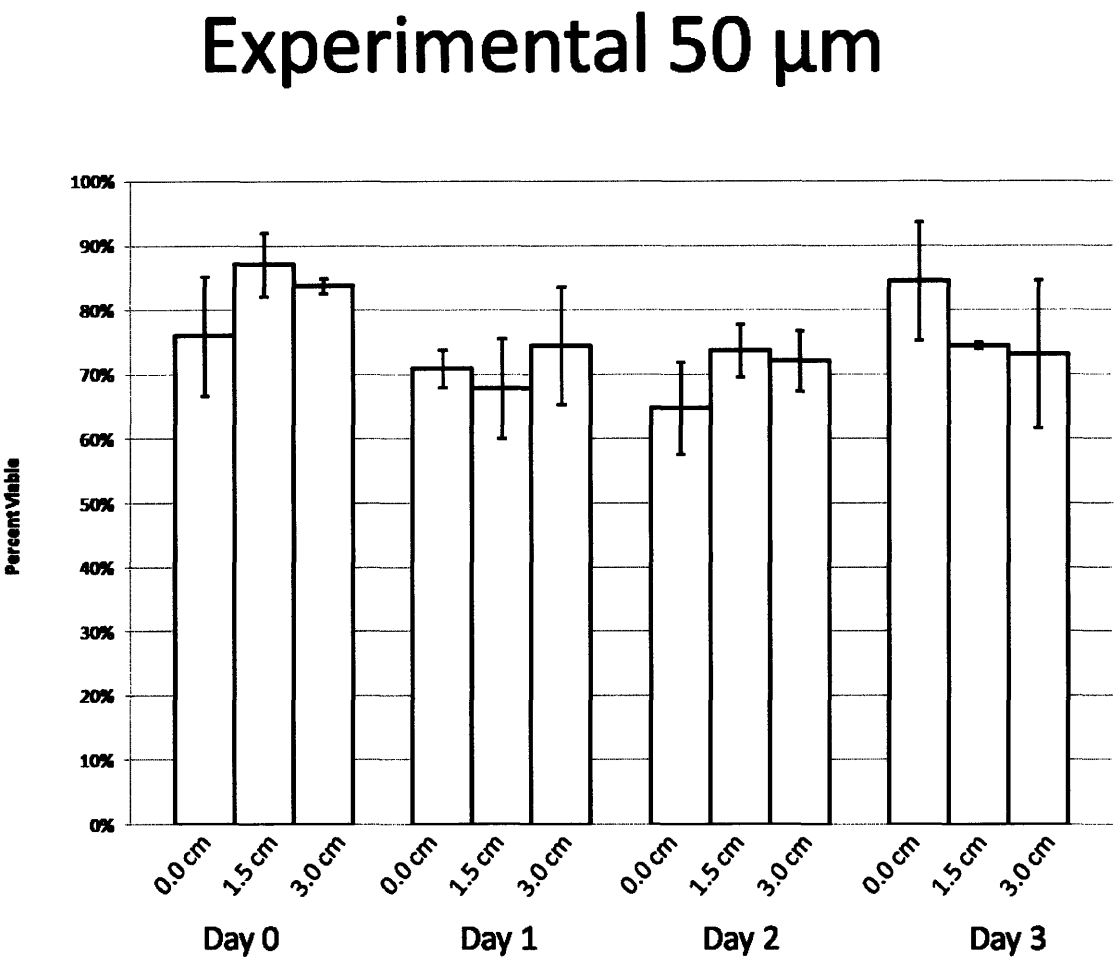

Figure 5.10: Viability data for media flow experimental conditions within a 1.25mm x 0.25mm zone 50 µm above the channel floor. Axial distance as well as time course data are plotted (n = 3). Error bars span 1 standard deviation from the mean.

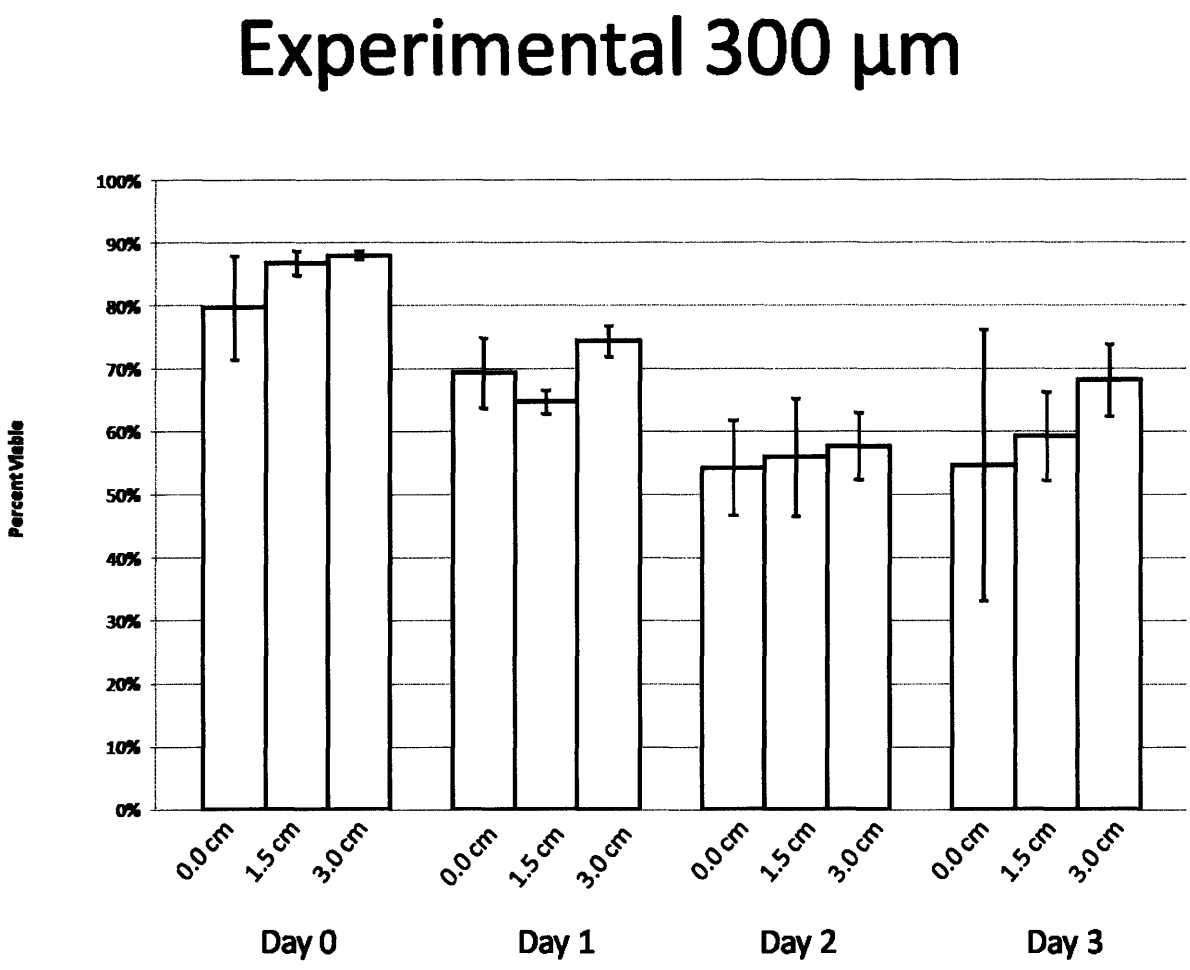

Figure 5.11: Viability data for media flow experimental conditions within a 1.25mm x 0.25mm zone 300 µm above the channel floor. Axial distance as well as time course data are plotted (n = 3). Error bars span 1 standard deviation from the mean.

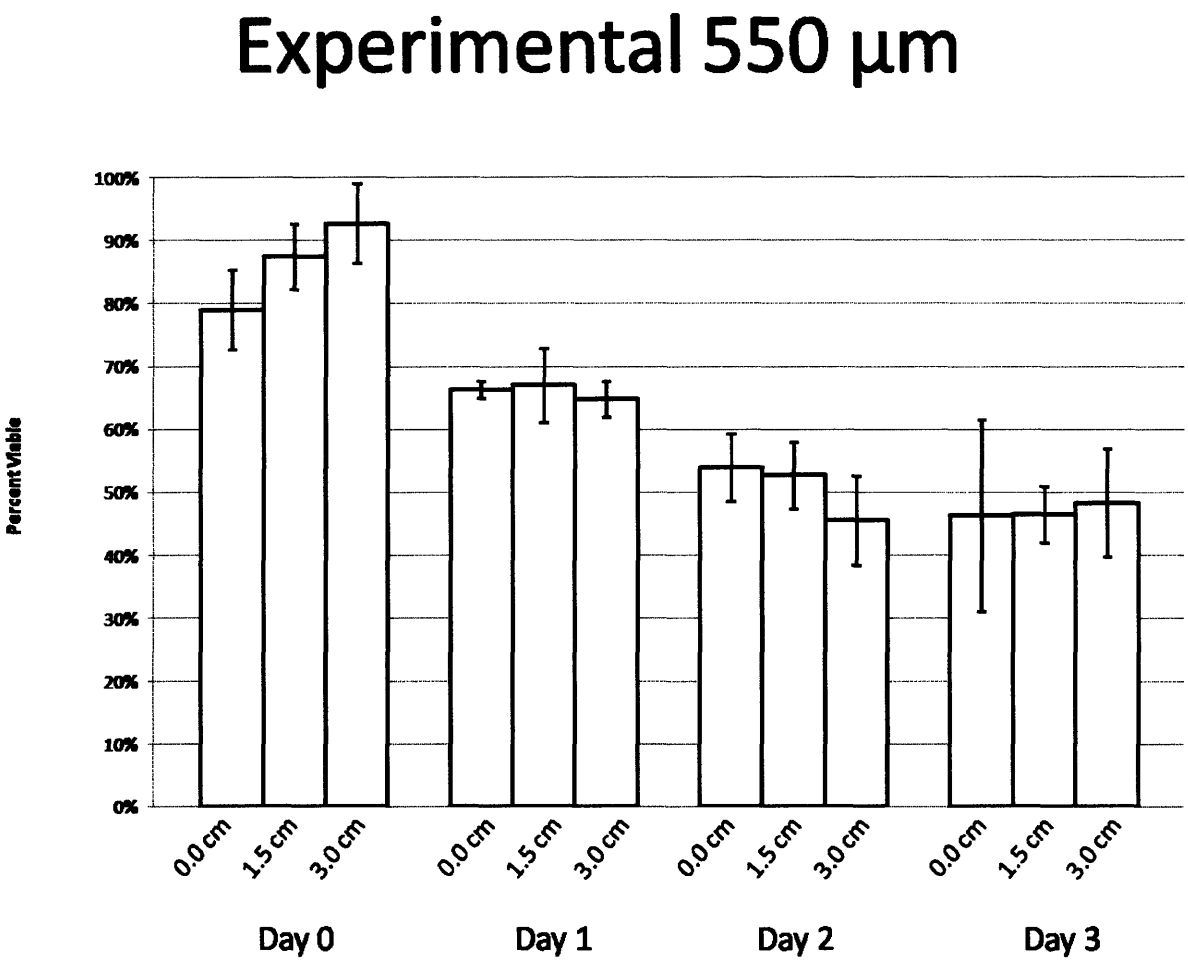

Figure 5.12: Viability data for media flow experimental conditions within a 1.25mm x 0.25mm zone 550 µm above the channel floor. Axial distance as well as time course data are plotted (n = 3). Error bars span 1 standard deviation from the mean.

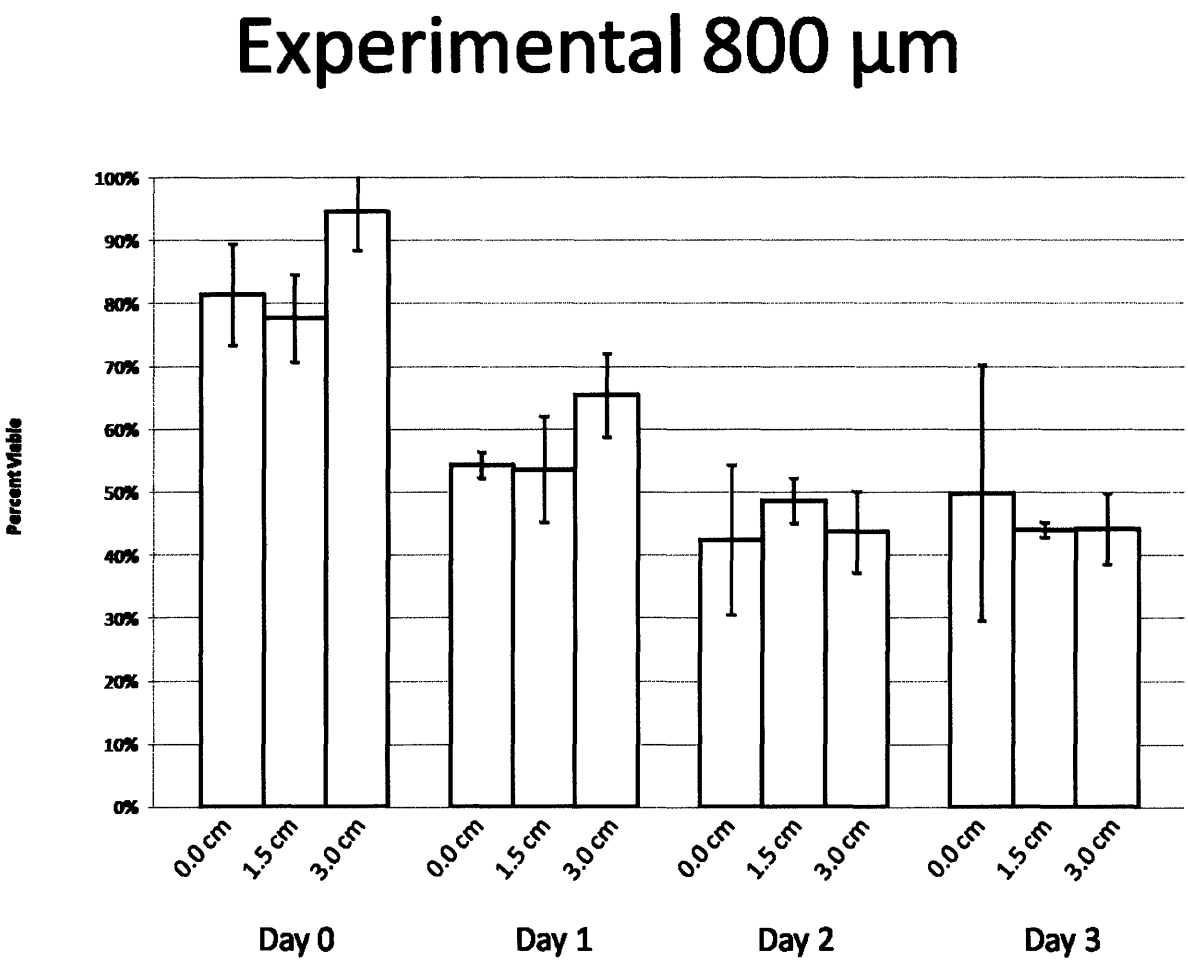

Figure 5.13: Viability data for media flow experimental conditions within a 1.25mm x 0.25mm zone 800 µm above the channel floor. Axial distance as well as time course data are plotted (n = 3). Error bars span 1 standard deviation from the mean.

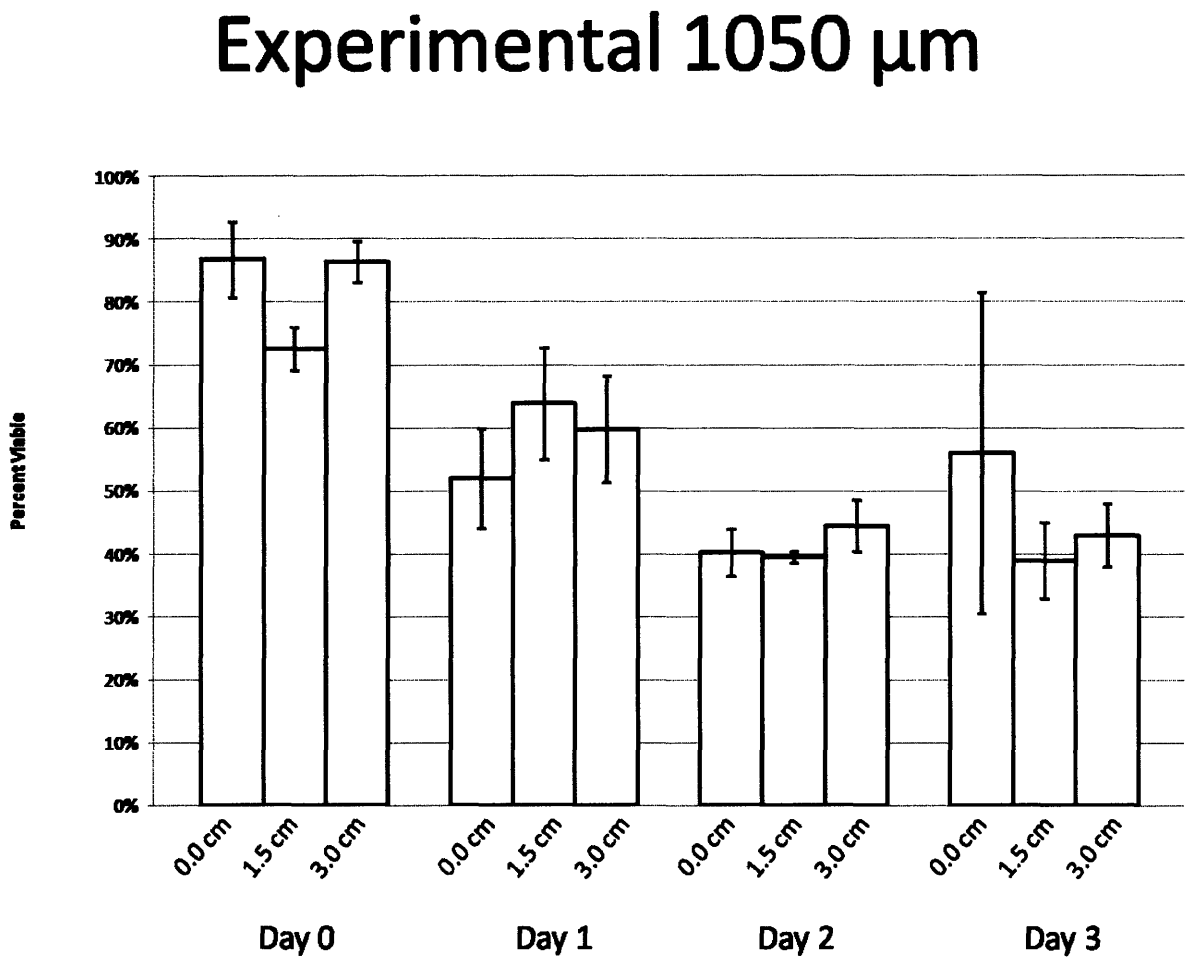

Figure 5.14: Viability data for media flow experimental conditions within a 1.25mm x 0.25mm zone 1050 µm above the channel floor. Axial distance as well as time course data are plotted (n = 3). Error bars span 1 standard deviation from the mean.

5.3 Discussion

5.3.1 Channel Fabrication

While soft lithography has previously been used to mold agarose[113,114] this work is to our knowledge the first demonstration of an agarose microfluidic device. Proper channel sealing is a non-trivial problem in soft lithography-based microfluidics, and so the initial question was whether sealing would be possible using agarose. Fortunately, the gelation of agarose can be reversed by thermal modulation, allowing for the sealing of channels by semi-melting surfaces before bonding.

Based on the well-known properties of agarose[121], our finding that stiffness and melting temperature tended to increase with increasing agarose concentration was in line with expectations. But this implies an important drawback of agarose as a microfluidic material—at lower concentrations it is fairly difficult to peel away from the mold without tearing. Though concentrations of higher than 3% might have further improved mechanical stability and decreased the likelihood of tearing during handling, this consideration was overridden by the downside of having to treat agarose surfaces to much higher, potentially cytotoxic temperatures, to facilitate bonding.

High porosity and ease of molecular diffusion are crucial for maintaining the viability of encapsulated cells since diffusion facilitates efficient nutrient delivery and waste removal. Though the plots somewhat resemble typical diffusion curves, they cannot be construed as actual diffusion profiles; this fluorescence microscopy technique is not amenable for

obtaining reliable diffusivity values (in the literature, D~6.4 x 10^{-7} cm^2/s [122]) since diffusion into the ceiling and floor of the channel skews the shape of the curves.

5.3.2 Viability of Encapsulated Cells

Due to processing requirements (cell-loaded devices were set for 2 hours to facilitate agarose gelation), the devices were fabricated with media (at 50%) to prevent compromise of initial cell viability. However, this introduced the likelihood of a partial maintenance of cell viability by pre-loaded rather than delivered media. This is likely the reason that cell viability did not drop to 0% under PBS flow and no flow control conditions even after 3 days.

The PBS control experiments were run to assess the effect of waste removal on cell viability. It is important to note that we cannot in these experiments segregate the effect of waste removal from dilution of the pre-loaded media; however, one reasonable explanation for the PBS results when compared to no-flow is that the initial (days 1 and 2) increases in viability are due to waste removal, which becomes insignificant by day 3. Therefore, the effect of waste removal in improving cell viability in this system does appear to overwhelm the detrimental effect of nutrient dilution in the first 2 days.

It is important to note that since the viability values of the two control conditions in Figure 5.6B were taken from a 1.25 mm x 1.25 mm region above the channel the experimental values were also taken from corresponding regions. However, by days 1-3 there is a distinct drop in cell viability at increasing distances above the channel. The high viability of the region nearest the channel is therefore attenuated by lower viabilities

farther away from the channels; this phenomenon necessitated the finer binning of data in Figure 5.6C. These findings (higher viability near the channel) were likely the result of diffusion limitations within the bulk agarose, preventing adequate nutrient and waste exchange to cells embedded at larger distances from the microchannel. This property is shared by the natural vasculature of tissues (capillaries in human tissues are typically found ~200 μm apart).

The finely binned results in Figures 5.7-5.14 indicate that nutrient depletion, or alternatively, waste accumulation, did not appear to impact cell viability within statistical error along the length of the channel used. This result is expected since the residence time of any particular volume of media within the channel (which can be modulated by adjusting flow rate) is less than half a minute. However, limitations due to axial nutrient depletion and waste accumulation would be expected to affect cell viability for longer channels and slower flow rates.

5.3.3 Future Work

The purpose of this work was to assess the capacity for a cell-laden agarose microfluidic system to facilitate cellular nutrient/waste exchange within the surrounding material. In the future it may be valuable to rigorously assess questions such as pressurization of the microchannels and shape maintenance over time. Furthermore, modeling of diffusion and cellular metabolism (as a function of cell type and density) would provide a more solid theoretical basis for choosing flow rates and the rational design of channel shape, size, length, and (in biomimetic microfluidic networks) distances apart.

The lithographic approach presented here is potentially compatible with other agarose mixtures. To overcome the absence of an attachment matrix, the agarose could be supplemented with ECM additives such as collagen or gelfoam. Signaling molecules may also be incorporated within the hydrogel, either dissolved within the liquid phase or conjugated to agarose via a Williams ether synthesis (attachable to amine group of ligand)[123]. Alternatively, the use of natural ECM molecules such as hyaluronic acid or collagen may provide a more chemically and mechanically *in vivo*-like environment, leading to superior assimilation of the resulting structures into the host tissue and cell migration and proliferation within the hydrogel matrix.

Cell-laden agarose microfluidic hydrogels can also be scaled up. In this process, biomimetic vascular patterns may be fabricated and stacked layer-by-layer, one upon another to generate multi-layer vascularization in many discrete planes. However, the basis for rational design of such a network would necessitate much work in modeling and empircally characterizing the mass transport of macromolecules from microfluidic channels into the surrounding material.

5.4 Conclusion

In summary, we have developed a soft lithographic technique for fabricating cell-laden agarose microfluidic devices. We have characterized the degree of surface heating necessary to form sealed channels and demonstrated flow within as well as diffusion into the surroundings of the microchannels. In addition, cells were embedded homogeneously within the agarose devices. The delivery of media from the channels allowed cells in

close proximity to the channels to remain significantly more viable than control conditions for up 3 days. This simple method may be useful as a means of generating synthetic vasculature within tissue engineered constructs.

Chapter 6

Future Work: Mesoscale Self-Assembly

This thesis described three techniques for producing cell-loaded structures that could be used for tissue engineering. In chapters 3 and 4 two methods for producing UV photocrosslinkable and chemically crosslinked shape- and size controlled microstructures were described. These works were originally aimed at creating structures that may be useful for a number of applications, but we here considered them primarily for their potential utilization as components in bottom-up tissue engineering. Though further characterization would be required before these microstructures could be used in self-assembly, we have demonstrated the techniques to be generally capable of producing shape- and size-controlled components with reasonable shape fidelity and cell viabilities. Chapter 5 described a technique for generating cell-loaded agarose structures that can be perfused by microfluidic channels. The results indicated that nutrient/waste exchange via diffusion from the channels can play a positive role in cell maintenance. The discussion of future work for further extending this general strategy for perfusion of tissue engineered constructs was straightforward and was therefore presented within Chapter 5 itself. However, a proper discussion of self-assembly for bottom-up tissue engineering would be substantially more involved. As such, it was restricted to this chapter.

The development of bottom-up tissue engineering requires the achievement of two essential objectives. Chapters three and four of this thesis describe the two strategies for generating shape- and size-controlled cell laden microstructures that constitute the

realization of the first of these two objectives. The purpose of this final chapter is to propose future work aimed at realizing the second objective: to develop methods for directing self-assembly of shape- and size-controlled microstructures into meso- and macroscale constructs.

Inspired by experimental observation of elf-assembling phenomena in biological systems, a series of experiments carried out in the past decade have demonstrated the viability of mesoscale self-assembly[124]. At the molecular scale, self-assembling phenomena are typically driven by reversible and relatively weak forces like van der Waals and Coulomb interactions, hydrophobic interactions, and hydrogen bonding[125,126]. In larger size regimes, similar phenomena may be reproduced by harnessing forces such as steric, entropic, magnetic, gravitational, and electrostatic interactions[125].

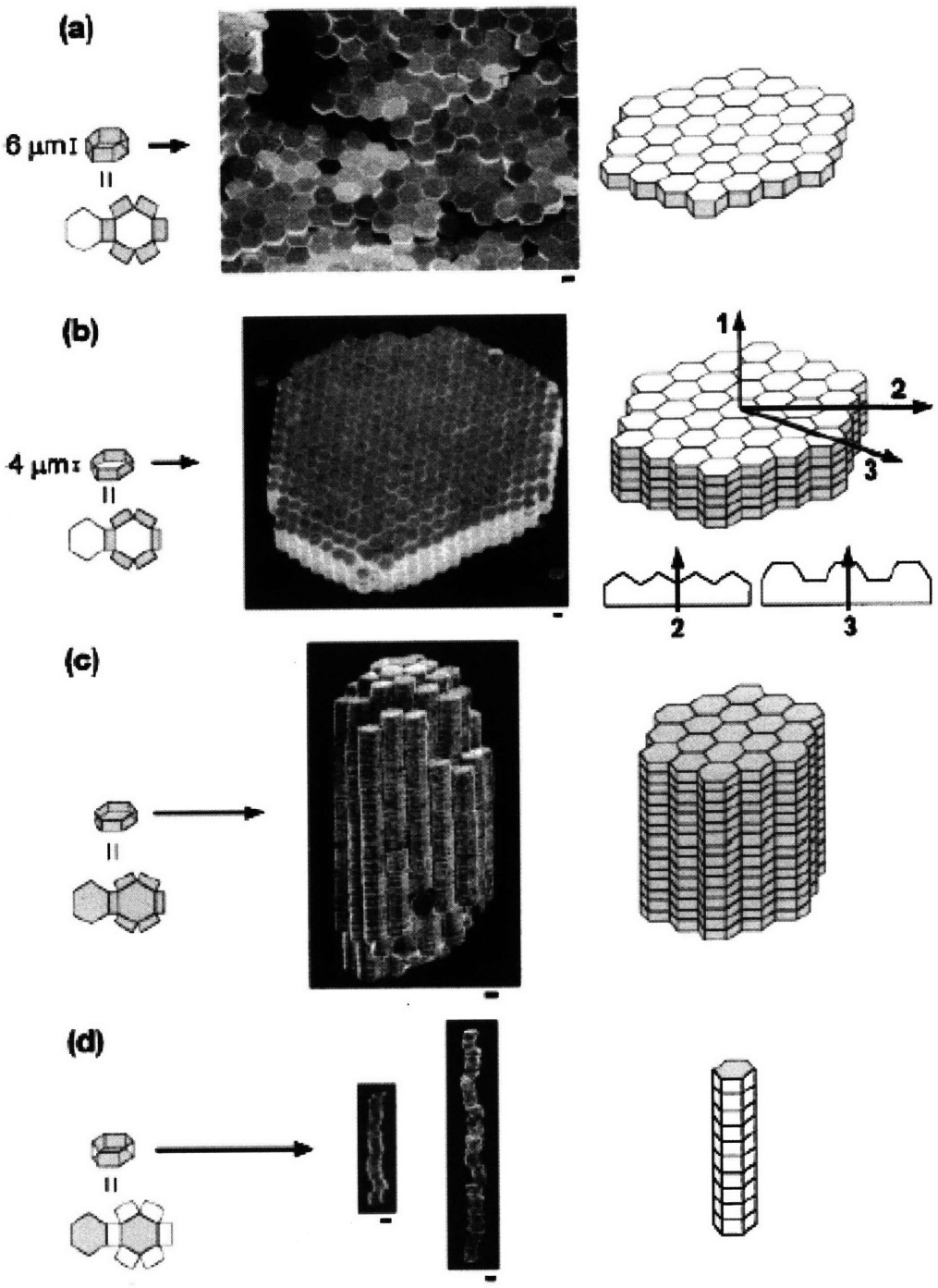

Figure 5.1: Mesoscale self-assembly. This set of schematics and images are taken from the Whitesides Group[127]. Metallic plates with hydrophobically functionalized surfaces (indicated in the schematic by darker surfaces) are coated with a liquid hydrophobic film. When agitated in an aqueous solution the coalescence of microstructures at the coated faces minimizes hydrophobic / hydrophilic interfacial areas thereby driving spontaneous self-assembly into consistent and reproducible ordered three-dimensional arrays.

Recent work at these larger size scales has shown that shape-fitting millimeter scale components can be self-assembled (with or without shaped templates) at floating and fluid-fluid interfaces[128,129] as well as in aqueous suspensions[77,130,131] by the clever exploitation of capillary forces, typically using liquids with high interfacial free energy (examples shown in Figure 5.1). For example, free units of hexagonal plates (hexagons were used to minimize the number of potential slip planes) floating at a water-perfluorodecalin interface were shown to spontaneously self-assemble into a honeycomb-like lattice[128]. Perhaps more importantly for bottom-up tissue engineering, components of a few hundred microns (the relevant size regime for bottom-up tissue engineering as proposed here) fabricated through photolithography have been self-assembled into ordered arrays via capillary interactions[132]. These experiments were motivated by potential applications in the microelectronics device industry and so demonstrate self-assembly of non-hydrogel polymeric and metallic microstructures in highly cell toxic environments; the self-assembly of cell encapsulation-compatible hydrogel microstructures has not yet been shown. Yet, the utilization of scale-relevant interactions to drive minimizations of interfacial free energy (necessitating shape- and size-controlled microstructures) should not be incompatible with microstructures derived from standard tissue engineering hydrogels.

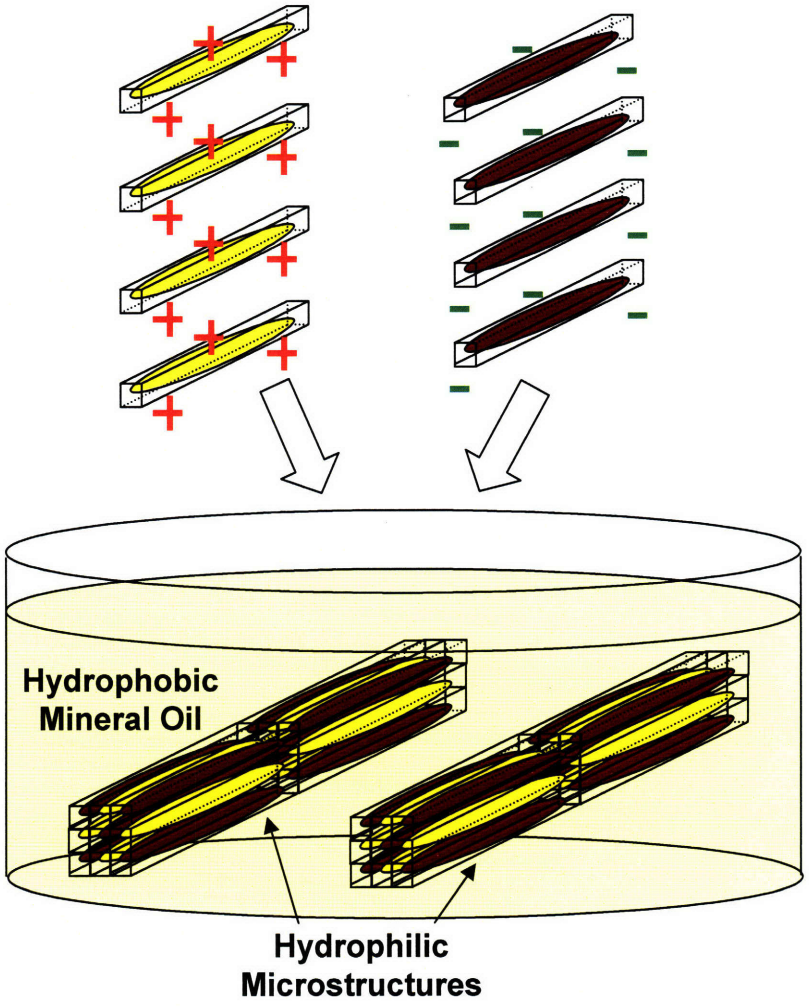

Figure 5.2: Non-ridged self-assembly. Hydrophilic microstructures of opposite charges (chitosan and hyaluronic acid) are placed into a hydrophobic mineral oil bath. Charge and hydrophobic / hydrophilic interactions facilitate self-assembly.

A similar self-assembly strategy that adopts cell compatible processing conditions may be extended to commonly used biocompatible hydrogels (poly(ethylene glycol), hyaluronic acid, alginate, chitosan, fibrin, polylysine, etc.). Any number of scale-relevant forces could be harnessed to drive self-assembly but initial experiments might utilize a combination of hydrophobic/hydrophilic and electrostatic interactions. Shape complementarities between fitting components would allow for these interactions to increase the specificity of self-assembly. In our initial experiments it may be valuable to apply this approach to the fabrication of cardiac tissues to enable facile validation (i.e. known and specific protein expression profiles, distinct phenotypes, etc.) of the approach although bottom-up tissue engineering is by no means an organ- or tissue-specific strategy.

5.1 Overview

To form three-dimensional (3D) tissues from cell-laden microstructures, we will develop approaches to self-assemble shape- and size-controlled components into directed and reproducible 3D configurations. Our initial experiments will focus on using a combination of hydrophobic/hydrophilic interactions and electrostatic interactions between differing hydrogel materials to induce self-assembly. Two useful model hydrogels may be hyaluronic acid and chitosan: both materials are largely hydrophilic but hyaluronic acid methacrylate hydrogels are negatively charged while chitosan hydrogels are positively charged. When placed in a chemically inert and non-toxic hydrophobic liquid such as mineral oil, these hydrogels should tend to aggregate to reduce interfacial free energy (Figure 5.2). Proper combinatorial mixing of positively charged chitosan and

negatively charged hyaluronic acid microstructures with shapes and sizes allowing for complementary coupling should increase the specificity of self-assembly. In order to reduce the number of potential slip planes, it is hypothesized that ridge-shaped surfaces (Figure 5.3) may facilitate superior self-orientation of microstructures during self-assembly.

5.2 General Experimental Design

Shape-Fitting Self-Assembly: A set of experiments using rectangular polyhedral microstructures with flat surfaces as well as a parallel set with ridged surfaces will be performed to assess the importance of precise shape-fitting to self-assembly. We anticipate the experiments involving ridged components to yield a relative reduction in the number of structural defects by reducing the number of potential slip planes (from 6 per component to 2). In either case, carefully controlled numbers of methacrylated hyaluronic acid (MeHA) and chitosan microstructures will be mixed together within a mineral oil solution (Figure 5.2) with MeHA prepolymer and photoinitiator (prepolymer and photoinitiator are hydrophilic and form around microstructures) and gently agitated to induce self-assembly. The assembled 3D macrostructures will then be exposed to UV light to covalently bond the microstructures to one another, removed from the mineral oil bath, and washed with PBS. Microscopy will be performed to assess the efficacy of self-assembly. Particular attention will be paid to the orientation of microstructures within the larger 3D structure and the number of defectively assembled components will be quantified and characterized.

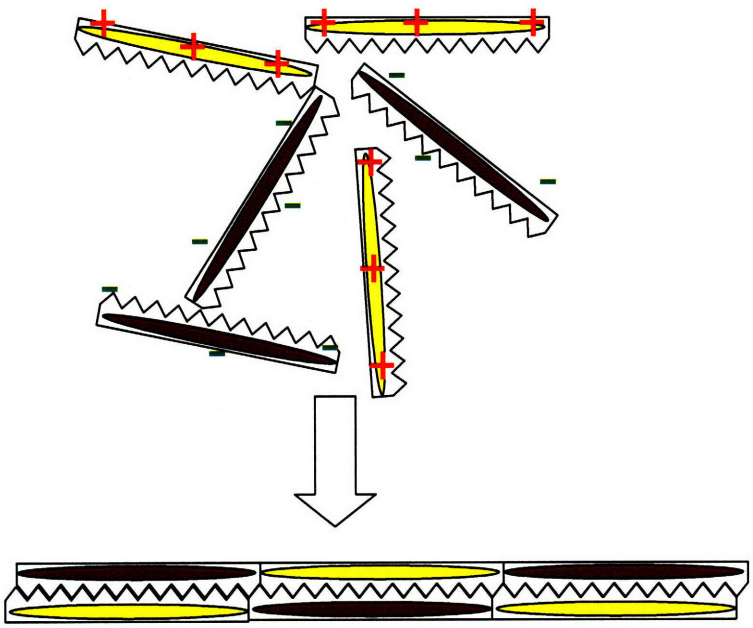

Figure 5.3: Ridged self-assembly. Ridge-shaped hydrophilic microstructures of opposite charge (chitosan and hyaluronic acid) are placed into a hydrophobic mineral oil bath. The complementary shape-fitting of opposing ridges are expected to act in unison with hydrophobic / hydrophilic interactions to further facilitate self-assembly.

Various parameters will be explored to minimize defects, such as the concentrations of the microstructures within the aqueous phase, size and shape of the microstructures, the ratio of the hydrophobic to hydrophilic components and the prepolymer and photoinitiator concentrations. Initial experiments will involve cell-free microstructures in order to characterize parameters; subsequent experiments will involve cell-loaded microstructures as required. If successful, these experiments would represent the first demonstration of the efficacy of electrostatic interactions in mesoscale self-assembly and demonstrate that processing conditions for bottom-up engineering *can* be sufficiently mild so as to facilitate high cell viability.

Characterization of Self-Assembled Constructs: As a model system for analyzing the proposed efficacy of bottom-up tissue engineering in enhancing tissue structure and function, cardiac myofibrils will be encapsulated within microstructures and self-assembled. We believe that this model tissue if successfully assembled would represent a powerful demonstration of bottom-up tissue engineering since cardiac function (contraction) requires alignment of myofibrils and the formation of load-transferring cell-cell junctions. Cell viability within thin samples of constructs will be analyzed with live-dead staining and MTT under fluorescence microscopy at reasonable (~daily) intervals for up to 60 days in culture. The viability of the cells within larger structures may be examined using confocal microscopy. We will also perform histological analysis on the resulting macrostructures at each of the above time points to visualize and capture remodeling characteristics such as the expression of intracellular myosin heavy chain (and other standard cardiac markers) and N-cadherins at fascia adherens junctions.

Bottom-up tissue engineering is premised on the hypothesis that different cell types when appropriately pre-configured within 3D environments would exhibit improved remodeling over cells randomly seeded within porous scaffolds. This set of analyses will represent a first step in testing that hypothesis. If indeed bottom-up engineered cardiac tissues exhibit improved *ex vivo* morphology and functionality, further *in vivo* work may follow.

5.3 Conclusions

Tissue engineering is an intriguing and promising regenerative technology with the potential to improve the quality of life for millions of individuals. Bottom-up tissue engineering constitutes a unique alternative to traditional tissue engineering strategies and when coupled with existing methodologies (physical stimuli and biochemical factors) may prove to be tremendously useful for producing many forms of complexity, including built-in vasculature. In this body of work two strategies for producing shape- and size-controlled microstructures for bottom-up tissue engineering were developed. This final chapter lays out concrete plans for bridging these microstructures with the concept of mesoscale self-assembly. The mastery of self-assembling phenomena may someday enable the recapitulation of all 3D structures within a tissue, from capillaries to veins, ducts to sinuses, glomeruli to glands.

References

1. Cohen, S. et al. Design of synthetic polymeric structures for cell transplantation and tissue engineering. *Clin Mater* **13**, 3-10 (1993).
2. Karp, J., Dalton, P. & Shoichet, M. Scaffolds for tissue engineering. *MRS BULLETIN* **28**, 301-306 (2003).
3. Cui, W., Kim, D.H., Imamura, M., Hyon, S.H. & Inoue, K. Tissue-engineered pancreatic islets: culturing rat islets in the chitosan sponge. *Cell Transplant* **10**, 499-502 (2001).
4. Murphy, W.L., Peters, M.C., Kohn, D.H. & Mooney, D.J. Sustained release of vascular endothelial growth factor from mineralized poly(lactide-co-glycolide) scaffolds for tissue engineering. *Biomaterials* **21**, 2521-7 (2000).
5. Seitz, H., Rieder, W., Irsen, S., Leukers, B. & Tille, C. Three-dimensional printing of porous ceramic scaffolds for bone tissue engineering. *J Biomed Mater Res B Appl Biomater* **74**, 782-8 (2005).
6. Vozzi, G., Flaim, C., Ahluwalia, A. & Bhatia, S. Fabrication of PLGA scaffolds using soft lithography and microsyringe deposition. *Biomaterials* **24**, 2533-2540 (2003).
7. Yeong, W.Y., Chua, C.K., Leong, K.F. & Chandrasekaran, M. Rapid prototyping in tissue engineering: challenges and potential. *Trends Biotechnol* **22**, 643-52 (2004).
8. Bhatia, S.N. & Chen, S.C. Tissue Engineering at the Micro-Scale. *Biomedical Microdevices* **2**, 131-144 (1999).
9. Tsang, V.L. & Bhatia, S.N. Three-dimensional tissue fabrication. *Adv Drug Deliv Rev* **56**, 1635-47 (2004).
10. Khademhosseini, A., Ling, Y., Karp, J.M., Langer, R. Micro- and Nanoscale Control of Cellular Environment for Tissue Engineering. in *Nanobiotechnology II* (ed. Mirkin, C.A., Niemeyer, C.M.) 349-366 (WILEY-VCH Verlag GmbH & Co. , 2007).
11. Yoshimoto, H., Shin, Y.M., Terai, H. & Vacanti, J.P. A biodegradable nanofiber scaffold by electrospinning and its potential for bone tissue engineering. *Biomaterials* **24**, 2077-82 (2003).
12. Fertala, A., Han, W.B. & Ko, F.K. Mapping critical sites in collagen II for rational design of gene-engineered proteins for cell-supporting materials. *J Biomed Mater Res* **57**, 48-58 (2001).
13. Zong, X. et al. Electrospun fine-textured scaffolds for heart tissue constructs. *Biomaterials* **26**, 5330-8 (2005).
14. Yoon, J.J., Song, S.H., Lee, D.S. & Park, T.G. Immobilization of cell adhesive RGD peptide onto the surface of highly porous biodegradable polymer scaffolds fabricated by a gas foaming/salt leaching method. *Biomaterials* **25**, 5613-20 (2004).
15. Benoit, D.S., Durney, A.R. & Anseth, K.S. The effect of heparin-functionalized PEG hydrogels on three-dimensional human mesenchymal stem cell osteogenic differentiation. *Biomaterials* **28**, 66-77 (2007).

16. Silva, G.A. et al. Selective differentiation of neural progenitor cells by high-epitope density nanofibers. *Science* **303**, 1352-5 (2004).
17. Leach, J.K., Kaigler, D., Wang, Z., Krebsbach, P.H. & Mooney, D.J. Coating of VEGF-releasing scaffolds with bioactive glass for angiogenesis and bone regeneration. *Biomaterials* **27**, 3249-55 (2006).
18. Luo, Y. & Shoichet, M.S. A photolabile hydrogel for guided three-dimensional cell growth and migration. *Nat Mater* **3**, 249-53 (2004).
19. Kim, B.S., Nikolovski, J., Bonadio, J. & Mooney, D.J. Cyclic mechanical strain regulates the development of engineered smooth muscle tissue. *Nat Biotechnol* **17**, 979-83 (1999).
20. den Braber, E.T., de Ruijter, J.E., Ginsel, L.A., von Recum, A.F. & Jansen, J.A. Orientation of ECM protein deposition, fibroblast cytoskeleton, and attachment complex components on silicone microgrooved surfaces. *J Biomed Mater Res* **40**, 291-300 (1998).
21. Walboomers, X.F., Croes, H.J., Ginsel, L.A. & Jansen, J.A. Contact guidance of rat fibroblasts on various implant materials. *J Biomed Mater Res* **47**, 204-12 (1999).
22. van Kooten, T.G., Whitesides, J.F. & von Recum, A. Influence of silicone (PDMS) surface texture on human skin fibroblast proliferation as determined by cell cycle analysis. *J Biomed Mater Res* **43**, 1-14 (1998).
23. Teixeira, A.I., Abrams, G.A., Bertics, P.J., Murphy, C.J. & Nealey, P.F. Epithelial contact guidance on well-defined micro- and nanostructured substrates. *J Cell Sci* **116**, 1881-92 (2003).
24. Sato, M. & Webster, T.J. Nanobiotechnology: implications for the future of nanotechnology in orthopedic applications. *Expert Rev Med Devices* **1**, 105-14 (2004).
25. de Oliveira, P.T. & Nanci, A. Nanotexturing of titanium-based surfaces upregulates expression of bone sialoprotein and osteopontin by cultured osteogenic cells. *Biomaterials* **25**, 403-13 (2004).
26. Price, R.L., Waid, M.C., Haberstroh, K.M. & Webster, T.J. Selective bone cell adhesion on formulations containing carbon nanofibers. *Biomaterials* **24**, 1877-87 (2003).
27. Webster, T.J., Siegel, R.W. & Bizios, R. Osteoblast adhesion on nanophase ceramics. *Biomaterials* **20**, 1221-7 (1999).
28. Webster, T.J. Nanophase ceramics: the future of orthopedic and dental implant material. in *Nanostructured materials* (ed. Ying, J.Y.) 126-166 (Academy Press, New York, 2001).
29. Webster, T.J., Ergun, C., Doremus, R.H., Siegel, R.W. & Bizios, R. Enhanced functions of osteoblasts on nanophase ceramics. *Biomaterials* **21**, 1803-10 (2000).
30. Webster, T.J., Ergun, C., Doremus, R.H., Siegel, R.W. & Bizios, R. Enhanced osteoclast-like cell functions on nanophase ceramics. *Biomaterials* **22**, 1327-33 (2001).
31. Folkman, J. & Hochberg, M. Self-regulation of growth in three dimensions. *J Exp Med* **138**, 745-53 (1973).

32. Hutmacher, D.W., Sittinger, M. & Risbud, M.V. Scaffold-based tissue engineering: rationale for computer-aided design and solid free-form fabrication systems. *Trends Biotechnol* **22**, 354-62 (2004).
33. Ennett, A.B. & Mooney, D.J. Tissue engineering strategies for in vivo neovascularisation. *Expert Opin Biol Ther* **2**, 805-18 (2002).
34. Ennett, A.B., Kaigler, D. & Mooney, D.J. Temporally regulated delivery of VEGF in vitro and in vivo. *J Biomed Mater Res A* **79**, 176-84 (2006).
35. Bouhadir, K.H. & Mooney, D.J. Promoting angiogenesis in engineered tissues. *J Drug Target* **9**, 397-406 (2001).
36. Tan, W. & Desai, T.A. Layer-by-layer microfluidics for biomimetic three-dimensional structures. *Biomaterials* **25**, 1355-64 (2004).
37. Tan, W. & Desai, T.A. Microscale multilayer cocultures for biomimetic blood vessels. *J Biomed Mater Res A* **72**, 146-60 (2005).
38. Wilson, W.C., Jr. & Boland, T. Cell and organ printing 1: protein and cell printers. *Anat Rec A Discov Mol Cell Evol Biol* **272**, 491-6 (2003).
39. Boland, T., Mironov, V., Gutowska, A., Roth, E.A. & Markwald, R.R. Cell and organ printing 2: fusion of cell aggregates in three-dimensional gels. *Anat Rec A Discov Mol Cell Evol Biol* **272**, 497-502 (2003).
40. Nicolson, P.C. & Vogt, J. Soft contact lens polymers: an evolution. *Biomaterials* **22**, 3273-83 (2001).
41. Wheeler, J.C. et al. Evolution of hydrogel polymers as contact lenses, surface coatings, dressings, and drug delivery systems. *J Long Term Eff Med Implants* **6**, 207-17 (1996).
42. Langer, R. & Peppas, N.A. Advances in biomaterials, drug delivery, and bionanotechnology. *Aiche Journal* **49**, 2990-3006 (2003).
43. Rowley, J.A., Madlambayan, G. & Mooney, D.J. Alginate hydrogels as synthetic extracellular matrix materials. *Biomaterials* **20**, 45-53 (1999).
44. Langer, R. & Vacanti, J.P. Tissue engineering. *Science* **260**, 920-6. (1993).
45. Langer, R. Biomaterials in drug delivery and tissue engineering: one laboratory's experience. *Acc Chem Res* **33**, 94-101 (2000).
46. Dar, A., Shachar, M., Leor, J. & Cohen, S. Optimization of cardiac cell seeding and distribution in 3D porous alginate scaffolds. *Biotechnol Bioeng* **80**, 305-12 (2002).
47. Kim, S.S. et al. Dynamic seeding and in vitro culture of hepatocytes in a flow perfusion system. *Tissue Eng* **6**, 39-44 (2000).
48. Carrier, R.L. et al. Cardiac tissue engineering: cell seeding, cultivation parameters, and tissue construct characterization. *Biotechnol Bioeng* **64**, 580-9 (1999).
49. Vunjak-Novakovic, G. et al. Dynamic cell seeding of polymer scaffolds for cartilage tissue engineering. *Biotechnol Prog* **14**, 193-202 (1998).
50. A.B. Scranton, C.N.B.e.a. Photopolymerization fundamentals and applications. *ACS Publishers* (1996).
51. Sakiyama, S.E., Schense, J.C. & Hubbell, J.A. Incorporation of heparin-binding peptides into fibrin gels enhances neurite extension: an example of designer matrices in tissue engineering. *Faseb J* **13**, 2214-24 (1999).

52. Burdick, J.A., Chung, C., Jia, X., Randolph, M.A. & Langer, R. Controlled degradation and mechanical behavior of photopolymerized hyaluronic acid networks. *Biomacromolecules* **6**, 386-91 (2005).
53. Khademhosseini, A., May, M.H. & Sefton, M.V. Conformal Coating of Mammalian Cells Immobilized onto Magnetically Driven Beads. *Tissue Eng* **11**, 1797-1806 (2005).
54. Halstenberg, S., Panitch, A., Rizzi, S., Hall, H. & Hubbell, J.A. Biologically engineered protein-graft-poly(ethylene glycol) hydrogels: a cell adhesive and plasmin-degradable biosynthetic material for tissue repair. *Biomacromolecules* **3**, 710-23 (2002).
55. Elisseeff, J. et al. Photoencapsulation of chondrocytes in poly(ethylene oxide)-based semi-interpenetrating networks. *J Biomed Mater Res* **51**, 164-71 (2000).
56. Chandrashekhar P. Pathak, A.S.S., and Jeffrey A. Hubbell. Rapid photopolymerization of immunoprotective gels in contact with cells and tissue. *J. Am. Chem. Soc.* **114**, 8311 - 8312 (1992).
57. Cruise, G.M. et al. In vitro and in vivo performance of porcine islets encapsulated in interfacially photopolymerized poly(ethylene glycol) diacrylate membranes. *Cell Transplantation* **8**, 293-306 (1999).
58. Sawhney, A.S., Pathak, C.P. & Hubbell, J.A. Interfacial photopolymerization of poly(ethylene glycol)-based hydrogels upon alginate-poly(l-lysine) microcapsules for enhanced biocompatibility. *Biomaterials* **14**, 1008-1016 (1993).
59. Ki Hyun Bae, J.J.Y., and Tae Gwan Park. Fabrication of Hyaluronic Acid Hydrogel Beads for Cell Encapsulation. *Biotechnol. Prog* **22**, 297-302 (2006).
60. Chandy, T., Mooradian, D.L. & Rao, G.H. Evaluation of modified alginate-chitosan-polyethylene glycol microcapsules for cell encapsulation. *Artif Organs* **23**, 894-903 (1999).
61. Uludag, H., De Vos, P. & Tresco, P.A. Technology of mammalian cell encapsulation. *Adv Drug Deliv Rev* **42**, 29-64 (2000).
62. Xia, Y.N. & Whitesides, G.M. Soft lithography. *Angewandte Chemie-International Edition* **37**, 551-575 (1998).
63. Khademhosseini, A. et al. Molded polyethylene glycol microstructures for capturing cells within microfluidic channels. *Lab Chip* **4**, 425-30 (2004).
64. Khademhosseini, A. et al. Direct Patterning of protein- and cell-resistant polymeric monolayers and microstructures. *Advanced Materials* **15**, 1995-2000 (2003).
65. Jeon, N.L. et al. Neutrophil chemotaxis in linear and complex gradients of interleukin-8 formed in a microfabricated device. *Nature Biotechnology* **20**, 826-830 (2002).
66. Khademhosseini, A. et al. Cell docking inside microwells within reversibly sealed microfluidic channels for fabricating multiphenotype cell arrays. *Lab Chip* **5**, 1380-6 (2005).
67. W. T. Godbey, A.A. In Vitro Systems for Tissue Engineering. *Annals of the New York Academy of Sciences* **961**, 10-26 (2002).
68. Batorsky, A., Liao, J., Lund, A.W., Plopper, G.E. & Stegemann, J.P. Encapsulation of adult human mesenchymal stem cells within collagen-agarose microenvironments. *Biotechnol Bioeng* **92**, 492-500 (2005).

69. Dang, S.M., Kyba, M., Perlingeiro, R., Daley, G.Q. & Zandstra, P.W. Efficiency of embryoid body formation and hematopoietic development from embryonic stem cells in different culture systems. *Biotechnol Bioeng* **78**, 442-53 (2002).
70. Koh, W.G., Itle, L.J. & Pishko, M.V. Molding of hydrogel multiphenotype cell microstructures to create microarrays. *Analytical Chemistry* **75**, 5783-5789 (2003).
71. Liu, V.A. & Bhatia, S.N. Three-dimensional photopatterning of hydrogels containing living cells. *Biomedical Microdevices* **4**, 257-266 (2002).
72. Koh, W.G., Revzin, A. & Pishko, M.V. Poly(ethylene glycol) hydrogel microstructures encapsulating living cells. *Langmuir* **18**, 2459-2462 (2002).
73. Tang, M.D., Golden, A.P. & Tien, J. Molding of three-dimensional microstructures of gels. *Journal of the American Chemical Society* **125**, 12988-12989 (2003).
74. Khademhosseini, A., Langer, R., Borenstein, J. & Vacanti, J.P. Microscale technologies for tissue engineering and biology. *Proc Natl Acad Sci U S A* **103**, 2480-7 (2006).
75. Cabodi, M. et al. A microfluidic biomaterial. *J Am Chem Soc* **127**, 13788-9 (2005).
76. Bryant, S.J., Nuttelman, C.R. & Anseth, K.S. Cytocompatibility of UV and visible light photoinitiating systems on cultured NIH/3T3 fibroblasts in vitro. *J Biomater Sci Polym Ed* **11**, 439-57 (2000).
77. Breen, T.L., Tien, J., Oliver, S.R., Hadzic, T. & Whitesides, G.M. Design and self-assembly of open, regular, 3D mesostructures. *Science* **284**, 948-51 (1999).
78. Hansen, C. & Quake, S.R. Microfluidics in structural biology: smaller, faster em leader better. *Curr Opin Struct Biol* **13**, 538-44 (2003).
79. Beebe, D.J., Mensing, G.A. & Walker, G.M. Physics and applications of microfluidics in biology. *Annu Rev Biomed Eng* **4**, 261-86 (2002).
80. Whitesides, G.M., Ostuni, E., Takayama, S., Jiang, X. & Ingber, D.E. Soft lithography in biology and biochemistry. *Annu Rev Biomed Eng* **3**, 335-73 (2001).
81. Takayama, S. et al. Patterning cells and their environments using multiple laminar fluid flows in capillary networks. *Proc Natl Acad Sci U S A* **96**, 5545-5548 (1999).
82. Stroock, A.D. et al. Chaotic mixer for microchannels. *Science* **295**, 647-651 (2002).
83. Beebe, D.J. et al. Functional hydrogel structures for autonomous flow control inside microfluidic channels. *Nature* **404**, 588-90 (2000).
84. Kenis, P.J.A., Ismagilov, R.F. & Whitesides, G.M. Microfabrication inside capillaries using multiphase laminar flow patterning. *Science* **285**, 83-85 (1999).
85. King, K., Wang, C., Kaazempur-Mofrad, M., Vacanti, J. & Borenstein, J. Biodegradable microfluidics. *Advanced Materials* **16**, 2007-2012 (2004).
86. Borenstein, J.T. et al. Microfabrication technology for vascularized tissue engineering. *Biomedical Microdevices* **4**, 167-175 (2002).
87. Bettinger, C.J., Weinberg, E.J., Kulig, K.M., Vacanti, J.P., Wang, Y., Borenstein, J.T., Langer R. Three-Dimensional Microfluidic Tissue-Engineering Scaffolds Using a Flexible Biodegradable Polymer. *Advanced Materials* **18**, 165-169 (2006).
88. Fidkowski, C. et al. Endothelialized microvasculature based on a biodegradable elastomer. *Tissue Eng* **11**, 302-9 (2005).
89. Paguirigan, A. & Beebe, D.J. Gelatin based microfluidic devices for cell culture. *Lab Chip* **6**, 407-13 (2006).

90. Morra, M. & Cassineli, C. Non-fouling properties of polysaccharide-coated surfaces. *Journal Of Biomaterials Science. Polymer Edition* **10**, 1107-1124 (1999).
91. Khademhosseini, A. et al. Micromolding of photocrosslinkable hyaluronic acid for cell encapsulation and entrapment. *J Biomed Mater Res A* (2006).
92. Mummert, M. Immunologic roles of hyaluronan. *Immunol Res* **31**, 189-206 (2005).
93. Lee, K.Y. & Mooney, D.J. Hydrogels for tissue engineering. *Chem Rev* **101**, 1869-79 (2001).
94. Cruise, G.M., Scharp, D.S. & Hubbell, J.A. Characterization of permeability and network structure of interfacially photopolymerized poly(ethylene glycol) diacrylate hydrogels. *Biomaterials* **19**, 1287-94. (1998).
95. Smeds, K.A. et al. Photocrosslinkable polysaccharides for in situ hydrogel formation. *J Biomed Mater Res* **54**, 115-21 (2001).
96. Khademhosseini, A. et al. Layer-by-layer deposition of hyaluronic acid and poly-l-lysine for patterned cell co-cultures. *Biomaterials* **25**, 3583-92 (2004).
97. Davis, K.A., Burdick, J.A. & Anseth, K.S. Photoinitiated crosslinked degradable copolymer networks for tissue engineering applications. *Biomaterials* **24**, 2485-95 (2003).
98. Khademhosseini, A. et al. Micromolding of photocrosslinkable hyaluronic acid for cell encapsulation and entrapment. *J Biomed Mater Res A* **79**, 522-32 (2006).
99. Barralet, J.E. et al. Comparison of bone marrow cell growth on 2D and 3D alginate hydrogels. *J Mater Sci Mater Med* **16**, 515-9 (2005).
100. Chang, S.C. et al. Injection molding of chondrocyte/alginate constructs in the shape of facial implants. *J Biomed Mater Res* **55**, 503-11 (2001).
101. Augst, A.D., Kong, H.J. & Mooney, D.J. Alginate hydrogels as biomaterials. *Macromol Biosci* **6**, 623-33 (2006).
102. Magyar, J.P. et al. Mass production of embryoid bodies in microbeads. *Ann N Y Acad Sci* **944**, 135-43 (2001).
103. Wee, S. & Gombotz, W.R. Protein release from alginate matrices. *Adv Drug Deliv Rev* **31**, 267-285 (1998).
104. Tonnesen, H.H. & Karlsen, J. Alginate in drug delivery systems. *Drug Dev Ind Pharm* **28**, 621-30 (2002).
105. Zekorn, T. et al. Alginate coating of islets of Langerhans: in vitro studies on a new method for microencapsulation for immuno-isolated transplantation. *Acta Diabetol* **29**, 41-5 (1992).
106. Wang, T. et al. An encapsulation system for the immunoisolation of pancreatic islets. *Nat Biotechnol* **15**, 358-62 (1997).
107. Mullen, Y., Maruyama, M. & Smith, C.V. Current progress and perspectives in immunoisolated islet transplantation. *J Hepatobiliary Pancreat Surg* **7**, 347-57 (2000).
108. Uludag, H., De Vos, P. & Tresco, P.A. Technology of mammalian cell encapsulation. *Adv Drug Deliv Rev* **42**, 29-64. (2000).
109. Peppas, N., Hilt, J.Z., Khademhosseini, A. & Langer, R. Hydrogels in biology and medicine. *Advanced Materials* **18**, 1345-60 (2006).

110. Shiong, P.S., Heintz, R.E., Merideth, N., Yao, Q.X., Yao, Z., Zheng, T. et al. . Insulin independence in a type 1 diabetic patient after encapsulated islet transplantation. *Lancet* **343**, 950–951 (1994).
111. Whitesides, G.M., Ostuni, E., Takayama, S., Jiang, X.Y. & Ingber, D.E. Soft lithography in biology and biochemistry. *Annual Review of Biomedical Engineering* **3**, 335-373 (2001).
112. Borst, P. Ethidium DNA agarose gel electrophoresis: how it started. *IUBMB Life* **57**, 745-7 (2005).
113. Weibel, D.B. et al. Bacterial printing press that regenerates its ink: contact-printing bacteria using hydrogel stamps. *Langmuir* **21**, 6436-42 (2005).
114. Stevens, M.M. et al. Direct patterning of mammalian cells onto porous tissue engineering substrates using agarose stamps. *Biomaterials* **26**, 7636-41 (2005).
115. Jones, K.S., Sefton, M.V. & Gorczynski, R.M. In vivo recognition by the host adaptive immune system of microencapsulated xenogeneic cells. *Transplantation* **78**, 1454-62 (2004).
116. Rahfoth, B. et al. Transplantation of allograft chondrocytes embedded in agarose gel into cartilage defects of rabbits. *Osteoarthritis Cartilage* **6**, 50-65 (1998).
117. Chen, Q., Suki, B. & An, K.N. Dynamic mechanical properties of agarose gels modeled by a fractional derivative model. *J Biomech Eng* **126**, 666-71 (2004).
118. Benkherourou, M., Rochas, C., Tracqui, P., Tranqui, L. & Gumery, P.Y. Standardization of a method for characterizing low-concentration biogels: elastic properties of low-concentration agarose gels. *J Biomech Eng* **121**, 184-7 (1999).
119. Farokhzad, O.C. et al. Microfluidic system for studying the interaction of nanoparticles and microparticles with cells. *Anal Chem* **77**, 5453-9 (2005).
120. R.S. Renemana, T.A., A.P.G. Hoeksb. Wall Shear Stress - an Important Determinant of Endothelial Cell Function and Structure - in the Arterial System in vivo

Discrepancies with Theory. *Journal of Vascular Research* **43**, 251-269 (2006).
121. Upcroft, P. & Upcroft, J.A. Comparison of properties of agarose for electrophoresis of DNA. *J Chromatogr* **618**, 79-93 (1993).
122. Pluen, A., Netti, P.A., Jain, R.K. & Berk, D.A. Diffusion of macromolecules in agarose gels: comparison of linear and globular configurations. *Biophys J* **77**, 542-52 (1999).
123. Inman, J.K. Affinity Chromatography: A Practical Approach. (ed. Dean, P.D.G., Johnson, W.S., Middle, F.A.) p. 53 (IRL Press Limited, Oxford, 1985).
124. Whitesides, G.M. & Boncheva, M. Beyond molecules: self-assembly of mesoscopic and macroscopic components. *Proc Natl Acad Sci U S A* **99**, 4769-74 (2002).
125. Whitesides, G.M. & Grzybowski, B. Self-assembly at all scales. *Science* **295**, 2418-21 (2002).
126. Whitesides, G.M., Mathias, J.P. & Seto, C.T. Molecular self-assembly and nanochemistry: a chemical strategy for the synthesis of nanostructures. *Science* **254**, 1312-9 (1991).
127. Clark, T.D., Tien, J., Duffy, D.C., Paul, K.E. & Whitesides, G.M. Self-assembly of 10-microm-sized objects into ordered three-dimensional arrays. *J Am Chem Soc* **123**, 7677-82 (2001).

128. Bowden, N., Terfort, A., Carbeck, J. & Whitesides, G.M. Self-Assembly of Mesoscale Objects into Ordered Two-Dimensional Arrays. *Science* **276**, 233-5 (1997).
129. Bowden, N.B., Weck, M., Choi, I.S. & Whitesides, G.M. Molecule-mimetic chemistry and mesoscale self-assembly. *Acc Chem Res* **34**, 231-8 (2001).
130. Clark, T.D., Ferrigno, R., Tien, J., Paul, K.E. & Whitesides, G.M. Template-directed self-assembly of 10-microm-sized hexagonal plates. *J Am Chem Soc* **124**, 5419-26 (2002).
131. Oliver, S.R., Bowden, N. & Whitesides, G.M. Self-Assembly of Hexagonal Rod Arrays Based on Capillary Forces. *J Colloid Interface Sci* **224**, 425-428 (2000).
132. Jacobs, H.O., Tao, A.R., Schwartz, A., Gracias, D.H. & Whitesides, G.M. Fabrication of a cylindrical display by patterned assembly. *Science* **296**, 323-5 (2002).

Biography

Yibo Ling (凌逸波) was born on November 4th, 1982 in Taiyuan, China. He immigrated with his parents to the United States in 1989 and graduated in 2001 from Plymouth-Salem High School (Canton, Michigan). He received his Bachelor of Science in Engineering in Biomedical Engineering and Bachelor of Arts in English Literature from the University of Michigan (Ann Arbor, Michigan) in May 2005. He is currently pursuing a doctorate in Medical Engineering and Medical Physics at the Harvard-MIT Division of Health Sciences and Technology.